Cardiomyocyte apicobasal polarity during cardiac trabeculation in zebrafish

---

Dissertation

zur Erlangung des Doktorgrades

der Naturwissenschaften

vorgelegt beim Fachbereich 15

der Johann Wolfgang Goethe-Universität

in Frankfurt am Main

von

Vanesa Jiménez-Amilburu

aus Logroño, La Rioja, Spanien

Frankfurt 2018

(D30)

vom Fachbereich Biowissenschaften (FB15) der Johann Wolfgang Goethe - Universität als Dissertation angenommen.

Dekan: Prof. Dr. Sven Klimpel

Gutachter: Prof. Didier Y. R. Stainier, Ph.D.
Prof. Amparo Acker-Palmer, Ph.D.

Datum der Disputation: August 21st, 2019

SUPERVISOR

Prof. Didier Y. R. Stainier, Ph.D.
Department of Developmental Genetics
Max Planck Institute for Heart and Lung Research
Bad Nauheim, Germany

REVIEWERS

Prof. Didier Y. R. Stainier, Ph.D.
Department of Developmental Genetics
Max Planck Institute for Heart and Lung Research
Bad Nauheim, Germany

and

Prof. Amparo Acker-Palmer, Ph.D.
Department of Molecular and Cellular Neurobiology
Institute for Cell Biology and Neuroscience
Johann Wolfgang Goethe University
Frankfurt am Main, Germany

Commonly used abbreviations

Abbreviation	Description
aa	Aminoacid
AJ	Adherens junction
aPKC	Atypical protein kinase C
At	Atrium
AVC	Atrioventricular canal
BMPs	Bone Morphogenetic Proteins
cDNA	Complementary DNA
CM(s)	Cardiomyocyte(s)
Crb	Crumbs
Crb2a	Crumbs2a
DAPI	4,6-diamino-2-phenylindole
DMSO	Dimethyl sulfoxide
DNA	Deoxyribonucleic acid
E.Coli	Escherichia coli
EGFP	Enhanced Green fluorescent protein
EMT	Epithelial to mesenchymal transition
ErbB2	V-Erb-B2 Avian ErythroblasticnLeukemia Viral Oncogene Homolog 2
EtBr	Ethidium Bromide
F-actin	Filamentous actin
g	Gram
hpf	Hours post fertilization
IHC	Immunohistochemistry
l	Liter
LVNC	Left ventricular non compaction
mg	Milligram
min	Minutes
ml	Milliliter
mM	Milimolar
MO	Morpholino
mRNA	Messenger RNA
MTZ	Metronidazol
myl7	Cardiac myosin light chain 7
NA	Numerical aperture

ng	Nanogram
nls	Nuclear localization signal
Nrg	Neuregulin
PATJ	Protein associated with tight junctions
PBS	Phosphate Buffered Saline
PCR	Polymerase Chain Reaction
PFA	Paraformaldehide
Podxl	Podocalyxin
PTU	N-Phenylthiourea
RNA	Ribonucleic acid
RT	Room temperature
SA node	Sinoatrial node
Sdt	Stardust
Taq	Thermus aqaticus
TBE	Tris-borate-EDTA
Tg	Transgenic
TJ	Tight junction
tnnt2a	Troponin T Type 2 (Cardiac)
Tricaine	Ethyl-m-aminobenzoate methanesulfonate
V	Ventricle
v/v	Volume/volume
WT	Wild Type
µl	Microliter
µm	Micromolar

1. Introduction

1. 1 Heart development in mammals

The heart is the first organ to develop. During development, the embryonic heart experiences numerous modifications in order to become a capable pumping organ (Brand, 2003; Moorman and Christoffels, 2003; Sedmera et al., 2000). The heart is an asymmetric organ that displays three different types of polarity patterns based on the body axes: anteroposterior, dorsoventral, and left–right. Derived from the mesoderm, the cardiac crescent is formed by the cardiac progenitors that establish the first heart field (FHF) and the second heart field (SHF). The two heart fields migrate and fuse to form the linear heart tube patterned along the anteroposterior axis (**Figure 1**). The early immature heart is a two-layer linear tube composed of an inner endothelial layer of cells (luminal) and an immature myocardial layer (abluminal), separated by extracellular matrix called cardiac jelly. Genes such as *Mesp1, Nkx2.5, Gata4,* and *Bmp4* are required at early stages to establish precise allocation of cardiac progenitors (Bondue and Blanpain, 2010; Pashmforoush et al., 2004; Peterkin et al., 2005; van Wijk et al., 2007). These transcription factors will also play roles later at other time points during cardiac development (Paige et al., 2015).

As the primitive heart tube elongates, it begins to loop acquiring sigmoid shape (Ivanovitch et al., 2017). During the looping, the original left and right sides of the linear heart tube evolve to the ventral and dorsal sides (Brand, 2003). Next, cardiac chamber specification takes place. At this stage, cardiac structures derived from the FHF and SHF are distinguishable. The left ventricle and part of the atrium derive from the FHF, while the right ventricle and the outflow tract, and the primitive common atria and the inflow tract arise from the anterior and posterior SHF respectively. Moreover, septation occurs in order to separate the left and the right ventricular chambers, thus preventing the mixing of the oxygenated an deoxygenated blood (Lamers and Moorman, 2002). Lastly, the endothelial cushions and the tricuspid and mitral valves develop mainly by epithelial-to-mesenchymal transition (EMT). These structures will ensure unidirectional blood flow (von Gise and Pu, 2012). Once the chambers of the heart are specified, the cardiac chamber maturation occurs. The ventricle forms a spongy-like network called trabeculae that helps to increase the cardiac output in the heart (Sedmera et al., 2000). At the same time, trabeculae experience extensive remodeling, the cardiac wall and conduction system mature, and the coronary vasculature is established (Samsa et al., 2013). Molecularly, *Tbx1/5*, *Tbx20, Pitx2, and Fgf10* are essential regulators of chamber looping and ballooning, ventricular growth and maturation (Franco et al., 2014; Singh et al., 2005; Steimle

and Moskowitz, 2017; Vega-Hernández et al., 2011). All these events result in the formation of a four-chambered heart integrated with the circulatory system.

Figure 1. Development of the heart. Diagram showing the development and maturation of the mouse

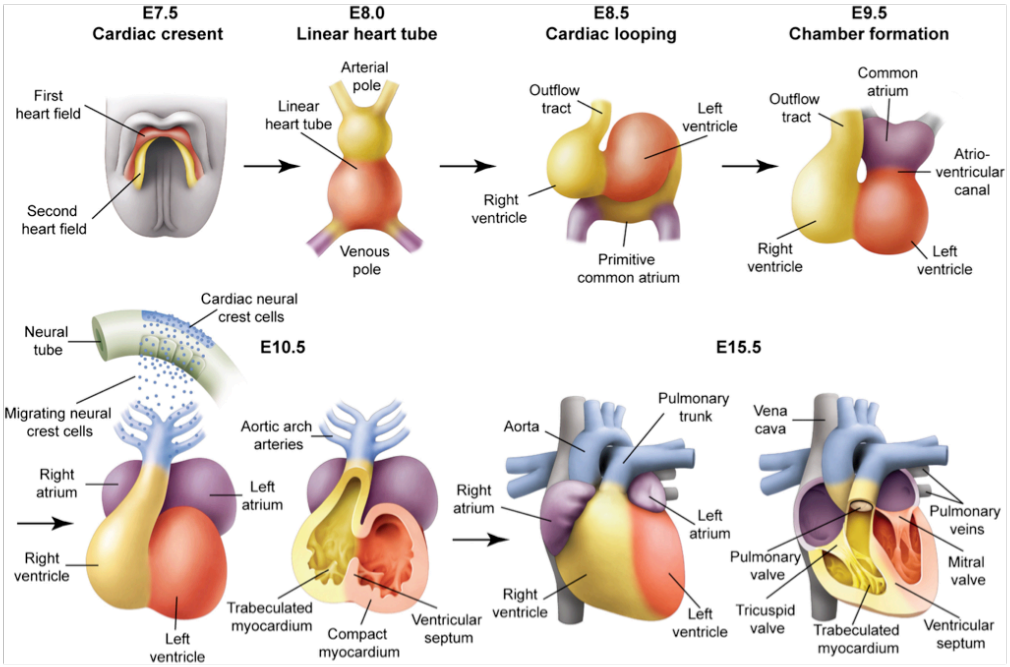

embryonic heart. During cardiac development, the first and second heart fields migrate and fuse to give raise to the linear heart tube. Later the nascent linear heart tube will undergo looping, chamber specification, septation, and valve morphogenesis. Adapted from Epstein et al., 2014.

1.1.1 Zebrafish heart development

The zebrafish, *Danio rerio*, has emerged as a valuable model organism to study cardiovascular diseases. Zebrafish embryos undergo fast development and are transparent, allowing visualization of the heart morphology by light or confocal microscopy. Additionally, diverse reverse and forward genetic approaches (gene editing, gene knockdown, mutagenesis, etc.) are possible and well-established. Heart contraction appears as early as 24 hours post fertilization (hpf). However, zebrafish do not require a functional cardiovascular system during the first week of life, which permits the study of heart defects during embryonic stages that in other vertebrate models like rodents lead to embryonic lethality. Altogether, these features and advantages make zebrafish ideally suited to study heart development and disease.

Although the zebrafish heart is simpler structurally than the mammalian heart, most of the steps that give rise to this essential organ are highly conserved **(Figure 2)**. The zebrafish heart is derived from mesodermal tissue. Before gastrulation, two different pools of myocardial progenitor cells (atrial and ventricular) can be observed in the blastula region (Bakkers, 2011). At 16-somites, the myocardial tissue expands and the endocardium migrates **(Figure 2A-C)**. Next, the fusion of the bilateral cardiac tubes at the midline at 22 hpf leads to the formation of the cardiac disc, where the endocardium locates in the middle with the atrial cardiomyocytes (CMs) around, and ventricular CMs localized in the periphery **(Figure 2D)**. At 28 hpf, the cardiac tube is already transformed into a linear heart tube and exhibits two distinct specialized chambers, one ventricle and one atrium, separated by the atrioventricular canal (AVC), and a valvular structure called *bulbus arteriosus* **(Figure 2E)**. Then, heart looping occurs at 30 hpf by twisting of the cardiac tube toward the right-hand side of the embryo **(Figure 2F)**. Once the heart has finished looping, a cluster of cells derived from the pro-epicardial organ migrates to form the third layer of the heart **(Figure 2G)**. Using *tcf21* and *wt1* markers, Serluca found that around 50 hpf, pro-epicardial cells migrate onto the surface of the heart towards the atrium and are located near the atrioventricular canal and the sinus venous. Later, around 60 hpf and coinciding with the onset of trabeculation, pro-epicardial cells start populating the outer layer of the ventricle in the heart to form the epicardium that will cover the myocardium. The epicardial layer is fully formed by 96 hpf (Serluca, 2008). Epicardial cues are essential for heart growth in zebrafish, mouse and chick (Männer, 1993; Ruiz-Villalba et al., 2015). However, although the physical interactions between epicardium and myocardium have been widely studied, the instructive molecular signals that drive these interactions and its implication during cardiac development remain to be elucidated.

Figure 2. Zebrafish heart development. (A) Two populations of myocardial progenitors cells are visible (atrial and ventricular). (B) Migration of cardiac progenitor cells towards the mid-line to end up in the anterior later plate mesoderm (ALPM). (C) Myocardial tissue expands and endocardium migrates. (D) Formation of the heart disc. (E) Heart disc transforms into a linear heart tube. (F) Heart looping has already started. (G) Looping continues and heart acquires S-shape. Adapted from Bakkers 2011.

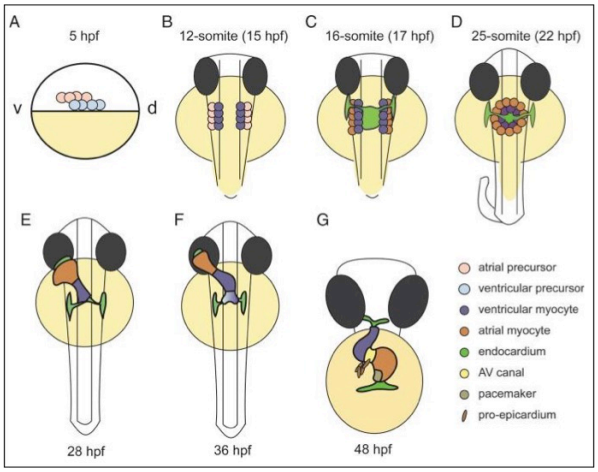

1.2 Cardiac trabeculation

Cardiac trabeculation is a highly conserved process among vertebrates. It initiates after looping and is one of the essential events that contribute to the formation of a functionally competent ventricular wall in the heart (Samsa et al., 2013). Cardiac trabeculation is a complex multi-step process that requires the tight coordination of events involving CM selection, delamination and proliferation.

The formation of trabeculae is typically divided in three different steps: emergence, trabeculation and remodeling (**Figure 3**).

1. Emergence. Before the initiation of cardiac trabeculation, the compact wall of the ventricle is composed of a single layer of myocardial cells and an inner layer of endocardial cells separated by extracellular matrix called "cardiac jelly". In human embryos at Carnegie stage 12, in mouse at the embryonic day 9.5 (E9.5), and in zebrafish around 60 hpf, the first CMs projecting towards the ventricular lumen can be observed. These first trabecular protruding CMs emerge in the outer curvature of the ventricle, located ventral to the AVC, in a stereotypical manner (Liu et al., 2010; Peshkovsky et al., 2011; Sedmera and Thomas Penny, 1996). Zebrafish studies show that the main process by which CMs reach the trabecular layer is delamination (Staudt et al., 2014). In mouse, a recent work demonstrates that both migration and oriented cell division contribute to the formation of the first trabeculae (Li et al., 2016)

2. Trabeculation. Next, a combination of both processes delamination/migration and proliferation/oriented cell division take place in order to increase the length and thickness of these protrusions towards the lumen of the ventricle in mice and zebrafish (Uribe, et al, unpublished; Zhang et al., 2013). At this point during vertebrate cardiac chamber maturation, the majority of the myocyte mass is found in the trabecular region rather than in the compact wall.

3. Remodeling. This is the last step during cardiac chamber maturation and is also called "compaction". The remodeling step dictates the differences in cardiac chamber morphology between species. Trabeculae stop growing towards the lumen in length. Now, the trabecular base thickens and fuses with the compact wall and the spaces between trabeculae are converted into capillaries.

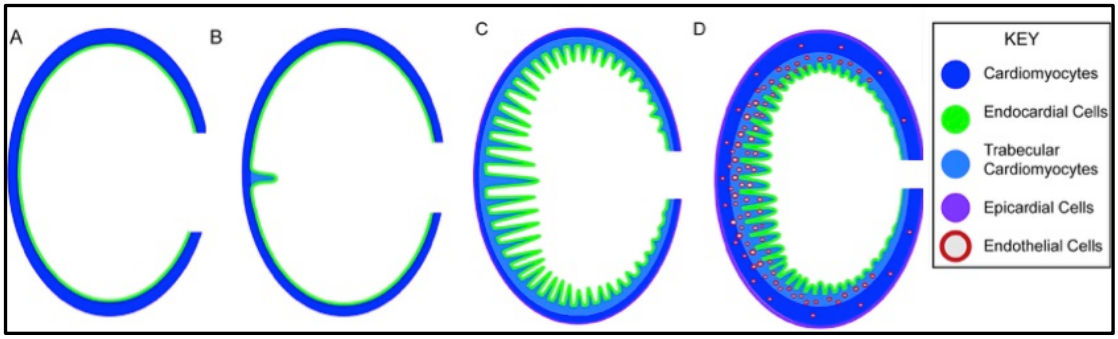

Figure 3. Cardiac chamber maturation. (A) Heart ventricle formed by a single layer of CMs (myocardium, outer layer) and a single layer of endothelial cells (endocardium, inner layer). **(B) Emergence:** During development, selected CMs leave the compact myocardial layer and reach a second layer in the lumen of the heart called trabecular layer**. (C) Trabeculation:** Later, myocardial protrusions grow in length and thickness in the whole ventricle from trabecular ridges in the lumen of the ventricle. **(D) Remodeling:** Compaction of the wall form by a radial network of trabeculae in the lumen of the ventricle. Figure modified from Samsa et al., 2013

Perturbations in any of these steps can lead to severe cardiac abnormalities. Some of these defects include a significant reduction in the number of trabeculae forming a "hypoplastic wall", which usually leads to embryonic lethality or embryonic heart failure (Jenni et al., 1999). On the other hand, excessive trabeculation (hypertrabeculation) and non-compaction during cardiac chamber maturation are also related to embryonic cardiac defects associated to Left Ventricle Non-Compaction (LVNC) (Jenni et al., 1999; Towbin, 2010; Zhang et al., 2013). Despite being critical for the development of the heart, the exact function of cardiac trabeculae is unknown. It is suggested that they might be relevant to contractility (Zhang et al., 2013), increase the cardiac output, permit nutrition and oxygen uptake by CMs prior to the formation of the coronary vasculature (Liu et al., 2010; Rychter 1971), and to be involved in the formation of a conduction system (van Weerd and Christoffels, 2016).

1.3 Factors involved in cardiac trabeculation

A number of signaling pathways and factors are required as part of the dynamic process of cardiac trabeculation.

1.3.1 Signaling pathways involved in trabeculation:

Here, I summarize the most relevant signaling pathways regulating different steps of cardiac trabeculation **(Figure 4**).

Neuregulin/ErbB2/ErbB4 signaling

The Neuregulin (Nrg)/ErbB2/ErbB4 signaling pathway is one of the master regulators of cardiac trabeculation. The transmembrane NRG1 acts as a paracrine ligand. It binds to receptors of the ERBB family to promote the formation of ERBB4/ERBB2 heterodimeric signaling complex. In mice, the lack of the either the ligand (NRG1) or any of the receptor tyrosine kinase (ERBB2 or ERBB4) causes embryonic lethality due to the failure in the formation of trabeculae (Gassmann et al., 1995; Lee et al., 1995; Meyer and Birchmeier, 1995). Recently in zebrafish, it has been found that the main ligand for ErbB2/ErbB4 tyrosine receptor in CMs is Nrg2a (Rasouli and Stainier, 2017). Moreover, similar to mammals *nrg2a* or *erbB* mutant animals display a strong reduction in CM delamination and trabecular formation (Liu et al., 2010), further confirming that the molecular axes governing cardiac trabeculation are highly conserved across vertebrates.

Angiopoetin1/Tie2 signaling

Angiopoetin1 (ANG1) is the major ligand of the endothelial-specific receptor tyrosine kinase TIE2. *Ang1* is expressed in ventricular trabeculae, while *Tie2* is highly expressed by endocardial cell adjacent to these trabecular CMs (Suri et al., 1996). Studies in *Ang1*$^{-/-}$ and *Tie2*$^{-/-}$ mice revealed that mutant hearts are devoid of trabeculae. These observations led to hypothesize that myocardial *Ang1* regulates the production of endocardial derived factors required for normal trabecular formation (Suri et al., 1996). Moreover, these data support the crucial association between these two layers, myocardium and endocardium, in the heart. These defects in trabeculation are very similar to phenotypes observed in mice lacking *Nrg1* or its receptors. In addition, studies using CM-specific *Ang1* knockout mice (*Ang1* CKO), also found mild defects in the formation of the trabecular layer and decreased CM proliferation (Yoh Arita, 2014). In addition, it was found that mRNA levels of *Nrg1* were lower in *Ang1* CKO compared to controls, suggesting that Nrg/ErbB2 signaling might act via ANG1 regulating processes involved in cardiac maturation like cardiac trabeculation (Arita et al., 2014; Nakaoka et al., 2007).

Semaphorin/Plexin signaling

Semaphorin/Plexin signaling is another pathway involved in trabeculae morphogenesis. Deletion of *Semaphorin6D* (*Sema6D)* and/or *Plexin-a1* (*Plxna1)* in chick embryos leads to a reduction in compact wall thickness and trabecular density (Toyofuku et al., 2004a; Toyofuku et al., 2004b). These studies showed that trabeculating CMs express *Sema6D* but not *Plxn1a.* Those trabecular CMs expressing *Sema6D* interact with compact-layer CMs expressing both

Sema6D and *Plxn1a,* preventing them to delaminate. These data suggest a role for *Sema6D* in the myocardium for the correct migration of CMs from the compact into the trabecular layer (Jongbloets and Pasterkamp, 2014; Toyofuku et al., 2004a; Toyofuku et al., 2004b).

EphrinB2/B4 signaling

Ephrins and Ephrin receptors are important for cardiovascular development (Adams et al., 2001). In the mouse heart, both the ligand EphrinB2 and one of its receptors, EphrinB4, are expressed in the ventricle, precisely in the endocardial cells lining the trabecular projections (Gerety et al., 1999; Wang et al., 1998). Global knockout mice for both *EphrinB2* (Wang et al., 1998) and *EphrinB4* (Gerety et al., 1999) result in failure of myocardial trabeculation. Interestingly, also the double knockout *EphrinB2* and *EphrinB3* (another receptor of the family) display a defects in development and maturation of the trabecular network (Adams et al., 1999). These data indicate that Ephrins via their receptors are required for the formation a mature trabecular network.

Bone Morphogenetic Proteins (BMPs)

BMP signals have been associated to different steps of cardiac development. BMP10 is enriched in the trabecular myocardium and it has been shown to be important for CM proliferation (Chen et al., 2004; Pashmforoush et al., 2004). BMP10-deficient mice display a significant reduction in CM proliferation at E9.0-E9.5. These mutants are embryonically lethal due to defects in cardiac development and function, including hypoplastic ventricular walls, the absence of trabecular structures, and defects in endocardial cushion formation (Chen et al., 2004).

Notch signaling

Activation of Notch signaling in endocardial cells controls the expression of genes required for the formation of the trabecular network into the cardiac lumen, including *EphrinB2/B4*, *Nrg1* and *Bmp10* (D'Amato et al., 2016; Del Monte et al., 2007; Grego-Bessa et al., 2007; VanDusen et al., 2014). The endocardium expresses *Notch1*, *Delta4* and *Notch4*, while the myocardium expresses *Jagged2* and *Notch2*. Mutations in components of this pathway such as *Notch1, Notch2, Hey1, Hey2 and Jagged1* lead to defective trabeculation in mice and zebrafish (Fischer et al., 2004; Krebs et al., 2000; Lai et al., 2018). Moreover, it was recently shown in zebrafish that cardiac contraction regulates trabeculation, at least in part, by activating *notch1b*

transcription in the endocardium. This activation triggers the expression of the downstream targets *ephrinB2* and *nrg1,* what in turn initiates trabeculation (Samsa et al., 2015).

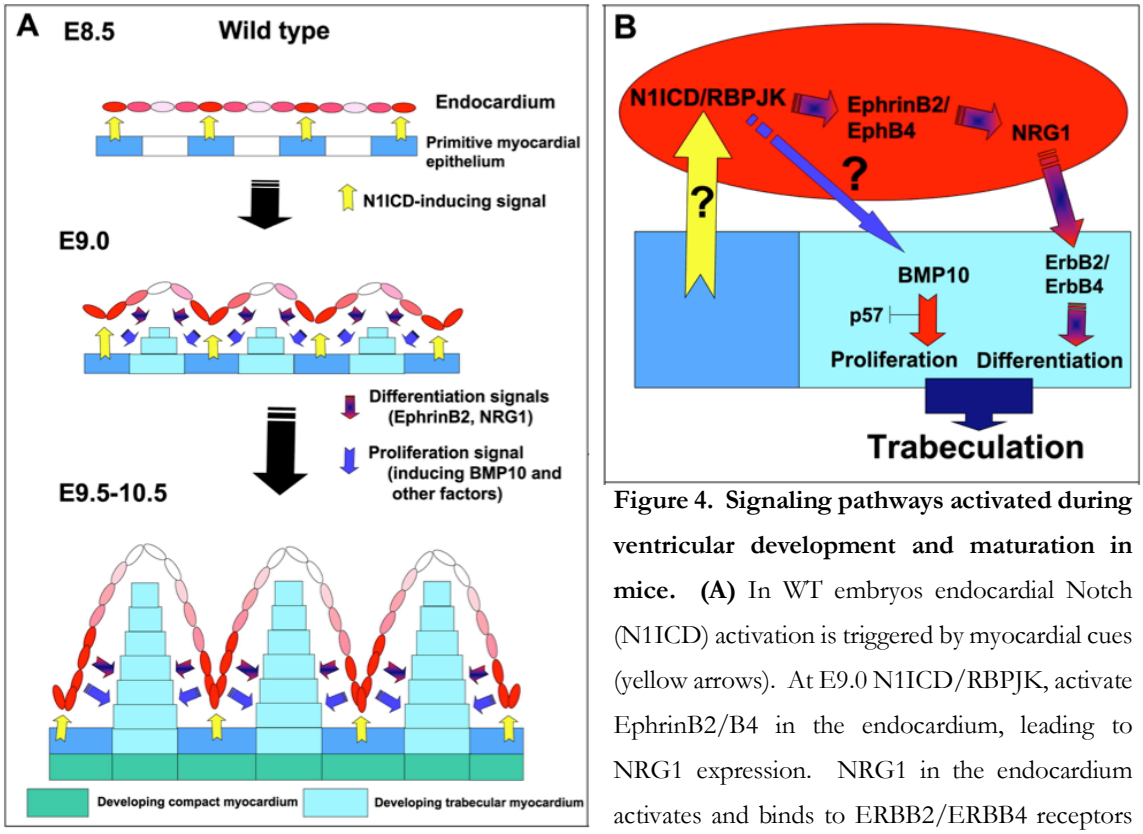

Figure 4. Signaling pathways activated during ventricular development and maturation in mice. (A) In WT embryos endocardial Notch (N1ICD) activation is triggered by myocardial cues (yellow arrows). At E9.0 N1ICD/RBPJK, activate EphrinB2/B4 in the endocardium, leading to NRG1 expression. NRG1 in the endocardium activates and binds to ERBB2/ERBB4 receptors in the myocardium triggering one of the most important pathways for myocardial differentiation. Next, myocardial proliferative signals, such as BMP10 signaling, are triggered in order to promote extension and growth of trabeculae (dark blue arrow). As the trabecular protrusions develop, the endocardium separates from the myocardium, N1ICD-inducing signals and N1ICD are downregulated (white/pink) at the tip of the trabeculae. At E9.5-10.5, N1ICD is highly expressed at the base of the trabeculae (red). At this time, the ventricular myocardium has differentiated into a compact wall (green) and a developing trabecular region (light blue). **(B)** Overview molecular pathways involved in ventricular chamber maturation. (Adapted from Grego-Bessa et al., 2007).

1.3.2 Blood flow and contractility

Unidirectional blood flow through the specialized cardiac chambers, and proper cardiac contractility are required to ensure optimal heart beating and delivery of oxygen and nutrients to the whole organism. Studies in different animal models including zebrafish have shown how mechanical forces like blood flow and contractility are key determinants of CM morphology and different processes during heart development, including trabeculation (Cherian et al., 2016; Chi et al., 2008; Lee et al., 2016; Peshkovsky et al., 2011; Samsa et al.,

2015; Staudt et al., 2014). Circulating blood exerts a pressure parallel to the endocardium called shear stress. Changes in shear stress can affect the signaling triggered in the endocardium to the myocardium, impacting chamber maturation.

In the chick, the development of the cardiac conduction system and trabeculation are both altered in the absence of mechanical loading (Sankova et al., 2010). Cilia are important fluid mechano-sensing organelles localize in different cell types including endothelial cells (Ando and Yamamoto, 2009). Mutations in *Ift88* in mice, which is involved in cilia assembly, cause decreased myocardial trabeculation (Clement et al., 2009). Similarly, mice lacking the Na^+/Ca^{2+} exchanger *Ncx*, which participates during cardiac contraction, show thinner ventricular wall and less developed trabeculae (Reuter et al., 2002).

Manipulation of mechanical forces has been also found to affect the initiation of cardiac trabeculation in zebrafish. In *cardiac troponin T type 2* (*tnnt2a)* mutants, where sarcomeres are defective and the heart does not contract, trabeculation is severely affected (Chi et al., 2008; Sehnert et al., 2002). *Weak atrium (wea)* encodes for *atrial myosin heavy chain (myh6)*, which is an atrial specific myosin gene that is required for atrial but not ventricular contractility. *wea/myh6* mutants display reduced atrial contractility and significant reduction of blood flow (Auman et al., 2007; Berdougo et al., 2003). As a consequence of the reduced blood flow in these mutants, trabecular morphogenesis is severely impaired (Peshkovsky et al., 2011) *gata1* morpholino (MO) injections cause reduction of blood viscosity and hematopoiesis, resulting in reduced hemodynamic shear stress (Lee et al., 2016). In consequence *gata1* morphants showed delayed in the initiation of trabeculation (Lee et al., 2016). However, the molecular bases for the regulation of CM behavior during trabeculation by blood flow and contractility remain still to be elucidated.

1.4 Tissue morphogenesis in epithelial cells

Organogenesis is a complex process that requires the coordination of both cell fate specification and tissue morphogenesis (Cavodeassi, 2018). Tissue morphogenesis includes changes in cell shape, proliferation, motility, and polarity. Coordinated cellular movements, as well as regulation of the actomyosin cytoskeleton and positioning of tight (TJs) and adherens junctions (AJs), translate into changes in the whole tissue. Therefore, it is of great interest to understand how the movement of an individual cell can influence the behavior of neighboring cells when these rearrangements take place during development.

1.4.1 Cellular rearrangements: cytoskeleton and junctional proteins

Cytoskeleton and junctions provide integrity and mechanical rigidity to epithelia (Ferrer-vaquer et al., 2010). In an epithelium, the apical side of epithelial cells is facing the environment, while the basal side is attached to the basal lamina by distinct junctional complexes (i.e, extracellular matrix also known as cardiac jelly in the heart). Moreover, lateral membranes of epithelial cells are anchored side-by-side by different junctional proteins. Actin filaments, one of the main components of the cytoskeleton, anchor to these junctions by establishing associations with AJs and TJs. Specifically, cytoskeletal proteins bind to proteins forming the cytoplasmic domain underlying the membrane of AJs and TJs also known as plaque. In this way, the cytoskeleton and junctional complexes establish an intercellular link by which forces can be transmitted between cells, coupling cell adhesion to cell shape modulation. It is well established that the interaction between cytoskeleton and AJs and TJs is a key determinant of cellular behavior during development, having a direct impact in the regulation of tissue morphogenesis. Yet, how the actomyosin cytoskeleton and the different junctional proteins are molecularly regulated during development warrants further attention (Hartsock and Nelson, 2008).

Actomyosin cytoskeleton. Filaments of actin and myosin are the main constituents of the eukaryotic cytoskeleton. Actin bundles are distributed mainly in the apical plasma membrane of epithelial cells. Myosin motors F-actin filaments generate forces that trigger contractile pulses as changes in cell shape occur. During contraction, F-actin filament organization is mainly controlled by the Rho family of small GTP-binding proteins, including RhoA, Rac1 and Cdc42 (Sit and Manser, 2011). Remodeling of cytoskeleton during mechanical processes is required for changes in cell shape and implies assembly and disassembly of F-actin and interaction with cell-cell adhesion proteins. This interaction is especially important with the proteins forming the cytoplasmatic plaque that contains PDZ domains, which modulate cell plasticity by anchoring actin and myosin to the TJs.

Tight junctions. The proposed function for TJ is to mediate the transport of ions and solutes between cells and to avoid mixing of membrane proteins between the apical and basolateral membranes. Moreover, TJs have been implicated in the establishment and

maintenance of apicobasal polarity, where they act as mediators in signaling pathways involved in proliferation and differentiation. In all these cases, they form the "TJs plaque". There are several transmembrane TJ proteins including Occludins, Claudins, and Zonula Ocludens (ZO). ZO-1 was the first TJ protein identified (Stevenson et al., 1986). However, the exact role of ZO-1 in the assembly and maturation of TJs was not described until 20 years later by Umeda *et al.* In that report, Umeda and co-workers showed that in epithelial cells lacking all members of ZO family, TJs were absent (Umeda et al., 2006). It has been suggested that AJs can affect TJ function and assembly, however, how do they interact is still unclear. As ZO-1 has a α-catenin region with strong binding affinity to Cadherin (Itoh et al., 1997), one possibility is that TJs function as a linker between cadherins and the cytoskeleton (Fanning et al., 2002). Alternatively, it could be that TJs can alter the biogenesis of Cadherins through polarity proteins, such us Crumbs (Crb) and Stardust (Std) in *Drosophila melanogaster* (*Drosophila*) (Grawe et al., 1996) or the Std ortholog (MPP5 in mammals) in zebrafish cardiac development (Rohr et al., 2006).

Adherens junctions. Epithelial apical junctions are formed by the classical Cadherins, including epithelial (E), neural (N) and vascular endothelium (VE)-Cadherins. Cadherins belong to the diverse cell adhesion molecule family and are transmembrane proteins dependent on calcium (Takeichi, 1990). In polarized epitheliums, they are found between cell-cell contacts and usually constituting a belt-like structure in the subapical region called zonula adherens (ZA) (Yonemura, 2011) or forming dynamic clusters in the lateral junctions below the ZA (Wu et al., 2014). AJs formed by both cadherins and nectins interact with specific linking proteins called catenins, mediating the binding of AJs to the actin filaments of the cytoskeleton (Drees et al., 2005) and regulating gene expression (Balda and Matter, 2009). The first studies supporting binding of cadherins to the cytoskeleton demonstrated that when using cytochalasin D, an actin-depolymerizing drug used to disrupt actin integrity, Cadherin adhesion was compromised (Jaffe et al., 1990). More recent reports have shown that Cadherins interact functionally and physically with actin filaments (Ratheesh and Yap, 2012). Furthermore, during changes in shape, cell junctions require remodeling and turnover, while Cadherins have been found to experience endocytosis and recycling (Le et al., 1999; Yap et al., 2007).

1.4.2 Epithelial to Mesenchymal Transition (EMT)

Tissue patterning and morphogenesis require control over cell shape changes and rearrangements. One key process that takes place during morphogenesis is EMT, and the reverse process Mesenchymal to Epithelial Transition (MET) (Shook and Keller, 2003). The typical epithelium is composed of layers of epithelial cells polarized along an apical-basal axis, perpendicular to the epithelial plane (**Figure 5**). Epithelial cells establish cell-cell cohesion with the neighboring cells by forming a belt of tight and adherens junctions (Ikenouchi et al., 2003). Usually, epithelial cells repose on a basal lamina, being the cell-basal lamina interaction necessary to stabilize and synchronize the epithelial architecture. Polarity and junctional rearrangements are important to maintain cell shape, tissue structure, and to define apical and basolateral membrane domains (von Gise and Pu, 2012). In order to undergo EMT, cells have to disassemble their cell-cell junctions and lose epithelial polarity to undergo cytoskeletal rearrangements. In consequence, epithelial cells gain plasticity and migratory properties, changing in shape and becoming mesenchymal cells (Micalizzi et al., 2010). Contrary to epithelial cells, mesenchymal cells do not form a belt of tight and adherens junctions. Consequently, they have a more amoeboid morphology, thus facilitating their movements through the extracellular matrix as individual cells.

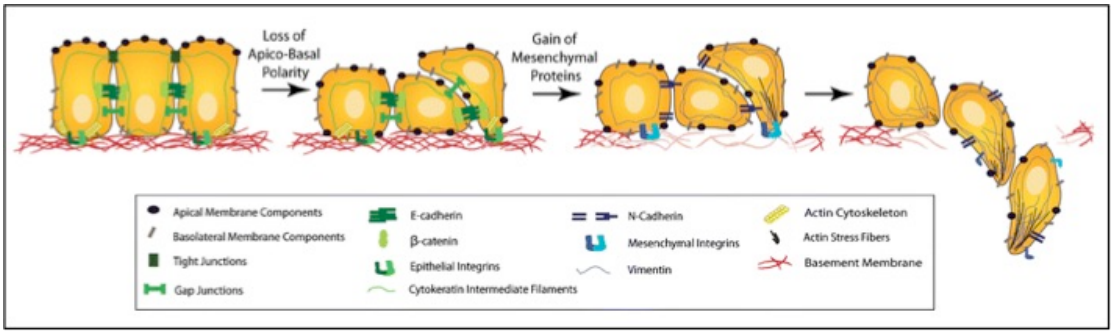

Figure 5. EMT. The scheme shows epithelial cells displaying polarity and establishing cell-cell junctions with surrounding cells. After disruption of their polarity, epithelial cells lose contacts and gain mesenchymal properties. Modified from Micalizzi et al., 2010

In the heart, endocardial EMT has been observed during endothelial valve formation and is driven by the coordination of TGFβ, BMPs, NOTCH, ERBB2 and VEGF signals. For example, in *ErbB2*$^{-/-}$ or *ErbB3*$^{-/-}$ cushion mesenchymal cells do not form (von Gise and Pu, 2012). Similarly, EMT takes place during development when pro-epicardial cells migrate onto the myocardium. Although endocardial and epicardial EMTs have been extensively studied

during heart development and regeneration, whether myocardial EMT takes place remains to be investigated.

EMT has been reported in pathological conditions such as fibrosis or cancer metastasis (López-Novoa and Nieto, 2009). In all cases, cells undergoing EMT lose apicobasal polarity and dissolve cell-cell junctions, causing the de-localization of apical and basolateral components. In addition, the composition of junctional components changes with proteins like E-Cadherin and Integrins being replaced by N-Cadherin and other types of Integrins. Furthermore, the cytoskeleton rearranges, including the replacement of actin filaments by stress fibers like Vimentin. All these changes enhance temporally cellular plasticity, thus facilitating the invasion of the extracellular matrix and subsequent migration towards their destination. In some pathological setups, like cancer, some of these phenomena take place, but in a less coordinated fashion (Gavert and Ben-Ze'ev, 2008). These similarities have led to the speculation that during cancer progression, some developmental programs are reactivated.

Therefore, currently the different types of EMTs are classified as follows:

- *"Type I"*: associated with embryo formation, implantation and organ development. Does not trigger fibrosis or induces an invasive phenotype.
- *"Type II"*: associated with organ fibrosis, wound healing and tissue regeneration. Is part of a repair-program and leads to the production of fibroblasts following a trauma and inflammatory response.
- *"Type III"*: associated with cancer progression and metastasis. Cells have excessive proliferation and angiogenesis, and acquire invasive properties.

1.4.3 Cardiac EMT

Most tissues and organs derive from a series of multiple EMT processes (Pérez-Pomares and Muñoz-Chápuli, 2002). The heart is one of these organs and all the cells that will form the heart result from one or more EMTs. The most characteristic EMT processes include endocardial and epicardial cells, and are involved in the formation of the cardiac valve and epicardial-derived tissues (Person et al., 2005; von Gise and Pu, 2012). Besides, EMT is also observed during cardiac regeneration (Zhou and Pu, 2011). Whereas numerous studies have focused on endocardial and epicardial EMT (Pérez-Pomares and de la Pompa, 2011; Sridurongrit et al., 2008) just a handful of studies have explored myocardial EMT during

cardiac trabeculation. It has been reported that, similarly to epithelial cells, CMs establish cell-cell contacts with the neighboring CMs (Cherian et al., 2016). In addition, CMs have the ability to migrate by delamination, requiring dynamic changes in cell shape during this process (Liu et al., 2010; Staudt et al., 2014). Along the same line, it has been shown that CMs experience changes in N-Cadherin localization (Cherian et al., 2016) and more recent data demonstrated changes in CM polarity during trabeculation (Jiménez-Amilburu et al., 2016).

1.5 Epithelial apicobasal polarity

Polarity is an essential feature of epithelial cells. Cell polarization is a conserved process during evolution that implies an asymmetry in shape, structure, and functions of cells. It is modified dynamically during physiological processes such as cell division, migration, and morphogenesis. Apicobasal polarity is a type of cell polarity specific to epithelial cells, where the epithelial cells adhere to one another through different kinds of junctions. The apical membrane is facing the outside surface of the cell or the lumen in internal cavities and the basolateral oriented away from the lumen. It has been shown using Madin-Darby canine kidney (MDCK) cultured cell monolayers, that cell-cell cohesion and adhesion to the extracellular matrix are important for organizing the apicobasal polarity axis in the cell (Yeaman et al., 1999). TJs and AJs in the cell participate in defining the apicobasal axis in epithelial polarity. TJs function as a barrier, preventing diffusion of membrane proteins between the apical and basal regions of a polarized epithelium (Zihni et al., 2016). There are many proteins involved in the regulation of cell polarity. The main complexes defining cellular apicobasal polarity are PAR and Crumbs in the apical membrane, and Scribble which sits on the basolateral domain of the cell. These complexes are highly conserved from worms to mammals **(Figure 6).** Recently, it has been shown that the maintenance of apicobasal polarity in cells is controlled by the crosstalk between polarity complexes and the cytoskeleton, and in turn is guided by an epithelial polarity programme (EPP) (Rodriguez-Boulan and Macara, 2014). Moreover, polarity complexes also interact with guanine nucleotide exchange factors (GEFs) and GTPase-activating proteins (GAPs) to control localization and activation of the Rho GTPase family members, mentioned above (Bos et al., 2007). The correct activation of Rho GTPase proteins has been shown to be indispensible for the specification of the apical and basal domains in polarized epithelial cells (Ngok et al., 2014).

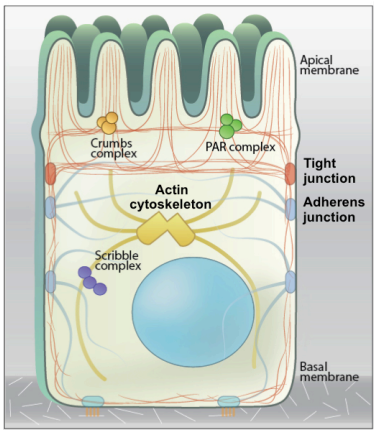

Figure 6. Distribution of different polarity complexes in epithelial cells. Apicobasal identity in epithelial cells is defined by Crumbs and PAR complexes at the apical side, and Scribble at the basolateral domain. The proteins forming these polarity complexes interact, producing molecular asymmetry along the apical–basal axis. At the same time, in order to support cell polarization, they regulate the maturation and maintenance of the different tight and adherens junctions between cells and cytoskeleton. Adapted from the website https://www.mechanobio.info/development/what-is-cell-polarity/.

1.5.1 PAR complex and regulation

The PAR complex was first described in *Caenorhabditis elegans* (*C.elegans*) in 1988 (Kemphues et al., 1988) and later in *Drosophila* and vertebrates. It is composed by two scaffold proteins, PAR3 and PAR6, that contain a PDZ-binding domain, and an atypical protein kinase C (aPKC). In epithelial cells, the PAR6-aPKC tandem establishes apicobasal polarity by interacting with their downstream effectors PAR3 and LGL (Yamanaka et al., 2003). Moreover, it has been shown that PAR3 regulates cytoskeletal dynamics (Mizuno et al., 2003), while activation of aPKC ensures TJ formation (Gopalakrishnan et al., 2007). In addition, small Rho GTP-binding proteins such as Cdc42 and Rac1 have been found to interact with PAR6 and PAR3, controlling the interactions between PAR proteins and thus regulating TJ assembly during the establishment of cell polarity (Johansson et al., 2000; Noda et al., 2001). This regulation defines the subcellular distribution of the PAR proteins and therefore suggests that PAR3, PAR6, and aPKC do not form always a constitutive complex.

1.5.2 Scribble complex and regulation

scribble (scrib) was first identified in *Drosophila* in a screening to find mutations that affect aspects of tissue morphogenesis (Bilder and Perrimon, 2000). It was found specifically in the basolateral membranes of epithelial cells. Later Bilder and Perrimon, found that Scrib might function together with two other two proteins, Lethal giant larvae (Lgl) and Lethal discs large (Dlg). Mutations in these two genes cause defects in cell shape, loss of epithelial polarity and organization, and overproliferation, phenocoping *scrib* mutants (Bilder et al., 2000). All three proteins localize to the basolateral membrane of cells and function establishing cell polarity by

excluding the apical polarity proteins, like Crumbs, from the basolateral domain (Bilder and Perrimon, 2000). Besides regulating cell polarity, this complex also controls cell proliferation and interacts with components of the TJs and AJs in order to support epithelial morphogenesis. Mammalian SCRIB has been found to interact with β-PIX, a guanine nucleotide exchange factor for RAC1 and CDC42 (Audebert et al., 2004). Some studies show that SCRIB localizes with β-PIX at the front edge of polarized astrocytes, and depletion of SCRIB using siRNA or expressing dominant-negative constructs inhibits astrocyte polarization (Osmani et al., 2006).

1.5.3 Crumbs complex and regulation

crb was first identified by Jürgens et al. in *Drosophila* in 1984, but it was Teppas et al. who established for the first time the link between this protein and cell polarity in 1990 (Tepaß and Knust, 1990; Tepass et al., 1990) Crb is also critical to regulate cytoskeleton and tissue integrity during physiological and pathological processes. In fact, it has been reported that the intracellular domain of Crb, specially the FERM binding domain, interacts with different cytoskeletal proteins through Moesin, in order to control cell shape (Wei et al., 2015). Different members of the Rho GTPase family mediate this interaction, controlling in this way epithelial cell polarity (Genova et al., 2000). Crb seems to activate Synectin-binding RhoA exchange factor (Syx) a Rho-specific GFE during angiogenesis in endothelial cells (Garnaas et al., 2008). Even though the role of Syx during epithelial cell polarity remains unclear, some reports suggest a role in regulating cell migration in breast cancer cells (Dachsel et al., 2013). On the other hand, Crb downregulates and excludes Rac1 and Cdc42 from the apical region to define and specify the apicobasal domains in epithelial cells (Wells et al., 2006; Yi et al., 2011).

Like other proteins, Crb has also different orthologs in different species. There is only one *crb* gene in *C.elegans* and *Drosophila,* three in mammals, *Crb1*, *Crb2* and *Crb3*, and five in zebrafish (due to the evolutionary genome duplication), *crb1, crb2a, crb2b, crb3a,* and *crb3b* (Omori and Malicki, 2006).

1.6. Components of Crumbs complex

Core components

In *Drosophila* there are four proteins that form the core components of the Crb complex: Crb, Sdt, Patj (Pals1-associated tight junction protein), and Lin-7 **(Figure 7)**.

Crb is a type I transmembrane protein that is composed of a large extracellular domain containing 29 EGF-like domains and 4 laminin-A globular domains, and one short but essential intracellular domain. This intracellular domain is composed of 37 amino acids, contains two highly conserved regions, the C-terminal PSD-95/Discs-large/ZO-1 (PDZ)-binding motif ERLI, and a 4.1/Ezrin/Radixin/Moesin (FERM)-binding domain, that harbor three of the four core components, Sdt, Patj and Lin-7. It has been reported that Crb and Sdt act together and are essential proteins to maintain the epithelial polarity in the embryo (Bachmann et al., 2001; Tepass and Knust, 1993). Several studies have shown that by expressing only the cytoplasmic domain of Crumbs is enough to rescue the phenotype of *crb* mutants in some embryonic epithelia, suggesting the importance of this domain and its PDZ and FERM-binding domains (Klebes and Knust, 2000; Wodarz et al., 1995). In most of the fly epithelia, Crb is localized in the apical membrane underneath the AJs, called subapical region (SAR) (Bachmann et al., 2001; Tepass, 1996).

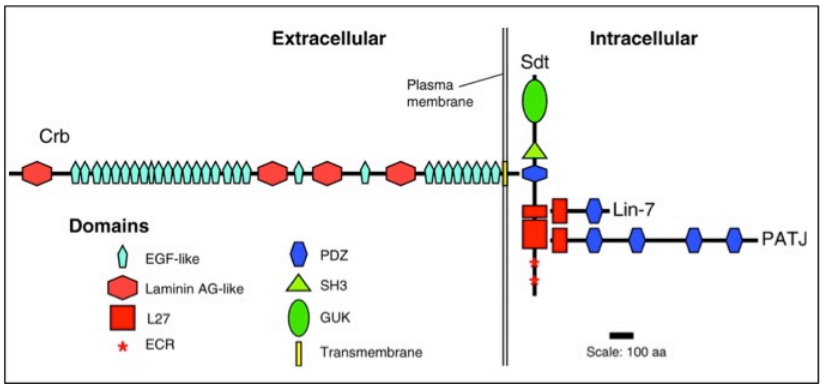

Figure 7. Core components of the Crumbs complex. Diagram showing the intracellular and extracellular domains of Crumbs, the four core components, (Crb, Sdt, Patj, and Lin-7), and their different domains. Adapted from Bulgakova and Knust, 2009.

Transient components

Three of the four proteins that constitute the Crb complex are scaffolding proteins with the capacity to form protein-protein interactions. Members of the PAR complex, especially PAR-6 and aPCK, are well known to interact with the Crb complex (Kempkens et al., 2006). Moesin is part of the ERM proteins and together with Ezrin and Radixin functions as linker between the plasma membrane and the cytoskeleton (Fiévet et al., 2007). Moesin is activated by phosphorylation and then binds to the FERM-binding domain of Crb and other membrane-associated protein (β_H-Spectrin) and F-actin, therefore acting as an important cross-linker of

apical membrane and cytoskeleton (Polesello et al., 2002). In *Drosophila, yurt* (the homolog of Moesin), which is important during morphogenesis of epithelial cells, associates transiently with the Crb complex. Loss of *yurt* causes expansion of the apical domain similar to the phenotype observed after overexpression of Crb, so Yurt is suggested as a negative regulator of the Crb complex (Laprise et al., 2006).

1.6.1 Importance of Crumbs

Mutations in human *CRB1* are mainly associated with retinopathies (den Hollander Anneke et al., 2004). Interestingly loss of *crb*, *Crb1,* and *crb2a* mutations in flies, mammals, and zebrafish respectively also cause retinal degeneration (Omori and Malicki, 2006). In general, loss of *crb* function causes the degradation of the other core components of the Crb complex and results in loss of cell polarity in many ectodermically derived epithelia (Wodarz et al., 1993). Overexpression of Crb causes expansion of the apical membrane domain leading to a complete "apicalization" of the plasma membrane, characterized by the ectopic expression of different apical markers (Chalmers et al., 2005; Klebes and Knust, 2000; Laprise et al., 2010). In addition, mutations in *crb* cause disruption of apicobasal polarity and consequent collapse of tissue integrity due to a failure in positioning and maintaining the ZA, leading to apoptosis (Grawe et al., 1996; Tepass, 1996; Tepass et al., 1990). In both *Drosophila* and mice it has been described a role for Crb in promoting cell ingression. Recent reports have shown that during salivary gland tubulogenesis in *Drosophila* and during gastrulation in mouse different levels of Crb (CRB2 in mouse) are observed amongst cells. Homophilic interactions between Crb on adjacent cell edges promote the recruitment of aPKC. aPKC, via negative regulation of Rok, prevents the formation of the Myosin II cable where Crb is localized. As a result, cells with low levels of Crb promote Myosin II assembly and cell ingression (Ramkumar et al., 2016; Röper, 2012).

An important role for Crb in regulating the positioning and stability of AJs has been found in the ectoderma and amnioserosa cell in *Drosophila*, where *crb* mutants showed defects in AJs shown by the lack of beta-catenin and DE-cadherin (Grawe et al., 1996). Crb is also required for AJ maintenance during the formation of the salivary gland and rhabdomere biogenesis during *Drosophila* pupal eye development (Izaddoost et al., 2002).

The specific role for the intracellular domain of Crb has been well characterized. It is responsible to maintain apicobasal polarity in cells and regulates tissue growth via Hippo signaling (Bulgakova and Knust, 2009; Chen et al., 2010; Richardson and Pichaud, 2010;

Tepass, 2012). For many years it was thought that the extracellular domain of Crb was dispensable, since experiments using only the intracellular domain were sufficient to rescue phenotypes derived from loss of Crb (Johnson et al., 2002; Klebes and Knust, 2000; Wodarz et al., 1995). The role for its extracellular domain is not well understood. However, recent reports indicated that this domain is involved in the regulation of homophilic Crb-Crb interactions at the cellular junctions (Das and Knust, 2018; Letizia et al., 2013).

In the heart, cardioblast (CB) polarity has been studied in *Drosophila* (Frémion et al., 1999; Medioni et al., 2008) and zebrafish (Rohr et al., 2006) during cardiac morphogenesis. For long time, CMs have been assumed to display "apicobasal" polarity, however due to the lack of precise tools it has never been conclusively demonstrated. CBs have been assumed to display "apicobasal" polarity based on the absence of α-Spectrin expression in the basolateral membrane located facing the dorsal midline (Frémion et al., 1999). Nevertheless, this membrane domain does not express the known classical apical markers of epithelial cells, including Crb, β-heavy-Spectrin, Bazooka, or aPKC (Qian et al., 2005; Tepass et al., 1990).

1.6.2 Crumbs in zebrafish

Although there are five different Crumbs proteins in zebrafish, not all of them have been studied and their role during organogenesis and development is unknown. All five genes have different patterns of expression. *crb1*, *crb2a,* and *crb2b* are expressed mainly in the central nervous system (CNS); while the first two exhibit complex expression patterns in brain and retina, *crb2b* is almost exclusively expressed in photoreceptors. *crb3a* is highly expressed in the otic vesicle and, together with *crb3a,* have been detected in the digestive tract (Omori and Malicki, 2006). The Crb complex has been widely studied in the context of polarization and morphogenesis of the neuroepithelia in zebrafish. In an extensive mutagenesis screening for embryonic defects in zebrafish, it was identified that the *oko meduzy (ome)* locus encodes for *crb2a* (Omori and Malicki, 2006). Mutations in *crb2a* locus cause loss of apicobasal polarity and, as a consequence, loss of neuronal patterning that affects severely the formation of the retina (Malicki and Driever, 1999; Malicki et al., 1996; Omori and Malicki, 2006; Wei and Malicki, 2002). Moreover, the similar phenotypes of *moe* and *crb2a* mutants suggest that Moesin might regulate negatively Crb by direct interaction with Crb2a and Nok (Pals1) (Hsu et al., 2006). In *crb2a* zebrafish mutants, the patterning of the three retinal layers is drastically disorganized due to loss of AJs (Malicki and Driever, 1999). This phenotype has also been shown in human cells, where CRB3 is able to promote TJ formation (Tilston-Lünel et al.,

2016). However, the role of Crumbs during heart development, and more specifically during the process of cardiac trabeculation remains to be investigated.

2. Aim of the project

The main goal of this project is to study apicobasal polarity in CMs and its regulation during cardiac trabeculation in zebrafish.

Cardiac trabeculation is a crucial process for the formation of a competent ventricular wall during heart development. In the last years, important contributions to the field have uncovered many aspects and questions related to trabeculation. However, essential questions remain to be addressed. Specifically, how CM polarity is relevant to cardiac trabeculation, and which polarity complexes govern this process is unknown. Zebrafish is a very powerful model. Taking advantage of the embryo transparency I will perform *in vivo* imaging that will allow me to visualize cardiac trabeculation events at single cell resolution. Moreover, thanks to the ability of the zebrafish embryos to survive early development even suffering heart defects, will allow me to study early cardiac dysfunctions in different mutants in the context of CM polarity and trabeculation.

To achieve the main goal of the project, specific aims were designed as follows:

AIM1: To establish apicobasal polarity in CMs during cardiac trabeculation

I will generate different transgenic lines to visualize apicobasal polarity in CMs. Time-lapse imaging of the beating heart will help to determine *in vivo* the different polarization events that take place in CMs during cardiac trabeculation.

AIM2: To understand the factors regulating changes in CM apicobasal polarity during cardiac trabeculation

Since Nrg/ErbB2 signaling and blood flow or contractility are required for the correct formation of trabeculae, I will study whether those affect CM polarization by combining different chemical and loss-of-function approaches. Moreover, I will also test whether myocardial Notch activation plays a role in regulating CM polarization and delamination.

AIM3: To study the role of the apical polarity complex Crumbs during cardiac trabeculation

I will examine the role of the polarity complex Crumbs during cardiac trabeculation in zebrafish. Combining transcriptomic analyses, loss-of-function tools, high-resolution imaging, immunohistochemistry, and cell-specific ablation experiments I will investigate how Crumbs is required for the formation of trabeculae.

3. Material and Methods

3.1 Material

3.1.1 Antibiotics

Table 1. List of antibiotics used in this thesis with their respective working concentration.

Antibiotic	Working concentration (ug/ml)
Ampicillin	100
Kanamycin	50

3.1.2 Antibodies

Table 2. List of antibodies used in this thesis with their respective isotype, supplier, catalog number and dilution.

Antibody	Isotype	Supplier	Catalog #	Dilution
Primary antibodies				
Anti-Crb2a	Mouse monoclonal	ZIRC	zs-4	1:100
Anti-ZO1	Mouse monoclonal	Invitrogen	33-9100	1:2000
Anti-EGFP	Chicken polyclonal	Aves Lab	gfp-1020	1:200
Anti-α-actinin	Mouse monoclonal	Sigma	A7811	1:1000
Anti-N-cadherin	Mouse monoclonal	Abcam	ab12221	1:250
Anti-tRFP	Rabbit polyclonal	Evrogen	AB233	1:500
Anti-Prkcζ (C20)	Goat polyclonal	Santa Cruz Biotechnology	sc-216	1:200
anti-myosin heavy chain (MF20)	Mouse monoclonal	eBioscience	14-6503-80	1:20
Secondary antibodies				
Alexa Fluor 488 anti-Chicken	goat IgG	Life Technologies	A11039	1:500
Alexa Fluor 488 anti-Rabbit	goat IgG	Life Technologies	A11034	1:500
Alexa Fluor 488 anti-Mouse	goat IgG	Life Technologies	A11029	1:500
Alexa Fluor 568 anti Mouse	goat IgG	Life Technologies	A11004	1:500
Alexa Fluor 488 anti-Mouse	goat IgG	Life Technologies	A21124	1:500
Alexa Fluor 647 anti-Mouse	goat IgG	Life Technologies	A21236	1:500

3.1.3 Bacterial strains

Table 3. List of bacterial strains used in this thesis with their purpose.

Bacterial strain	Purpose
DH5α	Competent cells
TOP10	Competent cells

3.1.4 Buffers and solutions

Table 4. List of buffers and solutions used in this thesis and their respective composition.

Buffer/Solution	Composition
10X PBS	10 PBS tablet (Sigma) 200 mL distilled water
10X TBE	121 g Tris 62 g Boric Acid 7.4 g EDTA 1 L final volume (distilled water)
1X PBDT	1% DMSO Dissolved in 1X PBST
1X PBST	0.1% Tween-20 Dissolved in 1X PBS
4% PFA	40 g PFA Dissolved in 1 L 1X PBS Adjust to pH 7.0 by HCl/NaOH
Bleaching solution	1.5% H202 + 1% KOH
Blocking buffer (immunofluorescence mouse)	3% BSA, 20 mM MgCl2, 0.3%Tween-20 and 5% FBS in PBS
Blocking buffer (immunostaining zebrafish) (5 mL)	4.05 mL PBS/0.1% Tween + 500 uL sheep serum + 200 µL 20% Triton-X + 250 Ul 20% BSA
Citrate buffer Antigen Retrieval	10 mM Citric Acid (anhydrous) + 0.05% Tween20 1L (distilled water) Adjust to ph 6.0 by HCl/NaOH
Egg water	3 g Instant Ocean 0.75 g Calcium sulfate 10 L final volume (distilled water)
Embryo disruption medium (EDM)	L15 medium + 10% Fetal bovine serum
Fish Fix (100 mL):	100 mL Fish Fix Buffer – prewarm to 60 degrees C, + 4g PFA + 1 mL 1M NaOH Adjust pH to 7.35 with HCl
Fish Fix Buffer (100 mL)	77 mL 0.1 M Na2HPO4 + 22.6 mL 0.1 M NaH2PO4 + 12 µl 1M CaCl2 + 4 g sucrose + 4 g PFA in 1X PBS Adjust to ph 7.35 by HCl/NaOH
Incubation buffer (immunostaining zebrafish) (5 mL)	4.5 mL PBS/0.1% Tween + 50 uL sheep serum + 200 µL 20% Triton-X + 250 Ul 20% BSA

3.1.5 Chemicals

Table 5. List of chemicals used in this thesis with their respective supplier and catalog number.

Chemical	Supplier	Catalog #
1-Phenyl-2-thiourea (PTU)	Sigma	P7629
2,3-butanedione monoxime (BDM)	Sigma	B0753
Agarose	Peqlab	35-1020
Agarose, low gelling temperature	Sigma	A9414
Alexa Fluor 568 Phalloidin	Thermo Scientific	A12380

Bovine serum albumin (BSA)	Sigma	A2153
Calcium Chloride (CaCl2)	Merck Millipore	10035-04-8
Chloroform	Merck	102445
Citric acid	Sigma	27487
CutSmart buffer	NEB	B7204S
DAPI	Sigma	D9542
DAPT	Merck Millipore	565770
Dimethylsulfoxide (DMSO)	Sigma	D4540
DNA ladder (100bp)	Thermo Scientific	SM0241
DNA ladder (1kbp)	Thermo Scientific	SM0311
ErbB2 inhibitor	Calbiochem	PD168393
Ethanol (denatured)	Roth	K928.3
Ethanol (molecular grade)	Roth	5054.4
Fetal bovine serum (FBS)	Sigma	12103C
Gel loading dye	Thermo Scientific	R0611
Glycerol	Millipore	356350
Hydrochloric acid (HCl)	Sigma	H1758
Heparin	Sigma	H5515
Isopropanol	Roth	6752,4
LY411575	MedChem Express	HY-50752
Methanol	Roth	4627.5
Methylene blue	Sigma	M9140
Mineral oil	Sigma	M8410
Sodium Chloride (NaCl)	Sigma	S3014
Sodium hydroxide (NaOH)	Sigma	221465
Nuclease-free water	Ambion	AM9938
OCT mounting medium for cryosection	Tissue-tek	4583
Paraformaldehyde (PFA)	Sigma	P6148
Phenol red	Sigma	P0290
Phosphate-buffered saline (PBS) tablets	Sigma	P4417
Pronase	Roche	10165921001
Proteinase K	Roche	1092766
Sheep serum	Sigma	S3772
Sucrose	Sigma	S0389
SYBR safe	Invitrogen	S33102
Tricaine	Pharmaq	NA

Tris	Roth	5429.2
Tris hydrochloride (TrisHcl)	Sigma	RES3098T-B701X
Triton X-100	Sigma	RES3103T-A101X
Trizol	Ambion	15596018
Tween-20	Sigma	P1379
Vectashield Antifade mounting Medium	Vector laboratories	H-1000
1-Phenyl-2-thiourea (PTU)	Sigma	P7629

3.1.6 Restriction Enzymes

Table 6. List of restriction enzymes used in this thesis and their respective supplier.

Restriction enzyme	Supplier
AgeI	NEB
BamHI-HF	NEB
BglII	NEB
BsmBI	NEB
EcoRI-HF	NEB
NheI	NEB
NotI	NEB
XbaI	NEB
XhoI	NEB

3.1.7 Growth media

Table 7. List of growth media used in this thesis with along with their composition.

Growth medium	Composition
SOC Medium	Tryptone 2% Yeast extract 0.5% NaCl 0.05% KCl 0.0186% Dissolve in distilled water and adjust to pH 7 and then add MgCl2 10 mM D-glucose 20 mM Autoclave
LB Medium	Roth
LB Agar	Roth
L-15 Medium	Invitrogen

3.1.8 Kits

Table 8. List of kits used in this thesis and their respective supplier and catalog number.

Kit	Supplier	Catalog #
Cold Fusion Cloning Kit	System Biosciences	MC101A-1
GeneJET G kit	Thermo Scientific	K0691
GeneJET PCR purification kit	Thermo Scientific	K0701
GeneJET plasmid miniprep kit	Thermo Scientific	K0502
iScript cDNA synthesis kit	Bio-Rad	1708891
miRNeasy Micro Kit	Qiagen	217084
pGEM-T Easy Vector cloning kit	Promega	A1360

3.1.9 PCR Enzyme/Master mix

Table 9. List of PCR Enzyme/Master mix used in this thesis with their respective supplier and catalog number.

PCR Enzyme/Master mix	Supplier	Catalog #
KAPA 2G master mix	KAPA biosystems	KM5101
Phusion taq DNA polymerase	NEB	M0530
DyNAmo ColorFlash SYBR Green qPCR Kit	Thermo Scientific	F-416
Takara Prime STAR™ HS DNA polymerase	Clontech	R010A
KOD plus neo	TOYOBO	KOD-401

3.1.10 Miscellaneous equipment

Table 10. List of miscellaneous equipment used in this thesis and their respective supplier.

Equipment	Supplier
Bacterial incubator	Heraeus
Bacterial incubator shaker	Infors HAT
CFX connect real time PCR detection system	Bio Rad
ChemiDoc MP	Bio Rad
Criterion SDS PAGE Chamber	Bio Rad
Dark reader transilluminator	Clare chemical
Electrophoresis power supply	Bio Rad
Gel Doc EZ System	Bio Rad
Glass bottles (100 ml, 250 ml, 500 ml, 1000 ml, 2000 ml)	Duran
Heating block	VWR
Injection micromanipulator	World precision instruments
Micropipette puller P-1000	Sutter Instrument
Microscale	Novex

Microwave	Bosch
NanoDrop 2000 c	Thermo scientific
PCR mastercycler Pro	Eppendorf
Picospritzer III	Parker
Pipetboy	Integra
Pipettes (2, 10, 20 100, 200, 1000 µl,)	Gilson
Printer	Mittsubishi P95
Trans Blot Turbo	Bio Rad
Weighing balance	Sartorius
Zebrafish aqua culture system	Tecniplast
Zebrafish breeding tanks	Tecniplast
Zebrafish incubator	Binder

3.1.11 Disposable equipment

Table 11. List of disposable equipment used in this thesis and their respective supplier.

Material	Supplier
Bacterial culture tubes (13 mL PP Tube Sterile)	Greiner Bio-one
Cell culture plates (6-and 12 well cell culture plate)	Greiner Bio-one
Centrifuge tubes (1,5 ml, 2 ml safe-lock tubes)	Eppendorf
Falcon tubes	Greiner Bio-one
Falcon tubes (15, 50 ml)	Greiner Bio-one
Glass bottom dish	MatTek
Glass Capillaries (1.00OD X 0.58ID X 100mm)	Hardvard Apparatus
Laboratory Film	Parafilm
Microloader pipette tips (20 µl Physio Care Concept)	Eppendorf
Needles (19-gauge needle, 1 ½ inches long)	HSK-Fine-Ject
Nitril gloves	WWR
Nylon mesh (105 µM, 40 µM)	Falcon
Pasteur pipettes (2,5 ml)	Sarstedt
PCR tubes (8er SoftStrips 0,2mL)	Bio Zym
Petri dish (35, 60, 90 mm)	Greiner Bio-one
Pipette filter tips (FT10, FT20, FT100, FT200,FT1000)	Greiner Bio-one
Pipette tips (10, 20. 100, 200, 1000 µl)	Greiner Bio-one
Plastic pipettes (5 ml, 10 ml, 25 ml)	Greiner Bio-one
Scalpel	Braun

Syringes (5 ml)	Terumo

3.1.12 Centrifuges

Table 12. List of centrifuges used in this thesis and their respective supplier.

Centrifuge	Supplier
Centrifuge (1.5-2ml tubes) 5418	Eppendorf
Centrifuge (200 µl tubes) 5417 R	Eppendorf
Centrifuge (15-50 ml tubes) 5810 Rf	Eppendorf
Centrifuge (1.5-2ml tubes) 5415D	Eppendorf

3.1.13 Morpholinos

Table 13. List of morpholinos used in this thesis and their respective sequences.

Gene	Sequence (5'>3')
tnnt2a	CATGTTTGCTCTGATCTGACACGCA
Standard control	CCTCTTACCTCAGTTACAATTTATA

3.1.14 Plasmids

Table 14. List of plasmids used in this thesis with their respective resistance and source.

Plasmid	Resistance	Source
PCR4-Blunt-TOPO	Ampicillin/Kanamycin	Thermo Fisher Scientific
pTol2 -0.2myl7:EGFP-Podocalyxin	Ampicillin	Mochizuki lab
pTol2- Mark3a-TagRFP-T	Ampicillin	Stainier Lab
pGEM-T	Ampicillin	Promega

3.1.15 Primers

Table 15. Primers used in this thesis with their respective sequences.

Gene	Forward	Reverse	
M13	TGTAAAACGACGGCCAGT	CAGGAAACAGCTATGAC	Sequencing
tol2	CATTAAAATTGTACTTGAGTAT	GTACTTATTTTTTGGAGATCAC	Sequencing
GFP	GTTCAGCGTGTCCGGCGA	TTGCTCAGGGCGGACTGG	Sequencing

rpl13a	TCGCTAGTTGGCATCGTTTATG	CGGAGGTTCGAAGACGATCA	qPCR
twist1a	GGCGCGTGGTCCATGTCAACATCC	GCTCCTTCCAGTGAGTTCAGCTCC	qPCR
twist1b	GGTTTGGAGGATGGAGGGCGCTTG	TGGTCCTCGTGTTTTCCCAGCTCACTG	qPCR
snai2	TCCAGGCCTTGGCTGCTGCAG	TCGATCTGCGAATGCACGACTGC	qPCR
snai1a	CACACACTGCCCTGCGTCTGTCC	GGAGGTTCGAGCGGTCTGCGA	qPCR
zf *podxl1*	TGACCATCACGTGGACAATCATCGTATTAG	TTACAAGTGAGTGTCCTCTTCGTCAGGTATG	To amplify zf Podocalyxin 1 for cloning
C-terminal side *podxl1*	AGAGATCTACCACAATACCCACCGCTTCTGAATC	GAAGATCTTTACAAGTGAGTGTCCTCTTCGTCAGG	To subclone C-terminal Podocalyxin 1 for cloning
mark3a-TagRFP-T	ATGTCAACAACGAGAGCCCCCCT	TTACTTGTACAGCTCGTCCATGCCA	Cloning fusion protein mark3a-TagRFP-T into a 0.2myl promoter
crb2a ATG	ATGGAGATCAGGAAAGTGCATCTGAAGG	TCATATTAACCGTTCTTCTGGTGGTACTTTC	To amplify Crb2a for mRNA injection
crb2a PCR BsrGI	TGTGTTGATCTCTGGACGAGCTACCGCTGTGACTTGTAC	AATAATAATCCGCTTGATTTAAGGGATCGAA	Genotyping Crb2a mutants
crb2a out	TCAGGCTTGTCCTTCAAGTC	TTACTTGGCTCAGGTGTGTC	Genotyping Crb2a mutants
crb2a in	TGTAAAACGACGGCCAGTTCAAGCATGCAGAGTTGAAG	AGGAAACAGCTATGACCATTATGCAAGACACTGGCACTC	Genotyping Crb2a mutants

3.1.16 Zebrafish food

Table 16. List of zebrafish food used at different developmental stages.

Food	Developmental stage
Brine Shrimp 5 dpf – 12 dpf	Brine Shrimp 5 dpf – 12 dpf
SDS 100 > 12 dpf – 1 month	SDS 100 > 12 dpf – 1 month
SDS 200 > 1 month – 2 months	SDS 200 > 1 month – 2 months
SDS 300 > 2 months – 3 months	SDS 300 > 2 months – 3 months
Tropical Breeder Mix and SDS 400	Adult fish

3.1.17 Zebrafish lines

Table 17. Zebrafish lines used in this thesis along with their publications where their were first described.

Zebrafish line	Abbreviation	Reference
AB (Wild type)		
Tg(−0.2myl7:EGFP-podocalyxin)^{bns103}	*Tg(−0.2myl7:EGFP-podxl)*	Jimenez-Amilburu et al. 2016
Tg(myl7-MKATE-CAAX)^{sd11}	*Tg(myl7:MKATE-CAAX)*	Lin et al. 2012
Tg(myl7:EGFP-Has.HRAS)^{s883}	*Tg(myl7:ras-EGFP)*	D'amico et al. 2007
Tg(myl7:Has.HRAS-mCherry)^{sd21}	*Tg(myl7:ras-mCherry)*	Yoruk et al. 2012
Tg(−5.1 myl7:DsRed2-NLS)^{f2}	*g(myl7:nDsRed2)*	Mably et al. 2003
Tg(myl7:mVenus-gmnn)^{ncv43Tg}	*Tg(myl7:mVenus-gmnn)*	Jimenez-Amilburu et al. 2016
Tg(myl7:LIFEACT-GFP)^{s974}	*Tg(myl7:LIFEACT-GFP)*	Reischauer et al. 2014
Tg(Tp1bglob:Venus-PEST)^{s940}	*Tg(TP1:VenusPEST)*	Ninov et al. 2012
Tg(tp1bglob:H2B-mCherry)^{s939}	*Tg(TP1:H2B-mCherry)*	Ninov et al. 2012
Tg(Tp1bglob:CreERT2)^{s951}	*Tg(TP1:CreERT2)*	Ninov et al. 2013
Tg(myl7:lox-mCherry-stop-lox-EGFP)^{s738}	*Tg(myl7:RSG)*	Jimenez-Amilburu et al. 2016
Tg(actb2:lox-dsRed-stop-lox-EGFP)^{s928}	*Tg(β-act2:RSG)*	Kikuchi et al. 2010
Tg(ubb:lox-EGFP-stop-lox- mCherry)^{z1701}	*Tg(ubi:Switch)*	Mosimann et al. 2011
Tg(kdrl:EGFP)^{s843}	*Tg(kdrl:EGFP)*	Jin et al. 2005
Tg(tcf21:mCherry-NTR)^{pd108}	*Tg(tcf21:mCherry-NTR)*	Wang J et al. 2015
TgBAC(cdh2:cdh2-EGFP,crybb1:ECFP)^{zf517}	*TgBAC(cdh2:cdh2-ECFP)*	Revenu C et al. 2014

3.1.18 Microscopes

Table 18. List of microscopes used for this thesis with their respective supplier.

Microscope	Supplier
Confocal Microscope, LSM 700	Zeiss
Confocal Microscope LSM 780	Zeiss
Confocal Microscope LSM 800	Zeiss
Confocal Microscope LSM 880	Zeiss
Spinning Disk Microscope, Cell observer SD	Zeiss
Lightsheet Microscope Z.1	Zeiss
Stereomicroscope Stemi 2000	Zeiss
Stereomicroscope Stereodiscovery V8 Zeiss	Zeiss
Stereomicroscope SMZ18	Nikon
Stereomicroscope SMZ23	Nikon
Confocal Microscope, LSM 700	Zeiss

3.1.19 Software

Table 19. List of software used in the thesis with their respective purpose.

Software	Purpose
Microsoft Office: Power point, Word and Excel	Writing, data analysis, image formatting and presentations
Fiji, Image J	Image processing
Imaris	Image processing
Graph Pad Prism	Data analysis
Ape, CLC	Sequence analysis
Oligo Calc	Primer design

3.2 Methods

3.2.1 Zebrafish maintenance

Zebrafish adults were kept and maintained as described in "The zebrafish book. A guide for the laboratory use of zebrafish (*Danio rerio*), 4th edition, 2000, Westerfield M." Zebrafish adults were kept in an aquaculture system (Tecniplast). The system is a circulating system that continuously filters the water providing a healthy aquatic environment. The tank temperature is always maintained at 26-28.5°C, the light-dark cycle consists of 14 hours of light and 10 hours of dark and the water pH should be around 6.8-7.5. The Tecniplast aquaculture system consists of fish tanks in a stainless steel rack structure connected to a fresh water reservoir and a water recycling system. Different types of filters help to keep the tanks clean from excess food and fish excreta. Moreover, the biological filters of the recycling system, made of sponge-like material (Siporax), allow growth of aerobic denitrifying bacteria, as *Nitrosomonas* and *Nitrobacter*. These bacteria, will maintain the nitrogen cycle in the aquarium, since an excess of ammonia or nitrite can be toxic for the fish. The water of each tank (around 20%) is automatically exchanged at precise intervals (every hour). UV light disinfects the water before re-entering the fresh water reservoir. Animal housing and experiments were approved by the MPG animal committee in concordance with the European regulations.

After collecting eggs, zebrafish embryos were kept in egg water in 90 mm Petri dish in an incubator set at 28.5°C. At 26 hpf, to avoid pigmentation in the embryos and facilitate the subsequent imaging, PTU was added in the medium. When imaging at early stages, removal of the chorion was necessary. For that, two different methods were applied, based on the need of the experiment: mechanical removal of the chorion by hand using two forceps, or adding 1mg/ml of pronase to 50 ml egg water at 26 hpf and keeping the embryos 28 °C

overnight (ON). Next day, water-containing PTU was removed and fresh egg water was added.

3.2.2 Zebrafish breeding

Zebrafish male and female adults (between 7-18 months old for maximum embryo production) were transferred into a mating tank that includes a removable insert with holes to allow eggs to pass through and a transparent divider. Next day, dividers that separated female and male were removed and the external fecundation takes place. After 30 to 45 minutes (min), eggs were collected using a mesh tea strainer and embryos were placed into 90 mm petri dish containing around 35 ml egg water (50 embryos per petri dish). Individual females were mated only once a week to ensure healthy embryos in every cross. Embryos were maintained in an incubator at 28.5ºC for optimal development. The same evening petri dishes with the embryos were cleaned and egg water was replaced for fresh one.

3.2.3 Preparation of injection plates

2% agarose was prepared with egg water. Then 30 mm petri dishes were filled with the agarose and a special mold with stripes. After solidifying, the agarose plates are ready to use.

3.2.4 Preparation of microinjection needles

Needles for injection were prepared using borosilicate glass capillaries and a micropipette puller. After placing the capillary under tension into the puller a chamber will heat the capillary in the middle. After stretching the hot capillary, a platinum heater filament will melt the capillary into two. The result is two needles with a very thin tip.

Table 20. Program used to prepare microinjection needles.

Ramp	Heat	Pull	Velocity	Time	Pressure
532	518	100	75	50	400

3.2.5 Microinjection

Samples were loaded using a microloader pipette tip into the glass needle. Under the dissecting microscope the thin tip of the needle was cut using forceps until opening a hole of 10-20 µm diameter. Then using a ruler, 1 nl drop was measured for the injection corresponding to 1.2 cm in the ruler. Embryos were aligned in the injection agarose plate at one-cell stage. Then, the needle was positioned with a slight angle respect to the plate and by pressing the foot

pedal, the solution was injected into the cell. To verify success of the injection, look for the presence of phenol red inside the cell.

3.2.6 *tnnt2a* morpholino injection

In order to stop contractility for some experiments 0.25 ng *tnnt2a* MO was injected into one-cell stage embryos.

3.2.7 Embryonic heart isolation from zebrafish

Isolation of embryonic *Tg(myl7:Hras-EGFP)* or *Tg(myl7:EGFP)* zebrafish heart at 52 hpf and larval hearts at 7 dpf was performed by following the protocol used by Burns & MacRae, 2006 (Geoffrey Burns and MacRae, 2006), with some modifications, for microarray analysis. This protocol was also used to extract embryonic hearts to analyzed different EMT markers by qPCR. In this case, zebrafish embryos were treated with an ErbB2 inhibitor, PD168393 starting at 54 hpf until 100 hpf, when the hearts were extracted. In both cases, embryos/larvae were first anesthetized using 0.04% tricaine methanesulfonate (MS-222), then collected into 1.5 ml microfuge tubes. I performed 3 X 15 min with embryo disruption medium (EDM), L15 medium containing 10% fetal bovine serum. All the washes were performed on ice. Hearts were then extracted from the embryos/larvae by mechanical disruption using a 5 ml syringe and a 19-gauge needle, 1 ½ inches long. Time of disruption was dependent of the embryos age, 2 dpf embryos were disrupted around 20 times while 7 dpf larvae around 35 times. Fragmented embryos/larvae were filter using a 105 μM nylon mesh to discard the death bodies and the flow-through was collected in a petri dish and applied to 40 μM nylon mesh. The 40 μM nylon mesh was inverted and the retained material (mostly zebrafish hearts with rest of tissue) was washed off with EDM into a 30 mm petri dish. EGFP positives hearts were then pick up one by one using a fluorescence stereomicroscope and collect into a new petri dish containing fresh EDM. Several washes were performed depending of the sample purity required. All these steps were also performed on ice. Then isolated EGFP positive hearts were placed into a 1.5 ml microfuge tube and centrifuged during 10 min at 14000 rpm. A total of 100 hearts were pooled per condition. Trizol was added then into the pellet and snap frozen on liquid nitrogen, consequently samples were kept at -80 °C.

3.2.8 RNA isolation

Prior to RNA isolation, extracted hearts were kept in TRIZOL at -80°C to preserve RNA and help in tissue dissociation. RNA extraction was performed using around 100 extracted hearts

per condition. Total RNA was isolated using RNeasy® Micro kit (QIAGEN) following the manufacturer's instructions.

3.2.9 cDNA synthesis

Five hundred nanograms of total RNA was reverse transcribed to cDNA with iScript cDNA synthesis kit from Biorad following manufactures' instructions. The protocol consisted on 5 min at 25 ºC followed by 20 min at 46 ºC and 1 min at 95 ºC for inactivation.

3.2.10 Real-time PCR

Real-time PCR were carried out in a Real-time system machine, CFX Connect Bundle 3, Biorad. Primers were designed using Ape and Oligo Calc softwares following specific criteria: the amplicon was not longer than 200 bp, and primers were designed to amplify an exon-exon junction. These two criteria made possible the duplication of the template in each cycle in a reliable manner and avoid possible amplification of genomic DNA in case is still present after RNA isolation. Primers used for the cloning are cited in section "3.1.15 Primers". Reactions were set up using SYBR Green PCR Master Mix that contains hot-start version of a modified *Thermus brockianos* DNA polymerase, SYBR Green I, optimized PCR buffer, 5 mM MgCl2, and dNTP mix including dUTP. Corresponding primers and 1/20 dilution of cDNA per sample was added to the mix.

Ct values in control/PD168393-treated hearts were as follows: *rpl13a*, 25/25; *snail1a*, 28/30; *snail2*, 17/19; *twist1a*, 30/31; and *twist1b*, 27/29.

Table 21. Standard real-time PCR conditions used.

Temperature	Time	Step	Cycles
95°C	7 minutes	Initial denaturation	1
95°C	10 seconds	Denaturation	X 40
60°C	30 seconds	Annealing	
72°C	10 minutes	Extension	
60°C	5 seconds	Final extension	1
92°C	1 minute		
4°C	Indefinite time	Hold	

3.2.11 Microarray analysis

RNA for microarray analyses was extracted as detailed in Section "3.2.8 RNA isolation". Two different conditions were analyzed: embryonic hearts collected at 52 hpf and 7 dpf. Microarray

was performed in duplicates (one duplicate per condition, each sample with a pool of 100 extracted hearts). Microarray analyses were performed by Oaklabs GmbH (Hennigsdorf, Germany). A 8 x 60K zebrafish expression array (XS-5090; Agilent 60-mer SurePrint technology) analysis was performed according to manufacturer's protocol.

3.2.12 PCR amplification for cDNA

PCR reactions were carried out in Eppendorf Mastercycler Pro thermal cyclers. PCR was performed in order to amplify EGFP-Podocalyxin and Mark3a-TagRFP-T plasmids using Phusion Taq polymerase or PrimeSTAR Takara HS polymerase. Primers were designed using ApE and Oligo Calc softwares following Cold Fusion Cloning manufactures. Primers used for the cloning are cited in section "3.1.15 Primers". Standard PCR reactions with both enzymes were set up according to manufacturer's instructions using 0.5 µl of cDNA and 1.5 µl each of forward and reverse primers (10 µM) in a 50 µl reaction. The PCR cycle parameters used were as follows:

Table 22. PCR to amplify EGFP-Podocalyxin fusion protein for Cold Fusion Cloning.

Temperature	Time	Step	Cycles
98°C	10 seconds	Denaturation	X 35
60°C	5 seconds	Annealing	
72°C	2 minutes	Extension	
72°C	2 minutes	Final extension	1
4°C	Indefinite time	Hold	

Table 23. PCR to amplify Mark3a-TagRFP-T fusion protein for Cold Fusion Cloning.

Temperature	Time	Step	Cycles
98°C	10 seconds	Denaturation	X 35
60°C	5 seconds	Annealing	
72°C	3 minutes	Extension	
72°C	3 minutes	Final extension	1
4°C	Indefinite time	Hold	

3.2.13 Agarose gel electrophoresis

Agarose gels were prepared by adding 1% agarose in 1 X TBE buffer and 2.5 µl SyBr Safe per 100 ml TBE buffer. PCR products samples were run in the gel together with loading buffer. Samples were run in the gel with the corresponding DNA ladder (100 bp or 1kb) depending on the size of the expected band. The gel was run at 120 v during 30-45 min depending also

on the product size. Gels were visualized with a blue light transiluminator and a picture of the gel was taking using a UV light in a gel imager system and printed using a thermal printer.

3.2.14 DNA extraction from agarose gel

Bands of interest visualized in the gel were purified using a gel extraction kit following manufacturer's instructions. The DNA was eluted with nuclease free water.

3.2.15 Measurement of nucleic acid concentrations

The concentrations of RNA and DNA were measured using Nanodrop, a spectrophotometer, by adding 1 µl of the sample. The nanodrop measures the absorbance and calculates the concentration of nucleic acids (260 nm) and purified proteins (280 nm). It is common to find a nucleic acid sample contaminated with other molecules. Then, the 260/280 ratio is used to assess the purity of the sample for both RNA and DNA. A 260/280 ratio of ~1.8 is generally accepted as "pure" for DNA; a ratio of ~2.0 is generally accepted as "pure" for RNA.

3.2.16 Cloning

- **Generation of -0.2myl7:EGFP-podocalyxin plasmid.**

First the zebrafish *podocalyxin1(podxl1)* was amplified using the following primers zf *podxl1* forward: TGACCATCACGTGGACAATCATCGTATTAG and zf *podxl1* reverse: TTACAAGTG AGTGTCCTCTTCG TCAGGTATG and the KOD plus neo polymerase (TOYOBO). The template used to amplify *podxl1* was cDNA of 36 hpf zebrafish embryos. The amplified zfPodxl1 (1338 bp) was cloned into PCR4-Blunt-TOPO vector generating the following plasmid, PCR4-zfPodocalyxin1. Next, C-terminal side of *podxl1* (24 aa-last aa) was subcloned adding BglII at both ends using the following primers: C-terminal side *podxl1* forward: AGAGATCTACCACAATACCCACCGCTTCTGAATC and C-terminal side *podxl1* reverse: GAAGATCTTTACAAGTGAGTGTCCTCTTCGTCAGG. A PCR product was cut by BglII and ligated into pEGFP-C1 at the BglII site. Because this plasmid (pEGFP-Podocalyxin(C1)) has a AgeI site in the immediate upstream of EGFP start codon, N-terminal side of Podocalyxin (1 aa - 23 aa) was ligated at the AgeI by annealing the following primers, forward: CCGGTATGACCATCACGTGGACAATCATCGTATTAGGTG CCTTCCTACATGACATGGCGTATGCACAGTCTGAAGCA and reverse: CCGGTGCTTCAGAC TGTGCATACGCCATGTCATGTAGGAAGGCACCTAATACGATGATTGTCCACGTGATGGTCATA. EGFP was located just after the signal peptide (Putative signal peptide is 1-20aa). Then, the pEGFP-podocalyxin1 plasmid was generated and finally inserted into pTol2:myl7 vector.

- **Generation of -0.2myl7:mark3a:TagRFP-T plasmid.**

The construct was generated using Cold Fusion Cloning system. Mark3a- TagRFP-T was amplified using the following primers mark3a-TagRFP-T forward: ATGTCAACAACGAGAGCCCCCCT and mark3a-TagRFP-T reverse: TTACTTGTACAGCTCGTCCATGCCA and the Phusion Tag HF Polymerase. Then the PCR product was run in a 1% agarose gel and the corresponding band of 2922 bp was extracted and purified with GeneJET Gel Extraction Kit. In parallel, 4 µg backbone plasmid was opened by using NheI and EcoRI restriction enzymes and digested for 3 hours at 37°C. Next, the digested plasmid was run in a 0.6% agarose gel and the band of 3755 bp was extracted and purified. After digestion, cold fusion cloning was performed using a ratio of 3:1 (insert:vector) following the manufacturer's instructions. Next, colonies containing the construct were sent for sequencing the correct integration of the construct.

3.2.17 DNA digestion

Digestion was used for cloning purpose. Backbones were digested for NheI and EcoRI for -0.2myl7:EGFP-Podocalyxin and -0.2myl7:mark3a:TagRFP-T cloning. Conditions for digestion were:

Enzyme	Incubation Temperature	Incubation Time
NheI/EcoRI	37°	3 hours

3.2.18 DNA ligation

Cold fusion cloning was used to generate -0.2myl7:EGFP-podocalyxin and -0.2myl7:mark3a:TagRFP-T constructs.

3.2.19 *Escherichia Coli* (*E.Coli*) competent cell preparation

DH5α competent cells were inoculated in LB liquid medium at 37°C ON. Next morning, 1 mL of the ON culture was added to a flask containing 200 ml of LB liquid medium and left in the shaker for 3-4 hours at 37°C. After this incubation, the culture was placed on ice for 20 min, cells were centrifuged for 10 min at 4000 rpm (4°C) and the supernatant medium was discarded. Once the pellet was dried, cells were resuspended in 5 ml cold 0.1M CaCl2 and kept on ice for 5min. Then the culture was centrifuged for 5 min at 4000 rpm (4°C). LB medium was discarded again and the pellet was dried. The final pellet was resuspended in 1 ml of cold 0.1M CaCl2 + 15% glycerol solution. Last, a metal 1.5 ml tube-rack was pre-chilled by immersing in liquid nitrogen and 20 µL of suspension cells was aliquoted in 1.5 ml tubes

and snap frozen quickly on the metal tube holder. Competent cells were stored in the freezer at -80 °C.

3.2.20 *E.coli* competent cell transformation

E.Coli competent cells were thawed on ice for few minutes. Plasmids to transform were added to the tube containing *E.Coli* competent cells and place on ice for 30 min. Then heat-shock was done at 42ºC for 40 min and then the tube was placed on ice for 10 more min. 5 ml LB agar per tube was added for 2 hours incubation in the shaker at 37ºC. Then, bacteria containing the plasmid were plated in 30 mm petri dishes prepared with LB agar containing the corresponding antibiotic, ampicillin or kanamycin, depending on the plasmid.

3.2.21 Plasmid DNA isolation

Mini-prep DNA isolation was performed to purify DNA for different downstream processes. One bacterial colony was inoculated in 5 ml LB liquid medium with the corresponding antibiotic and kept in the bacterial shaker a 37ºC ON. The following morning, the culture was centrifuged at 4000 rpm for 10 min and the supernatant was discarded. The DNA contained in the pellet was isolated using the GeneJET Plasmid Miniprep kit, following manufacture's instructions. Finally, the plasmid DNA was eluted in 40 µl of Elution Buffer.

3.2.22 Genomic DNA preparation for genotyping

To genotype embryos/larvae after each experiment or to identify founders, first genomic DNA was isolated. Embryos/larvae were disposed individually in 0.2 µl tubes. 50 µl (embryos/larvae) or 100 µl (fin clip) 10 mM NaOH were added and incubated at 95ºC during 10 min followed by addition of 1/10 1 mM TrisHCl. Then, samples were kept at 4ºC. In some cases 2 mg/ml final concentration Proteinase K was used to extract genomic DNA. In this case, samples were incubated at 55ºC for 2-3 hours and then heated at 95ºC for 10 min, thus inactivating the Proteinase K.

3.2.23 Screening of founders and mutants using PCR and sequencing

In order to screen for *crb2a*$^{-/-}$, *crb2a*$^{+/-}$ and wild-type fish I performed PCR 1 using genomic DNA extracted from fin clipped in adults or whole embryos/larvae. PCR 2 was done by using a 1/10 dilution of PCR 1 product. The PCR protocol is indicated in tables 24 and 25.

Table 24. PCR 1

Temperature	Time	Step	Cycles
95°C	3 minutes	Initial denaturation	1
94°C	30 seconds	Denaturation	X 35
57°C	30 seconds	Annealing	
72°C	30 seconds	Extension	
72°C	1 minute	Final extension	1
4°C	Indefinite time	Hold	

Table 25. PCR 2

Temperature	Time	Step	Cycles
95°C	3 minutes	Initial denaturation	1
94°C	30 seconds	Denaturation	X 35
57°C	30 seconds	Annealing	
72°C	1 minute	Extension	
72°C	3 minutes	Final extension	1
4°C	Indefinite time	Hold	

Then the PCR 2 product was sent for sequencing using M13 (-20) forward primer (Cited in section "3.1.15 Primers"). Sequences were analyzed using the ABI chromatogram file. The sequence containing the mutation is 5'- TGACTGTTAC (A>T) GACCCCATTA -3'. Wild-type sequence contains an "A", while mutant sequence a "T".

3.2.24 DNA sequencing

In order to verify that the sequences of interest were inserted correctly into the vectors, samples for sequencing were prepared as suggested by GATC or Seqlab companies according to the Sanger chain termination method.

3.2.25 Immunofluorescence mouse heart sections

Wild-type mouse embryos at E8.5 were collected and fixed ON in 4% PFA at 4ºC. Next day, they were embedded in OCT and stored right after at -80ºC for cryosections. Cryosections had a thickness of 10 μm and samples were collected in slides for histological analysis. Sections for immunofluorescence were post-fixed in 4% PFA for 20 min and then washed 2 X 15 min with PBS/Tween. Then, sections were antigen retrieved adding 10 mM citrate buffer (pH 6.0) and heating for 15 min in the microwave, followed by cooling the samples for 15 min at RT and washed with PBS and permeabilized with PBS 0.5% Tween20. After permeabilization,

samples were incubated in blocking solution for 1 hour. Primary antibodies were incubated ON at 4ºC. Next day, primary antibodies were removed, samples were washed 2 x 10 min with PBS/Tween followed incubation with secondary antibodies during 1 hour at RT. Slides were washed with PBS/Tween and nuclei were stained with DAPI dissolved in PBS/Tween before mounting with the antifade mounting medium Vectashield. Images were taken using a Zeiss LSM780 confocal microscope.

3.2.26 Immunostaining zebrafish: embryo preparation

Embryos were treated with PTU to avoid pigmentation and dechorionated using pronase at 1 dpf. Embryos/larvae were fixed at the stage of interest in 2 ml Fish fix buffer ON at 4ºC on nutator. Then the Fish fix buffer was removed and embryos were washed 3 X 15 min with PBS/Tween. Next, the yolk of the embryos/larvae was removed manually using forceps ("deyolking").

- **Immunostaining day 1: primary antibody incubation**

Deyolking was followed by permeabilization with Proteinase K (3 µm/ml) in 1 ml PBS/Tween (58 hpf → 30 min; 72 hpf → 50 min; >72 hpf → 1 hour). After permeabilization embryos/larvae were rinsed quickly with PBDT to stop the proteinase K reaction. Then, embryos/larvae were washed 3 X 15 min in PBDT. Blocking was done using Blocking buffer during 2 hours. Then embryos were incubated with the primary antibody(ies) with Incubation buffer ON at 4ºC in the rotator (gently shaking).

- **Immunostaining day 2: secondary antibody incubation**

Next day, after incubation, the primary antibody(ies) was/were removed and embryos were washed 4 X 20 min with PBDT. Then, embryos were incubated with the secondary(ies) in 200 or 500 µl depending on the antibody dilution, in Incubation buffer for 4 hours at RT in the rotator (gentle shaking). Next, secondary antibody(ies) were removed and embryos were washed first with DAPI in PBS/Tween for 10 min, followed by 6 X 15 min washes in PBS/Tween. All these steps were performed in dark conditions. Once the washes were finished, embryos were kept in PBS/Tween at 4ºC in the darkness until the day of imaging.

3.2.27 Imaging 36 hpf hearts: embryo preparation

Embryos were treated with PTU to avoid pigmentation and dechorionated using pronase at 1 dpf. At 36 hpf embryos were fixed with 4% PFA ON at 4ºC. Next day, PFA was removed and embryos were washed with PBS/Tween 2 X 10 min. After PFA removal, the heads of

the embryos were cut using forceps and a blade. The cut was performed right under the head in an angle of 15 degrees respect the base of the head. Removing the head at early stages help to visualize the heart. Embryos were kept in PBS/Tween at 4ºC until the day of imaging.

3.2.28 Chemical treatments

Embryos were treated with 10 μM of the ErbB2 inhibitor PD168393, 10 mM 2,3-butanedione monoxime (BDM), 0.08% tricaine, 50–100 μM DAPT, and 10 μM LY411575. In all the treatments, ten embryos per well were placed in 1 mL PTU egg water in 12-well plates containing the corresponding drug. DMSO was used as a control. In the case of PD168393 and DAPT treatments, drugs were added into egg water containing PTU and 1% DMSO to help with solubilization.

3.2.29 Lineage tracing

Tg(TP1:CreERT2) embryos were treated with 5 μM 4-OHT (Sigma, H7904) from 2 to 5 dpf. The drug was washed out and larvae were allowed to develop to the specific developmental stage for imaging.

3.2.30 Cell transplantation

Donor cells for transplantation were obtained from a cross between *crb2a*$^{+/-}$*;Tg(myl7:MKATE-CAAX)* animals. Host WT embryos were obtained from a cross between *Tg(myl7:ras:EGFP)* animals. For transplantation, embryos were first dechorionated by treating with 1 mg/ml pronase in Danieau buffer and embryos were maintained on agarose-coated Petri dishes until 1-cell stage. Embryos were then transferred into 12-well plates where each well is filled with agarose. Being in Ringer's buffer containing Penicillin/Streptomycin, donor cells were transplanted into 2-3 different WT host embryos along the blastoderm margin at mid-blastula stage. Donor larvae were maintained alive for genotyping. Prior to imaging, selection of mosaic larvae was done by screening for double positive larvae expressing both MKATE-CAAX and ras-EGFP transgenes. Imaging was done using LSM800 confocal microscope and contribution of transplanted cells in trabecular or compact-layer was quantified analyzing plane by plane the whole ventricle using the ZEN software.

3.2.31 Imaging with confocal microscope

Embryos and larvae were mounted in 1% low melt agarose on glass-bottom dishes. In order to stop the heart beating before imaging 0.2% (w/v) tricaine was added to the agarose. Z-plane images were taken using a spinning disk confocal microscope (Zeiss, CSU-X1

Yokogawa), Zeiss LSM700, LSM780, LSM800 or LSM880. A 40× (1.1 numerical aperture [NA]) water-immersion objective was used to acquire the images. The optical sections were 1 µm thick.

3.2.32 Time-lapse imaging

Time-lapse imaging was used to image *in vivo* at single-cell resolution the different polarization events taking place in CMs during cardiac trabeculation. Embryos/larvae were mounted in 1% low melt agarose containing 0.2% (w/v) tricaine on glass-bottom dishes. During the time of live imaging animals were kept in a temperature-controlled chamber at 27 ºC -28 ºC. Time-lapses images were taken using a spinning-disk confocal microscope (Zeiss, CSU-X1 Yokogawa) using a 40× (1.15 NA) water-immersion objective. Movies were acquired at four different Z positions 0.2 µm apart at each developmental time point. The acquisition time between each developmental time point was 10 min and the duration of the movie was of 3-5 hours. Data were aligned in Fiji.

3.2.33 Quantification of trabecular versus compact-layer CMs

To quantify trabecular versus compact-layer CMs, confocal images were acquired with a LSM800 microscope. For this specific experiment, the mid-sagittal plane of the ventricle was set up under the objective and then counted 12 planes up and 12 planes down at an increment of 1 µm per plane for the imaging. A total set of 24 planes was used for the analysis. Then, confocal images were processed and analyzed using ZEN software as follow. Two different ways were used for the counting. First, I drew two lines forming a 90° angle in the ventricle that includes the part of the outer curvature, which is right across from the atrioventricular (AV) canal and is usually where the first delaminated CMs can be observed. Second, I drew a line along the long axis of the ventricle in order to include now the whole outer curvature (See **Figures 15C and 15D**). I then counted the number of CMs in the trabecular and in the compact-layer in each individual plane (total 24 planes). Last, I calculated the percentage of trabecular CMs in each condition by dividing the number of trabecular CMs by the total number of CMs.

3.2.34 Image processing and analysis

3D images were processed using Imaris x64 (Bitplane, 7.7.2). To quantify the number of CMs in trabecular versus compact-layer CMs, ZEN 2011 software was used. Fiji or Zen softwares were used for the rest of 2D image processing. Images were prepared with the help of Adobe Illustrator or Microsoft PowerPoint.

3.2.35 Statistical analysis

Data are expressed as mean ± SEM. Differences between groups were compared with a two-tailed Student's t distribution test. All tests were performed with a confidence level of 95%. (*P< 0.05; **P< 0.01; ***P<0.001; ****P< 0.0001; ns: no significant changes observed).

4. Results

Part of chapter "4. Results" has been published as an article in the journal Cell Reports (Jiménez-Amilburu et al., 2016; Dec 6;17(10):2687-2699;11.023 (Jiménez-Amilburu et al. 2016).

The author contribution was described in the paper as follows:

V.J.A., S.J.R., D.W.S., and D.Y.R.S. designed the experiments; V.J.A., S.J.R., and D.W.S. performed the experiments; V.J.A., S.J.R., D.W.S., and D.Y.R.S. interpreted the data; H.N. constructed the EGFP-podocalyxin plasmid; N.M. and A.C. generated the *Tg(myl7:mVenus-gmnn)*^{ncv43Tg} line; and V.J.A. and D.Y.R.S. wrote the paper with feedback from all the authors.

4.1 Establishment of apicobasal polarity in cardiomyocytes and its regulation during cardiac trabeculation in zebrafish

4.1.1 Establishing apicobasal polarity in cardiomyocytes

As cellular rearrangements taking place during cardiac trabeculation are reminiscent of those observed in epithelial cells, I hypothesized that apicobasal polarity might be dynamically regulated in delaminating CMs.

Due to the lack of acknowledge in the field about polarity dynamics in CMs, I decided to investigate whether CMs display apicobasal polarity similar to epithelial cells during cardiac trabeculation. In order to study changes in CM apicobasal polarity during heart development, I first generated a zebrafish transgenic line, *Tg(−0.2myl7:EGFP-podocalyxin)*^{bns103Tg}, hereafter *Tg(−0.2myl7:EGFP-podxl),* which expresses the apical protein Podocalyxin fused to EGFP specifically in CMs (Figures 1A–1B″). Podocalyxin is the major component of the pericellular matrix of podocytes in the Bowman's capsule of the kidney and is found in the apical side of the plasma membrane (Bu and Callaway, 2011). In zebrafish it has also been shown to localize apically in glomerular podocytes (Ichimura et al., 2013) and other organs like Kupffer's vesicles (Navis et al., 2013) or the gut (Alvers et al., 2014). In order to clearly visualize Podocalyxin localization in CMs, I crossed and raised *Tg(−0.2myl7:EGFP-podxl)* fish into the background of the *Tg(myl7:MKATE-CAAX)*^{sd11Tg} reporter, hereafter *Tg(myl7:MKATE-CAAX),* to better distinguish CM morphology as this transgenic line labels the membrane of CMs (Lin et al., 2012). Next, I performed live imaging at different time points during the process of cardiac trabeculation. At 54 hpf, when trabeculation has not been initiated yet, the compact wall is

formed by a single layer of CMs. I analyzed embryonic hearts at 54 hpf and found that EGFP-Podocalyxin localization is restricted to the abluminal side of CMs (**Figures 1A–A″**).

It is well establish in the field that once trabeculation starts, around 60 hpf in zebrafish, specific CMs in a stochastic manner leave the compact-layer and seed the trabecular layer towards the lumen of heart (Staudt et al., 2014). To further investigate how CM polarity changes during delamination, I performed *in vivo* imaging of *Tg(−0.2myl7:EGFP-podxl);Tg(myl7:MKATE-CAAX)* fish after the initiation of cardiac trabeculation. At 82 hpf, trabecular CMs experience changes in EGFP-Podocalyxin localization (**Figures 1B-B"**). Interestingly, delaminated CMs in the trabecular layer present EGFP-Podocalyxin all around their membrane, while CMs that remain in the compact-layer retain EGFP-Podocalyxin at the apical side (**Figures 1B–B″**).

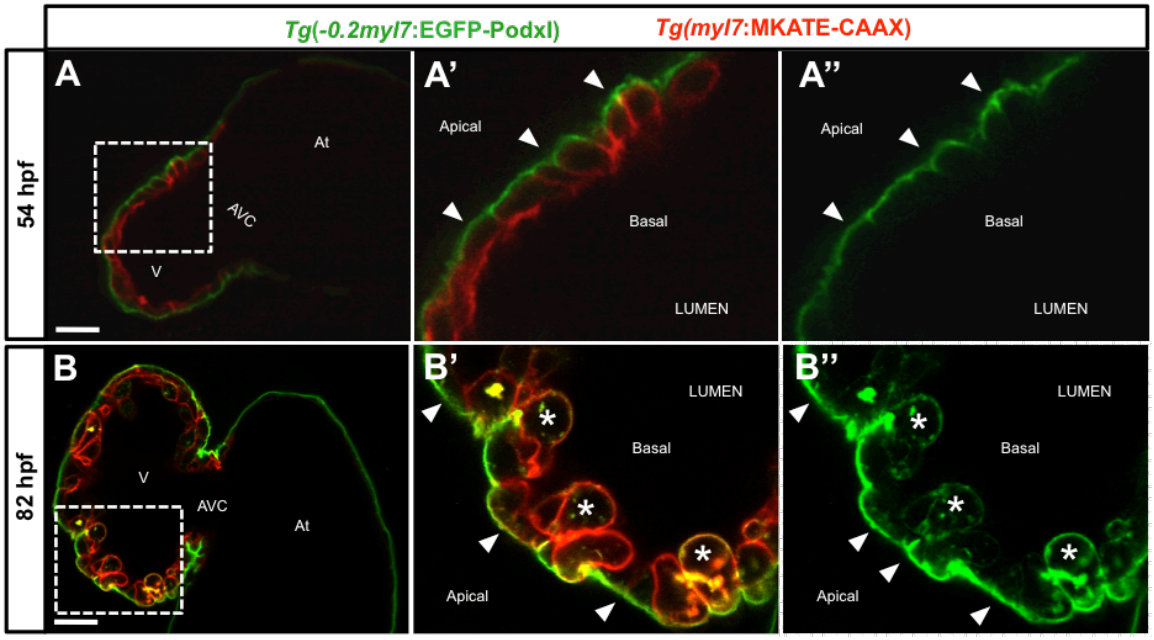

Figure 1. Changes in apical localization of Podocalyxin during cardiac trabeculation.

(**A-B"**) Confocal images (mid-sagittal sections) of *Tg(−0.2myl7:EGFP-podxl); Tg(myl7:MKATE-CAAX)* zebrafish hearts at 54 (**A-A"**) and 84 (**B-B"**) hpf. (**A-A"**) Higher magnification images show EGFP-Podocalyxin restricted to the abluminal side of compact-layer CMs. (**B-B"**) Higher magnification images show EGFP-Podocalyxin all around the membrane of delaminated CMs (asterisks) and apical in CMs staying in the compact-layer (white arrowheads). V, ventricle; At, atrium; AVC, atrioventricular canal. Scale bars, 20 µm. Modified figure reprinted with permission from Jiménez-Amilburu et al., Cell Reports, 2016 Dec 6;17(10):2687-2699;11.023.

To complement these results, I analyzed *Tg(myl7:EGFP-Has-HRAS)*^{s883Tg} line, hereafter *Tg(myl7:ras-GFP)* larvae, which specifically labels membranes of CMs (D'Amico et al., 2007), injected with the *-0.2myl7:mark3a-TagRFP-T* construct, which expresses the basolateral marker

Mark3a specifically in CMs (**Figures 2A-B"**). Mark3a (MAP/microtubule affinity-regulating kinase 3a) in zebrafish, also known as PAR1 in mammals, is involved in cell polarization and localizes basolaterally in mammalian epithelial cells (Böhm et al., 1997).

I analyzed the expression *in vivo* of *-0.2myl7:mark3a-TagRFP-T* injected larvae at 74 hpf, when delaminated CMs cannot be found yet, and found that Mark3a-TagRFP-T was expressed in the basolateral membrane of compact-layer CMs, which is facing the lumen of the heart (**Figures 2A–A″**).

Interestingly, at 82 hpf, CMs forming the trabecular layer show Mark3a-TagRFP-T expression localized all around their cell membrane, contrary compact-layer CMs that do not delaminate maintain basolateral identity and Mark3a-TagRFP-T is retained basolaterally (**Figures 2B–B″**). All these observations have been validated in the stable transgenic line *Tg(-0.2myl7:mark3a-TagRFP-T)*^{bns240Tg}.

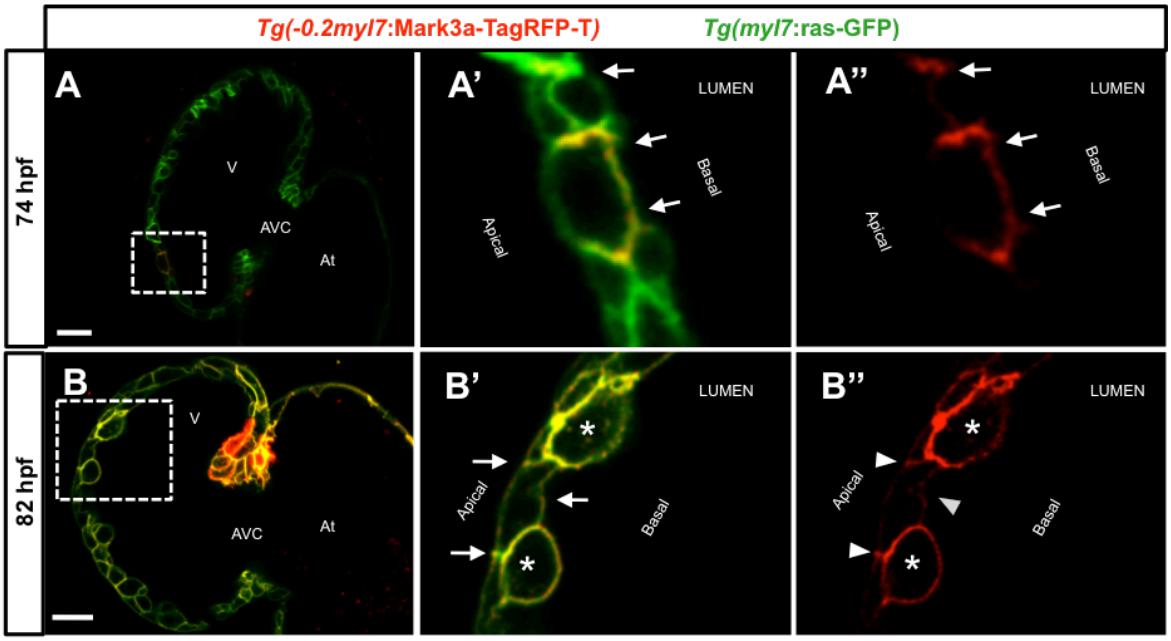

Figure 2. Changes in basolateral localization of Mark3a during cardiac trabeculation.

(**A-B"**) Confocal images (mid-sagittal sections) of *Tg(−0.2myl7:mark3a-TagRFP-T); Tg(myl7:ras-GFP)* zebrafish hearts. (**A-A"**) Higher magnification images of Mark3a-TagRFP-T show that basal in CMs is facing the lumen of the heart. (**B-B"**) Higher magnification images show Mark3a-TagRFP-T all around the membrane of delaminated CMs (asterisks) and basolateral in CMs staying in the compact-layer (white arrowheads). V, ventricle; At, atrium; AVC, atrioventricular canal. Scale bars, 20 μm. Modified figure reprinted with permission from Jiménez-Amilburu et al., Cell Reports, 2016 Dec 6;17(10):2687-2699;11.023.

These data together suggest that similar to epithelial cells, CMs display apicobasal polarity. I have shown for the first time apicobasal polarity in CMs, establishing as apical the CM membrane facing the outside surface of heart (abluminal), while basolateral membranes face the lumen of heart (luminal). Interestingly, I have described that delaminating CMs have to lose both, apical and basal identities, in order to migrate and reach the trabecular layer.

In order to confirm that apicobasal polarization is conserved across species, I analyzed embryonic mouse hearts. For this purpose, I immunostained embryonic day 8.5 (E8.5) mouse hearts for one of the PAR complex components, Prkci (**Figure 3A**), an apical polarity protein**.** Indeed, I could observe that Prkci localizes facing the abluminal membrane of compact-layer CMs (**Figures 3A'–A"'**). Besides confirming my observations in zebrafish, these data helped to solve the discrepancies with the work from Passer et al. where the authors proposed that the apical membrane of CMs is facing the lumen of the mouse heart. (Passer et al., 2016). (Certain lines in this section 4.1.1 have been quoted verbatim from Jiménez-Amilburu et al., Cell reports, 2016 Dec 6;17(10):2687-2699).

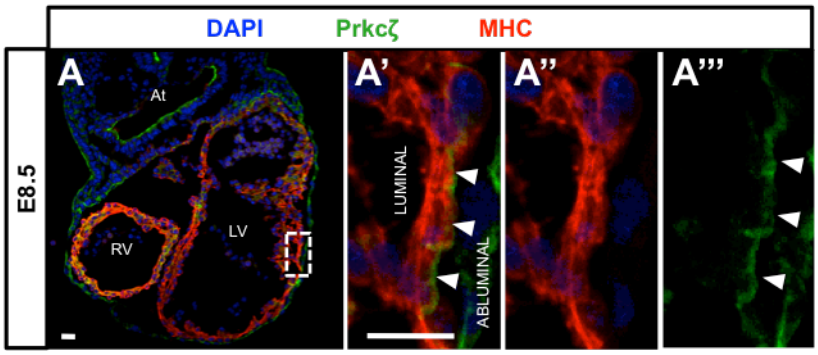

Figure 3. CM apicobasal polarity is conserved among vertebrates.

(**A-A'"**) Confocal images of E8.5 mouse hearts co-stained for Prkcζ (green), myosin heavy chain (MHC) (red), and DAPI (blue). (**A'-A'"**) Higher magnification images show the apical polarity protein Prkζ expresses in the abluminal side of compact wall CMs (white arrowheads). LF, left ventricle; RV, right ventricle; At, atrium. Scale bars, 20 μm. Modified figure reprinted with permission from Jiménez-Amilburu et al., Cell Reports, 2016 Dec 6;17(10):2687-2699;11.023.

4.1.2 Podocalyxin localization in cardiomyocytes during heart trabeculation

Apicobasal polarity in other cell types is very dynamic (Campanale et al., 2017). To understand how apicobasal polarity changes in CMs during cardiac trabeculation, I used the *Tg(−0.2myl7:EGFP-podxl);Tg(myl7:MKATE-CAAX)* line and followed EGFP-Podocalyxin localization at different stages of early heart development. I decided to examine zebrafish

hearts at 54, 77, 102, and 118 hpf. At 54 hpf, I found that EGFP-podocalyxin expression is restricted to the apical (abluminal) side of compact-layer CMs (**Figures 4A-A′**). At this stage, the basal membrane of CMs faces the ventricular lumen and is directly adjacent to the cardiac jelly, a specialized extracellular matrix (ECM), which separates the myocardium and endocardium. At 77 hpf, once trabeculation has been initiated, some delaminated CMs can be observed in the trabecular layer. EGFP-Podocalyxin localization is no longer exclusively apical in all CMs and delaminating CMs experience changes in their polarity. EGFP-Podocalyxin reorganizes and is now observed all around the cell membrane of the first delaminating CMs in the outer curvature of the ventricle, while those CMs that stay in the compact wall maintain their apical identity (**Figures 4B-B′**). At 102 hpf, larval hearts show trabecular protrusions formed by several CMs. Interestingly, all CMs forming the trabecula were depolarized, as shown by the expression of EGFP-Podocalyxin all around the cell membrane, while CMs staying in the compact-layer maintained their apical polarization (**Figures 4C-C′**). By 118 hpf, trabeculae form a complex network in the lumen of the ventricle and consist of depolarized CMs, while the CMs forming the compact-layer remain polarized (**Figures 4D-D′**). These findings help to understand the polarity changes that CMs experience during trabecular development and growth. (Certain lines in this section 4.1.7 have been quoted verbatim from Jiménez-Amilburu et al., Cell reports, 2016; 17(10):2687-2699;11.023)

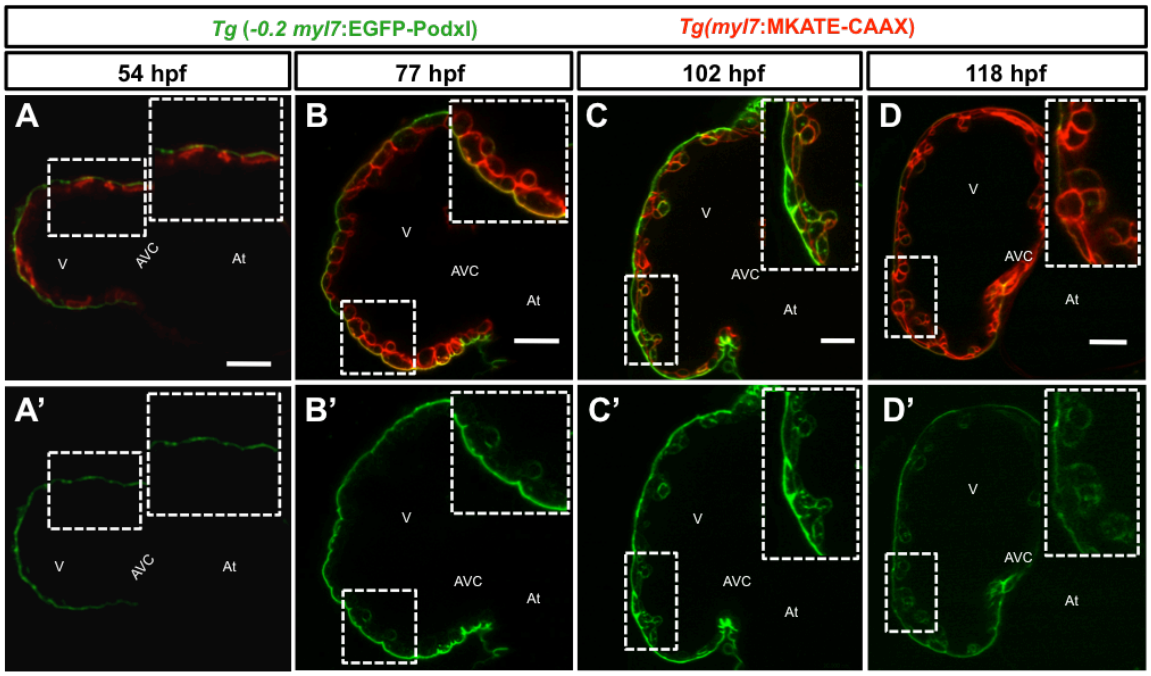

Figure 4. EGFP-Podocalyxin localization in CMs at different stages during zebrafish heart development.

(**A-D'**) Confocal images (mid-sagittal sections) of *Tg(−0.2myl7:EGFP-podxl); Tg(myl7:MKATE-CAAX)* zebrafish hearts at 54 (**A-A'**), 77 (**B-B'**), 102 (**C-C'**) and 118 (**D-D'**) hpf. Insets show higher magnification images of MKATE-CAAX and EGFP-Podocalyxin at the different stages studied. V, ventricle; At, atrium; AVC, atrioventricular canal. Scale bars, 20 μm. Modified figure reprinted with permission from Jiménez-Amilburu et al., Cell Reports, 2016 Dec 6;17(10):2687-2699;11.023.

4.1.3 Live imaging at single-cell resolution of cardiomyocyte polarization during cardiac trabeculation

Zebrafish in combination with high-resolution confocal microscopy offers many advantages for live imaging. In an attempt to study in more detail the different events taking place during CM depolarization, I analyzed spinning-disc time-lapse movies of beating *Tg(−0.2myl7:EGFP-podxl)*;*Tg(myl7:MKATE-CAAX*) zebrafish hearts during cardiac trabeculation. Live imaging at single-cell resolution showed that the first event that CMs undergo in the compact wall is apical constriction. I observed that random CMs in the outer curvature of the compact wall experience a progressive accumulation of EGFP-Podocalyxin in the abluminal side, where some CMs acquire a wedged shape (**Figure 5A**). These CMs will later ingress in the trabecular layer, showing that apical constriction precedes CM delamination. Next, I found that CMs depolarize while remaining in the compact-layer (**Figure 5B**). Depolarization was followed by the reorganization of EGFP-Podocalyxin all around the cell membrane of the compact-layer CMs. Then, depolarized CMs delaminate and leave the compact-layer to seed the trabecular layer, supporting previous observations (Staudt et al., 2014). Interestingly I found that once in the trabecular layer, some CMs undergo a partial repolarization; EGFP-Podocalyxin accumulates in the abluminal side of these CMs (**Figure 5C**). The CMs that repolarize inside the trabecular layer then undergo a second wave of depolarization where EGFP-Podocalyxin eventually redistributes all around their membranes (**Figure 5D**). My observations that CMs undergo apical constriction and apicobasal depolarization, together with previous reports (Cherian et al., 2016; Liu et al., 2010; Staudt et al., 2014), suggest cardiac trabeculation as an EMT-like process.

EMT and EMT-like processes imply upregulation of mesenchymal markers, such as *snail* or *twist*, whereas epithelial markers switch off (Wu et al., 2016). In order to further investigate whether trabeculation is an EMT-like process, I analyzed by qPCR the expression levels of different mesenchymal genes in pooled-hearts extracted from 96-hpf larvae treated with the ErbB2 inhibitor PD168393 starting at 55 hpf to block trabeculation. I found that *snail1a, snail2, twist1a*, and *twist1b* expression was downregulated in PD168393-treated hearts compared

to DMSO controls (**Figure 5E**). In these studies, I show how apical constriction of CMs can be used as a marker for delamination and that we can anticipate the process of delamination and follow those CMs that will delaminate from the compact-layer.

Altogether, these data show how CM apicobasal polarity is dynamically regulated during trabeculation (**Figure 5F**). (Certain lines in this section 4.1.7 have been quoted verbatim from Jiménez-Amilburu et al., Cell reports, 2016; 17(10):2687-2699;11.023).

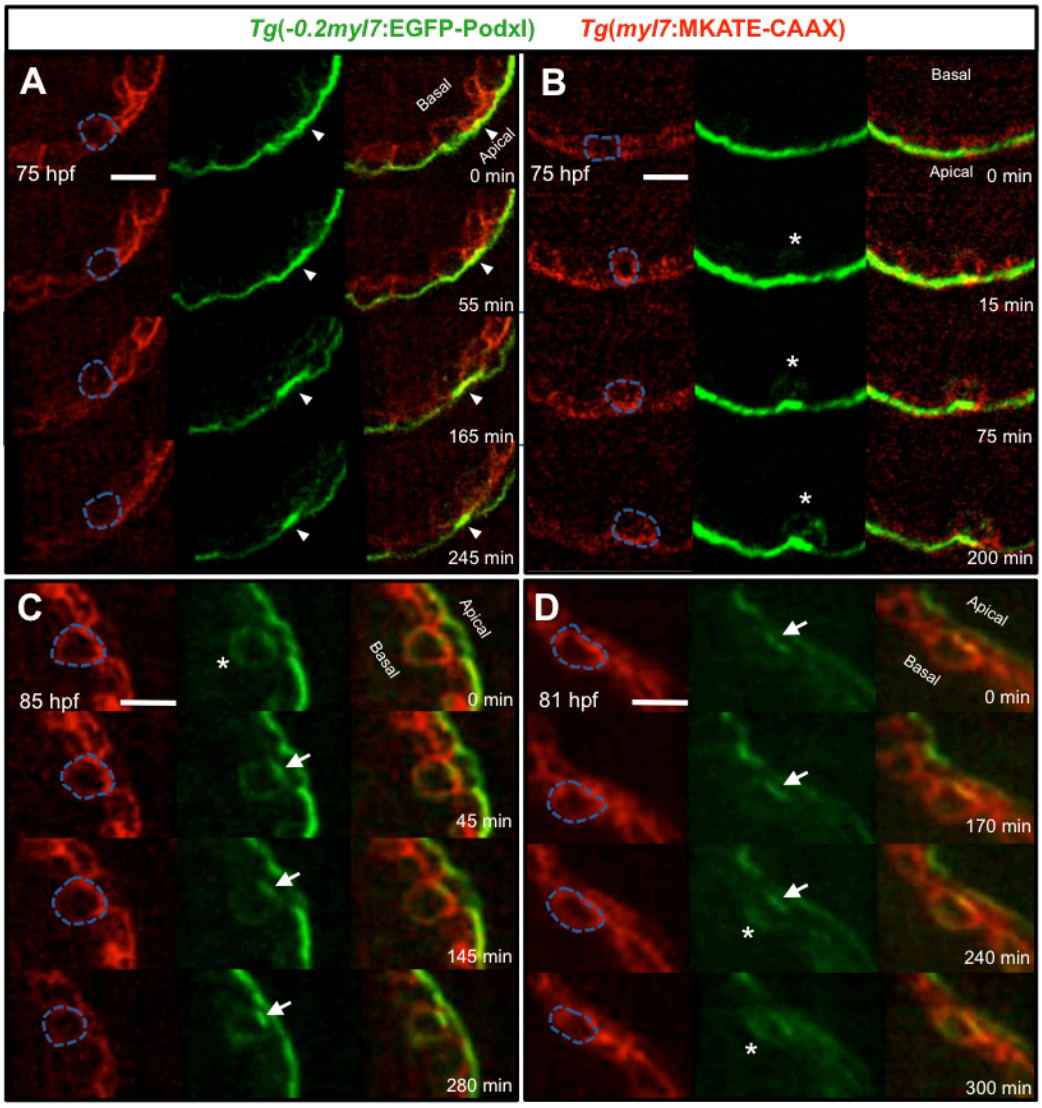

Figure 5. Live imaging shows how CMs undergo apical constriction prior to depolarization.

(**A-D**) Time-lapse movies of *Tg(−0.2myl7:EGFP-podxl);Tg(myl7:MKATE-CAAX)* beating zebrafish hearts between 75 and 90 hpf. (**A**) A CM undergoing apical constriction is indicated by white arrowheads. (**B**) Depolarized CM is marked by the asterisks. (**C**) Sometimes CM repolarization can be observed in the trabecular layer (white arrows). (**D**) Second wave of CM depolarization in the trabecular layer, arrows point to EGFP-Podxl

enrichment. Asterisks indicate the new depolarization event. Blue dashed lines outline the delaminating CMs examined (A–D). Scale bars, 10 μm. Modified figure reprinted with permission from Jiménez-Amilburu et al., Cell Reports, 2016 Dec 6;17(10):2687-2699;11.023.

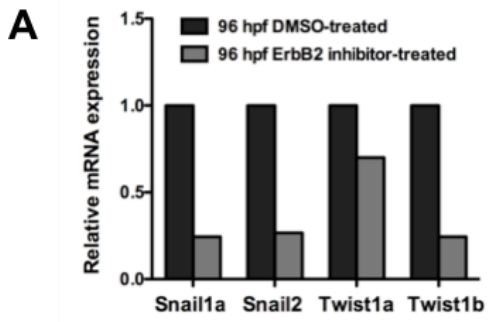

Figure 6. EMTs markers during cardiac trabeculation.

(**A**) qPCR expression data of *snail1a, snail2, twist1a, twist1b* in 96-hpf zebrafish hearts from DMSO- and PD168393-treated larvae. Modified figure reprinted with permission from Jiménez-Amilburu et al., Cell Reports, 2016 Dec 6;17(10):2687-2699;11.023.

In order to gain further insight into the apical constriction formation, I have reconstructed in 3D the core of CMs that might be involved in apical constriction (**Figure 6**). 3D modeling of individual CMs allowed me to observe in more detail how the constricting CM was acquiring the characteristic wedge shape in the abluminal side.

Moreover, I was able to identify that only two neighboring CMs are in close contact with the constricting CMs, one more superior and the other one inferior. These detailed morphological analyses of CMs neighboring apical constrictions at single cell resolution illustrate the complex cellular rearrangements required during trabeculation and will help to unravel questions about the process of CM delamination.

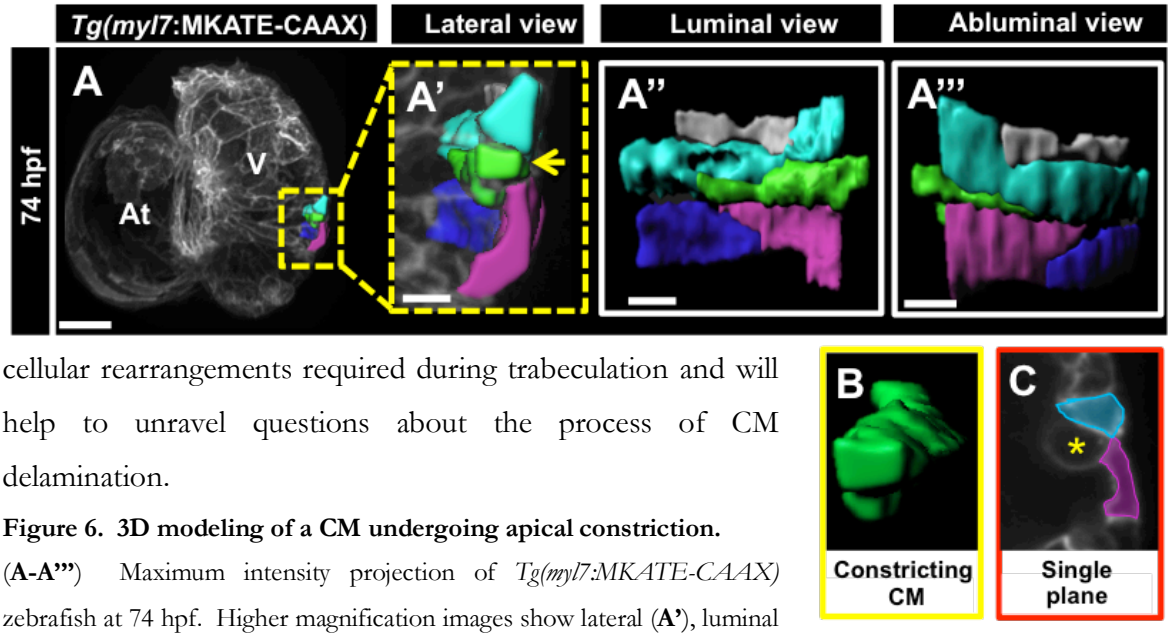

Figure 6. 3D modeling of a CM undergoing apical constriction.

(**A-A'''**) Maximum intensity projection of *Tg(myl7:MKATE-CAAX)* zebrafish at 74 hpf. Higher magnification images show lateral (**A'**), luminal

(**A"**) and abluminal (**A"'**) views of a 3D reconstructed set of CMs. The constricting CM is shown in green (A', yellow arrow). Different views show that CMs color coded in cyan and magenta are in close contact with the apically constricting CM. (**B**) 3D reconstruction using IMARIS of an individual
CM undergoing apical constriction. (**C**) Single z-stack of the constricting CM. The asterisk marks a constricting CM. At, atrium; V, ventricle. Scale bars, 20 µm.

4.1.4 Cardiomyocyte depolarization Is Nrg/ErbB2 signaling-dependent

Nrg/ErbB2 signaling has been previously reported as one of the essential pathways required for the correct formation of trabeculae during development in zebrafish (Liu et al., 2010) and mouse (Gassmann et al., 1995; Lee et al., 1995; Meyer and Birchmeier, 1995). To test whether ErbB2 signaling is necessary for CM depolarization, I treated *Tg(−0.2myl7:EGFP-podxl)*;*Tg(myl7:MKATE-CAAX)* zebrafish with the ErbB2 inhibitor PD168393 starting at 56 hpf. At 100 hpf, one can observe in untreated larvae CMs undergoing apical constriction as well as others experiencing depolarization (**Figures 7A-A″**). PD168393-treated larvae at 100 hpf did not exhibit any CM apical constriction or depolarized CMs (**Figures 7B-B″**).

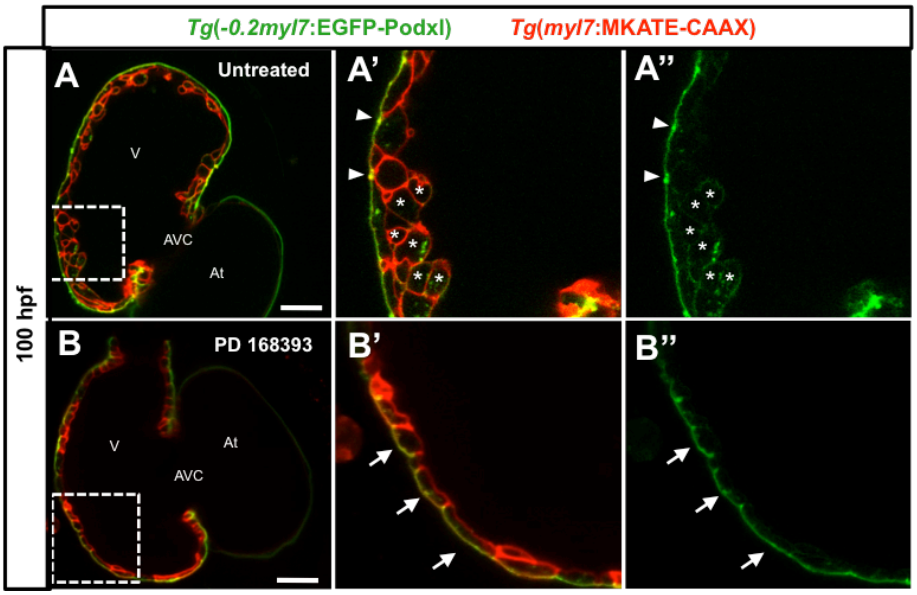

Figure 7. Embryos treated with and ErbB2 signaling inhibitor do not exhibit CM apical constriction. (**A-B"**) Confocal images (mid-sagittal sections) of *Tg(−0.2myl7:EGFP-podxl); Tg(myl7:MKATE-CAAX)* zebrafish hearts treated with 10 µM PD168393. (**A'-A"**) Untreated larvae at 100 hpf show apical constrictions (white arrowheads) and depolarization in trabecular CM (asterisks). (**B'-B"**) PD 168393-treated larvae show no apical constriction or depolarized CMs (white arrows). V, ventricle; At, atrium; AVC, atrioventricular canal. Scale bars, 20 µm. Modified figure reprinted with permission from Jiménez-Amilburu et al., Cell Reports, 2016 Dec 6;17(10):2687-2699;11.023.

Next, I also studied the possible role of the ErbB2 ligand controlling the formation of apical constriction or the depolarization of CMs. In zebrafish, it has been recently published that the main ligand for ErbB2 in the context of trabeculation is Neuregulin 2a (Nrg2a) (Rasouli and Stainier, 2017). In order to investigate this regulation, I used a recently developed *nrg2a* gene trap mutant (Westcot et al., 2015). I crossed *Tg(−0.2myl7:EGFP-podxl)* fish with *nrg2a*$^{+/mn0237Gt}$ animals. At 82 hpf, I found that heterozygous larvae (*nrg2a*$^{+/mn0237Gt}$) exhibit an average of 3.25 apical constrictions per ventricle per ventricular mid-sagittal plane (**Figures 8A-A'** and **Figure 8E**). Interestingly, *nrg2a*$^{mn0237Gt/mn0237Gt}$ larvae showed absence or lower number of apical constrictions compared to *nrg2a*$^{+/mn0237Gt}$ larvae (average of one apical constriction per ventricular mid-sagittal plane) (**Figures 8B-B'** and **Figure 8E**). EGFP-Podocalyxin expression in zebrafish hearts was also analyzed in *nrg2a*$^{+/mn0237Gt}$ and *nrg2a* $^{mn0237Gt/mn0237Gt}$ larvae at later stages. At 100 hpf, *nrg2a*$^{+/mn0237Gt}$ larvae exhibit a more complex trabecular network composed of many depolarized CMs (average of 5.6 per ventricular mid-sagittal plane) (**Figures 8C-C'** and **Figure 8F**). In contrast, *nrg2a* $^{mn0237Gt/mn0237Gt}$ larvae display a significantly lower number of delaminated CMs compared to *nrg2a*$^{+/mn0237Gt}$ (average of 1.6 delaminated CMs per ventricular mid-sagittal plane) (**Figures 8D-D'** and **Figure 8E**). Altogether, our data evidence the importance of the Nrg/ErbB2 signaling for the formation of apical constriction and depolarization during cardiac trabeculation. (Certain lines in this section 4.1.7 have been quoted verbatim from Jiménez-Amilburu et al., Cell reports, 2016; 17(10):2687-2699;11.023).

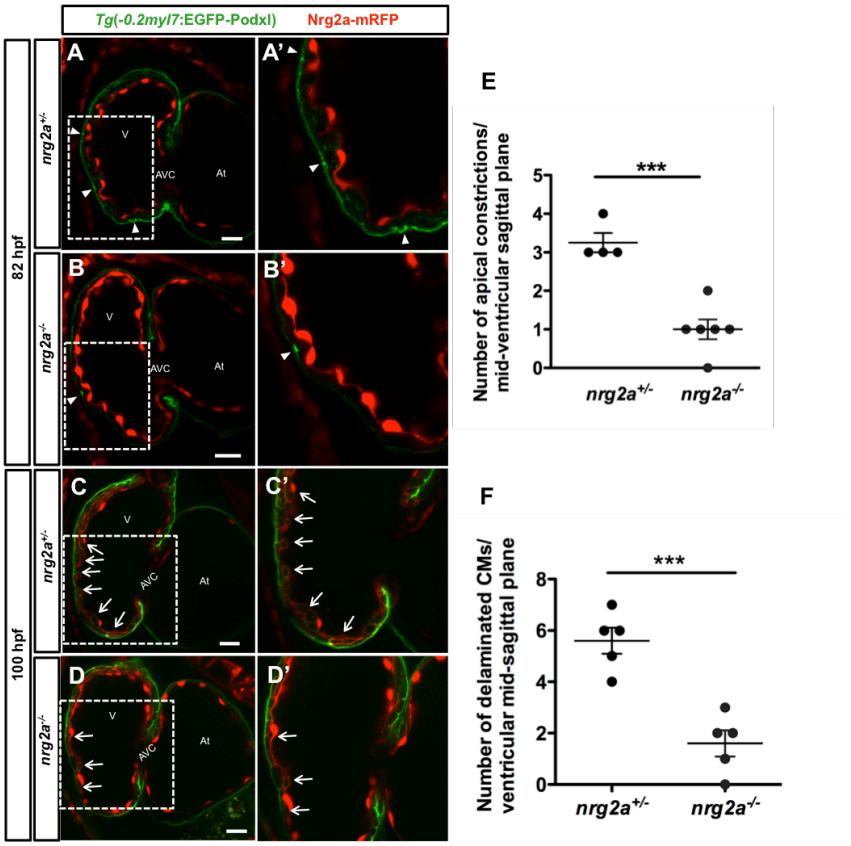

Figure 8. *nrg2a*$^{mn0237Gt/mn0237Gt}$ do not show apical constriction or CM depolarization.

(**A-D'**) Confocal images (mid-sagittal sections) of *Tg(−0.2myl7:EGFP-podxl)* zebrafish hearts from a *nrg2a*$^{+/mn0237Gt}$ incross at 82 (**A-C'**) and 100 (**C-D'**) hpf. Higher magnification images showing apical constrictions (white arrowheads) in *nrg2a*$^{+/mn0237Gt}$ (**A'**) and *nrg2a*$^{mn0237Gt/mn0237Gt}$ (**B'**). Higher magnification images showing delaminated CMs (white arrows) in *nrg2a*$^{+/mn0237Gt}$ (**C'**) and *nrg2a*$^{mn0237Gt/mn0237Gt}$ (**D'**). (**E**) Graphs showing the quantification of total number of apical constrictions in *nrg2a* heterozygous (n=4) homozygous mutants (n=6). (**F**) Graphs showing the quantification of total number of delaminated CMs in *nrg2a* heterozygous (n=5) homozygous mutants (n=5). Data are shown as mean ± SEM. ***$P < 0.001$ by Student's t test. V, ventricle; At, atrium; AVC, atrioventricular canal. Scale bars, 20 µm. Modified figure reprinted with permission from Jiménez-Amilburu et al., Cell Reports, 2016 Dec 6;17(10):2687-2699;11.023.

4.1.5 Cardiomyocyte depolarization is blood flow and cardiac contractility dependent

Cardiac contractility as well as blood flow have previously been shown to modulate trabecular formation in both mice (Sedmera et al., 2000) and zebrafish (Chi et al., 2008; Peshkovsky et al., 2011; Staudt et al., 2014). Based on these previous observations, I decided to investigate whether blood flow/contractility were also required for apical constriction formation and CM depolarization in the context of trabeculation. For this purpose, I followed three different approaches to stop cardiac contraction, each of them with its own limitations. First, I used

tricaine (MS-222), a sodium channel blocker (Malone et al., 2007). I treated *Tg(−0.2myl7:EGFP-podxl)*;*Tg(myl7:MKATE-CAAX)* larvae with tricaine at 58 (long-term treatment) and 72 (short-term treatment) hpf. I found that at 100 hpf, while controls exhibit apical constrictions and depolarized CMs (**Figures 9A-A"**), tricaine-treated animals do not exhibit apical constrictions or depolarized CMs in any of both treatments from 58 (**Figures 9B–B"**) or 72 (**Figures 9C–C″**) hpf. To complement these studies and in order to inhibit heart contraction as well, I injected the *tnnt2a* MO (Sehnert et al., 2002) into *Tg(−0.2myl7:EGFP-podxl)*;*Tg(myl7:MKATE-CAAX)* one-cell stage embryos. At 100 hpf, untreated larvae show apical constrictions and depolarized trabecular CMs (**Figures 9A-A"**), in contrast *tnnt2a* morphant hearts did not exhibit apical constrictions or depolarized CMs (**Figures 9C–C″**). Furthermore, I also used 2,3-butanedione monoxime (BDM), a myosin ATPase inhibitor (Higuchi and Takemori, 1989), to prevent cardiac contractility. At 100 hpf, I observed that, in contrast to controls (**Figures 10A–A"**) that showed depolarized CMs in the trabecular network, BDM-treated larvae showed no apical constrictions or depolarized CMs (**Figures 10B–B"**).

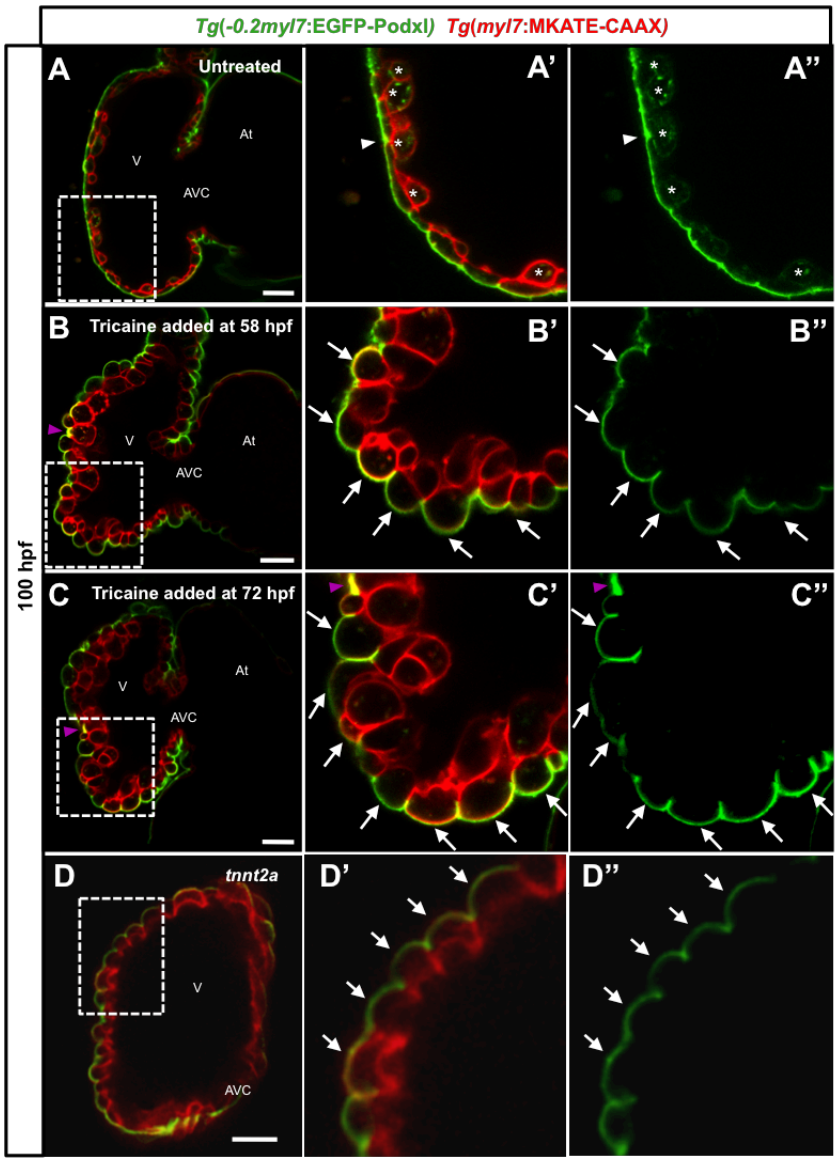

Figure 9. Blood flow/contractility regulates apical constriction formation and CM depolarization. (**A-D"**) Confocal images (mid-sagittal sections) of *Tg(−0.2myl7:EGFP-podxl);Tg(myl7:MKATE-CAAX)* zebrafish hearts. (**A-A"**) At 100 hpf, untreated larvae show apical constriction (white arrowheads) and depolarized CMs (asterisks). Tricaine-treated larvae at 58 (**B-B"**) and 72 (**C-C"**) hpf do not show apical constrictions or depolarized CMs (white arrows). (**D-D"**) *tnnt2a* morphants show no apical constrictions or depolarized CMs (white arrows). Purple arrowheads in B and C-C" point to apical Podocalyxin accumulation due to the heart collapse after tricaine exposure. V, ventricle; At, atrium; AVC, atrioventricular canal. Scale bars, 20 µm. Modified figure reprinted with permission from Jiménez-Amilburu et al., Cell Reports, 2016 Dec 6;17(10):2687-2699;11.023.

Based on these results, I reasoned that restoring contraction/circulation after temporal cessation of heart beating should be enough to rescue the formation of apical constrictions. To test this hypothesis, I carried out transient exposure treatments with BDM (**Figures 10C–**

E'). I treated larvae with BDM from 72 to 79 hpf. Larvae were imaged at 79 hpf, when the first apical constrictions can be observed in controls (**Figures 10C-C"**). As previously shown, BDM-treated larvae did not exhibit apical constrictions (**Figures 10D–D'**). Then, BDM was removed at 79 hpf and blood flow was restored by adding fresh water. The same larvae were imaged at 100 hpf, and interestingly I was able to observe apical constrictions (**Figures 10E-E″**). Overall, these results show that blood flow and cardiac contractility are required for CM apical constriction and depolarization. Furthermore, transient BDM exposure experiments indicate that CMs remain competent to undergo apical constriction even after temporary cessation of blood flow. (Certain lines in this section 4.1.7 have been quoted verbatim from Jiménez-Amilburu et al., Cell reports, 2016; 17(10):2687-2699;11.023).\

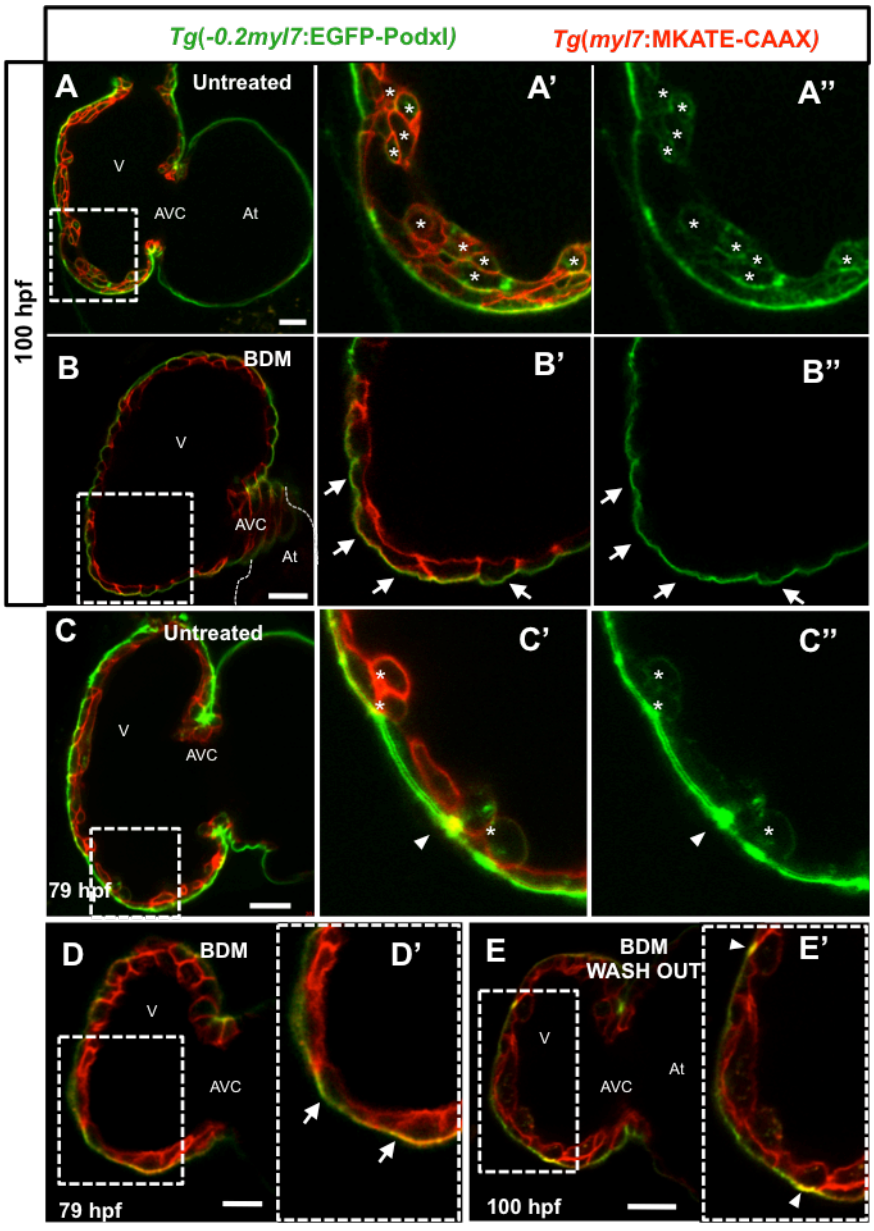

Figure 10. Apical constriction is recovered after restoring blood flow in zebrafish hearts.
(**A-E'**) Confocal images (mid-sagittal sections) of *Tg(−0.2myl7:EGFP-podxl);Tg(myl7:MKATE-CAAX)* zebrafish hearts after 20mM BDM treatment. At 100 hpf, untreated larvae showing depolarized delaminated CMs (**A-A"**, asterisks). Larvae were treated with BDM from 56 to 100 hpf. BDM-treated larvae at 100 hpf show no apical constriction or depolarized CMs (**B-B"**, white arrows). At 79 hpf, untreated larvae show apical constriction (white arrowheads) and depolarized CMs (asterisks) (**C-C"**). Larvae were treated with BDM from 72 to 79 hpf. After 7 hours of treatment, BDM-treated larvae show no apical constriction or depolarized CMs (**D-D'**, white arrows). At 79 hpf, BDM was washed out, and larvae were subsequently imaged at 100 hpf, images show presence of apical constrictions (**E-E'**, white arrowheads). V, ventricle; At, atrium; AVC, atrioventricular canal. Scale bars, 20 μm. Modified figure reprinted with permission from Jiménez-Amilburu et al., Cell Reports, 2016 Dec 6;17(10):2687-2699;11.023.

4.1.6 Differential expression of Notch reporter lines in zebrafish cardiomyocytes

Notch signaling has been widely reported to control the fate of several cell types and the organ patterning during developmental processes and in the adult (Artavanis-Tsakonas et al., 1999). In the heart, Notch has been shown to function in the endocardium allowing interaction with other signaling pathways and controlling thus cardiac morphogenesis in mouse (Grego-Bessa et al., 2007; Luxán et al., 2016) and zebrafish (Samsa et al., 2015). However, though a differential activation within the endocardium has been observed, it was unclear whether this activation contributed to the behavior of the underlying myocardium, or whether Notch reporter lines were active in the myocardium during trabecular stages. In order to examine Notch activity in the myocardium and to study its possible role during cardiac trabeculation, I took advantage of a number of transgenic zebrafish lines that act as reporters of the Notch pathway. First, I examined the *Tg(Tp1bglob:Venus-PEST)*^{s940Tg} line, hereafter *Tg(TP1:VenusPEST)*, which expresses destabilized YFP in cells with an active Notch signaling (Ninov et al., 2012). These reporter lines use 12 repeats of a region of the Tp1 promoter region, which is Notch-responsive, to mark Notch responsive cells. In addition, due to the short half-life of the fluorescent protein VenusPEST, this line enabled me to observe those cells that have recently activated the Notch pathway. Then, I crossed these fish with the *Tg(myl7:Has.HRAS-mCherry)*^{sd21} (Yoruk et al., 2012), hereafter *Tg(myl7:ras-mCherry)* and examined the expression of this reporter line at different stages during heart development. Before 76 hpf, I could only observed a strong expression of the reporter line in the endocardium and no reporter expression was detected in the myocardium (data not included). At 76hpf, I analyzed *Tg(TP1:VenusPEST)* larvae and found that not only the endocardium and

AVC but also few compact-layer CMs show activation of the reporter (**Figure 11A**). By 100 hpf, the endocardial expression of *Tg(TP1:VenusPEST)* line starts to disappear. Interestingly, at the same time, several compact-layer CMs expressing Tg(*TP1:*VenusPEST) can still be observed, however, expression in the complex network of trabecular CMs was not found (**Figure 11B**). Later in the development, at 125 hpf the same pattern of expression was found within the endocardium and myocardium (**Figure 11C**). To summarize, I did not observe *Tg(TP1:*VenusPEST) expression in the trabecular CMs at any of the different stages analyzed. Similar observations using the *Tg(Tp1:d2GFP)^{um43}* line (Clark et al., 2012) were also published (Han et al., 2016). Next, in order to determine the extent of the CMs that activate the Notch pathway during early development, I performed lineage tracing experiments using the *Tg(Tp1bglob:CreERT2)^{s951Tg}* line, hereafter, *Tg(TP1:CreERT2)*, which expresses the CreERT2 fusion protein in a Notch responsive manner (Ninov et al., 2013). This line was crossed to a *Tg(myl7:lox-mCherry-stop-lox-EGFP)^{s738Tg}* line, hereafter *Tg(myl7:RSG)* and *Tg(actb2:lox-dsRed-stop-lox-GFP)^{s928Tg}* line, hereafter *Tg(β-act2:RSG)* (Kikuchi et al., 2010), in which CMs are labeled in red, and turn green in the presence of Cre activity. Recombination was induced in CMs expressing the Notch reporter upon incubation with 4-hydroxytamoxifen (4-OHT). By growing the larvae in 4-OHT starting before the onset of trabeculation (from 60-120 hpf), I was able to label all CMs that will express Notch during trabecular stages. Interestingly, when I used this approach, I found that only compact-layer CMs were recombined (**Figures 11D-F**). Next, I crossed *Tg(TP1:CreERT2)* fish into the ubiquitous *Tg(ubb:lox-EGFP-lox-stop-mCherry)^{z1701Tg}* background, hereafter *Tg(ubi:Switch)* (Mosimann et al., 2011). Analysis of these double transgenic larvae, in which CM recombination takes place switching from green to red, recapitulated our observations with the other lines for lineage tracing (**Figure 11F**). (Certain lines in this section 4.1.7 have been quoted verbatim from Jiménez-Amilburu et al., Cell reports, 2016; 17(10):2687-2699;11.023).

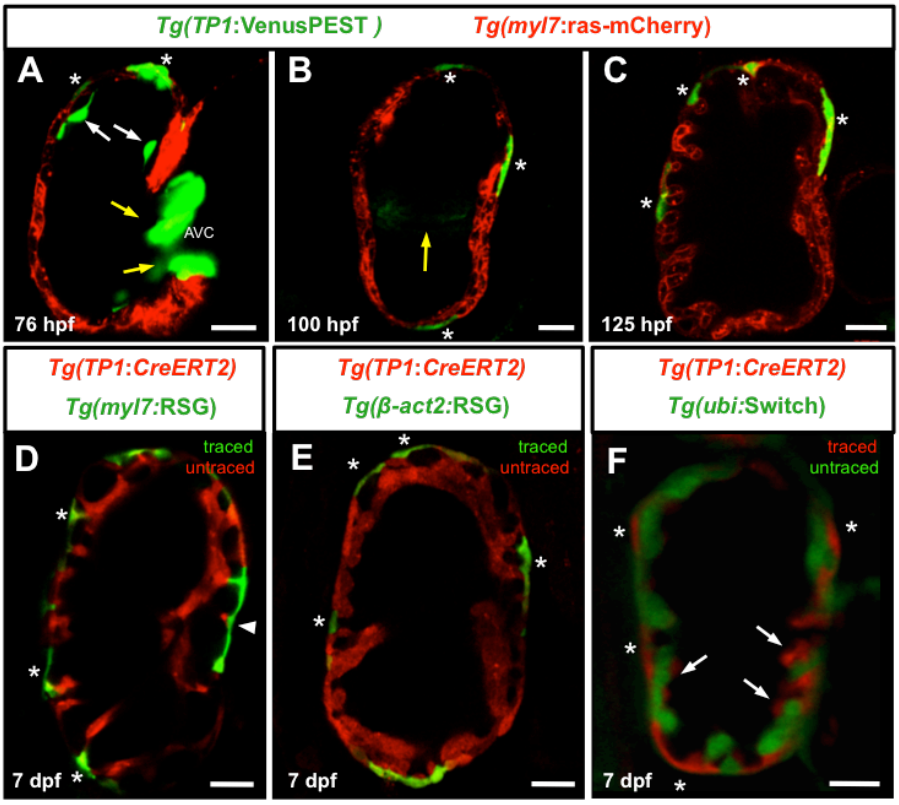

Figure 11. Expression of Notch reporter lines in the zebrafish myocardium.

(**A-C**) Confocal images (mid-sagittal sections) of *Tg(TP1:VenusPEST); Tg(myl7:ras-mCherry)* zebrafish hearts at 76 (**A**), 100 (**B**) and 125 (**C**) hpf. Asterisks indicate CMs expressing the Notch signaling reporter. White arrows in (A) point to fading *TP1*:VenusPEST expression in the endocardium. Yellow arrows point to the developing AV valve in (A) and (B). (**D-F**) Confocal sections of 7 dpf lineage-traced larval hearts obtained by crossing *Tg(TP1:CreERT2)* crossed into *Tg(myl7:RSG)* (**D**), *Tg(β-act2:RSG)* (**E**) or *Tg(ubi:Switch)* (**F**). Asterisks indicate labeled CMs in the compact-layer. Arrowhead points to a CM neighboring the AV canal. Note that in F, lineage-traced cells are in in red and that white arrows point to labeled endocardial cells. AVC, atrioventricular canal. Scale bars, 20 μm. Modified figure reprinted with permission from Jiménez-Amilburu et al., Cell Reports, 2016 Dec 6;17(10):2687-2699;11.023.

4.1.7 Notch reporter positive cardiomyocytes appear in the compact-layer adjacent to those undergoing apical constriction

To further understand whether Notch signaling in the developing myocardium plays a role in these fate decisions, I studied Notch activity in individual CMs during delamination. I crossed the *Tg(tp1bglob:H2B-mCherry)*^{s939Tg} (Ninov et al., 2012), hereafter *Tg(TP1:H2B-mCherry)*, which expresses mCherry in the nucleus of cells where Notch is activated, into the *Tg(−0.2myl7:EGFP-podxl);Tg(myl7:MKATE-CAAX)* background. Next, I analyzed these hearts at 79 hpf, when several apical constrictions and delaminated CMs can be observed.

Confocal images of the ventricular mid-sagittal plane at this developmental stage showed few *TP1*:H2B-mCherry-positive CMs localized in the compact-layer. Strikingly, those *TP1*:H2B-mCherry-positive CMs were found adjacent to CMs undergoing apical constriction (**Figures 12A–B′**). Similarly, when CMs had already delaminated and populated the trabecular layer, *Tg(TP1:H2B-mCherry)*-positive CMs were found directly adjacent to delaminated CMs (**Figures 12C–D′**). After quantification I found that 70% of CMs undergoing apical constriction were neighbored by Notch-reporter-positive CMs (**Figure 12E**). Overall, I identified an interesting subpopulation of compact-layer CMs during trabeculation. These data suggest a role for Notch signaling in preventing CMs from entering the trabecular layer. (Certain lines in this section 4.1.7 have been quoted verbatim from Jiménez-Amilburu et al., Cell reports, 2016; 17(10):2687-2699;11.023).

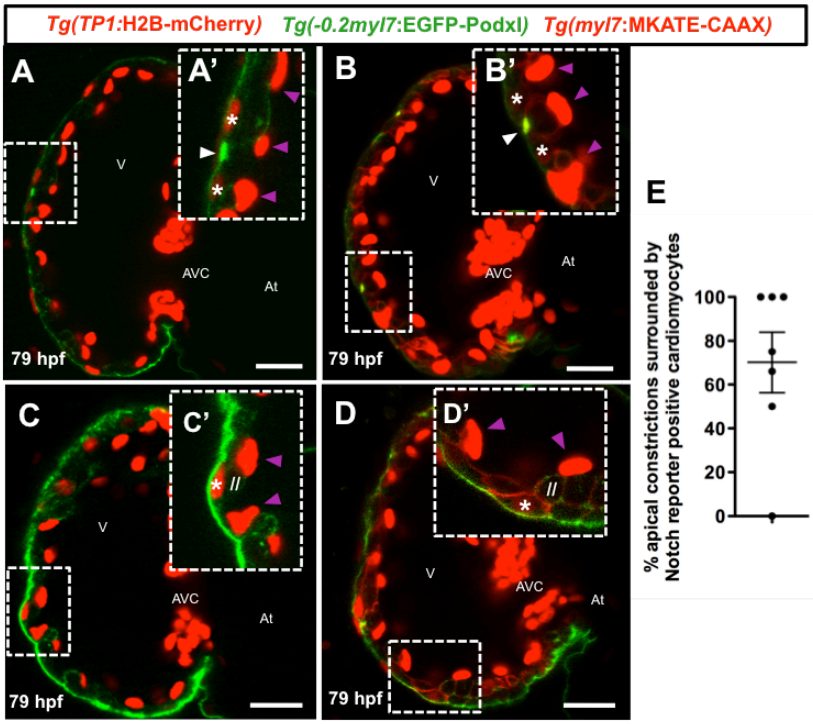

Figure 12. Notch reporter positve CMs appear in compact-layer adjacent to those undegoing apical constriciton.

(**A-D'**) Confocal images (mid-sagittal sections) of *Tg(TP1:H2B-mCherry);Tg(−0.2myl7:EGFP-podxl);Tg(myl7:MKATE-CAAX)* 79 hpf larval hearts. Images show Notch positive CMs surrounded by a CM undergoing apical constriction (**A-B'**) or adjacent to a delaminated CM (**C-D'**). (**E**) Graph showing percentage of CMs undergoing apical constriction surrounded by Notch reporter positive CMs. Each dot represents a heart. V, ventricle; At, atrium; AVC, atrioventricular canal. Scale bars, 20 μm. Modified figure reprinted with permission from Jiménez-Amilburu et al., Cell Reports, 2016 Dec 6;17(10):2687-2699;11.023.

4.1.8 Nrg2a signaling is required for Notch reporter activity in zebrafish cardiomyocytes

Recent studies in zebrafish suggest that Nrg2a rather than Nrg1 could be the preferential ligand for the tyrosine kinase receptor in zebrafish heart (Rasouli and Stainier, 2017). To better understand whether Nrg signaling might be involved in the modulation of myocardial Notch activity, I crossed *nrg2a* mutant animals with *Tg(tp1:VenusPEST)* line. Similar to WT (WT) animals, at 78 hpf in *nrg2a*$^{+/mn0237Gt}$ larvae I was able to observe *TP1:*VenusPEST-positive CMs in the compact-layer, AVC and endocardial cells (**Figures 13A-A"**). Interestingly, I noticed that in the *nrg2a*$^{mn0237Gt/mn0237Gt}$ animals, I could not find Notch expression in any compact-layer CM, however endocardial Notch activity remained unaffected (**Figures 13B-B"**). To better analyze this phenomenon, I imaged larval hearts at 96 hpf, and observed that in *nrg2a*$^{+/mn0237Gt}$ animals, Notch is still active in the myocardium while its expression in the endocardium decreases (**Figures 13C-C"**). Strikingly, 96 hpf *nrg2a*$^{mn0237Gt/mn0237Gt}$ animals lack Notch activation in CMs (**Figures 13D-D"**). The number of Notch reporter positive CMs in *nrg2a*$^{+/mn0237Gt}$ and *nrg2a* $^{mn0237Gt/mn0237Gt}$ was also quantified at 79 hpf, observing a significant reduction in homozygous larvae (**Figure 13E**). In view of these results, I set out to test whether Nrg2a signaling could be directly inducing Notch activation in a specific subset of CMs. To this end, I overexpressed Nrg2a fused to tdTomato protein via a p2A element (Rasouli and Stainier, 2017) specifically in *tnnt2a* morphant CMs, which do not exhibit Notch reporter activity (Samsa et al., 2015). Analysis of these hearts at 96 hpf revealed that, contrary to the WT situation, *tnnt2* morphant CMs failed to upregulate the Notch reporter (**Figure 13G**). Conversely, Nrg2a overexpression in CMs was able to activate *TP1*:VenusPEST expression in the surrounding tdTomato-positive CMs in *tnnt2a* morphants (**Figure 13H**). The percentage of *TP1*:VenusPEST-positive CMs in non-injected larvae, *tnnt2a* morphants, and *tnnt2a* morphants overexpressing *nrg2a* in the myocardium was quantified to confirm differences in Notch activation (**Figure 13I**).

Overall these data demonstrate a key role for Nrg signaling in activating Notch signaling in the myocardium during cardiac trabeculation in zebrafish. (Certain lines in this section 4.1.7 have been quoted verbatim from Jiménez-Amilburu et al., Cell reports, 2016; 17(10):2687-2699;11.023).

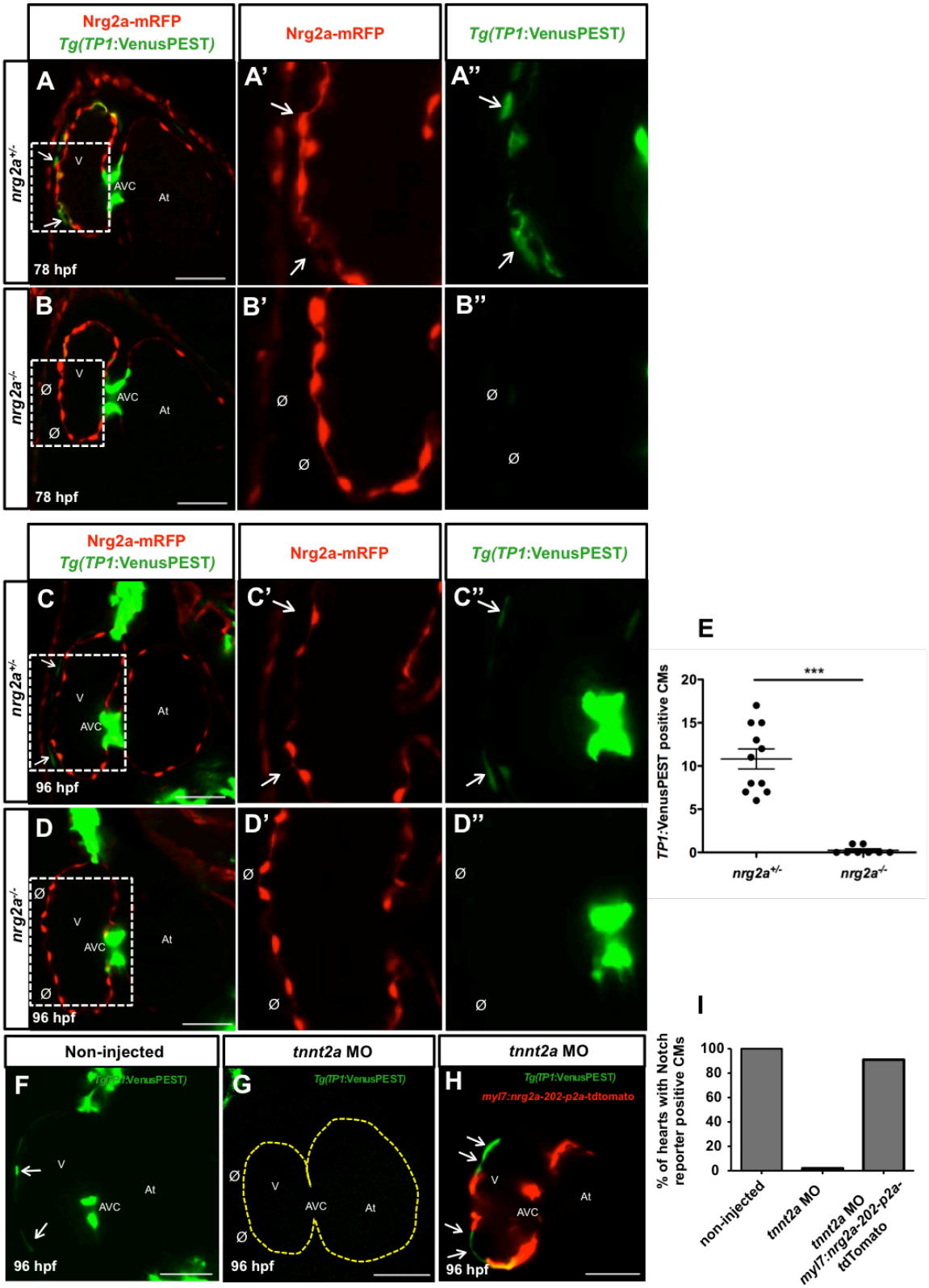

Figure 13. Nrg signaling plays a role in Notch signaling activation in the myocardium.

(**A-D"**) Confocal images (mid-sagittal sections) of *Tg(TP1:VenusPEST)* larval hearts from an *nrg2a*$^{+/mn0237Gt}$ incross at 78 (**A-B"**) and 96 (**C-D"**) hpf. At both stages, the number of *TP1*:VenusPEST-positive CMs is dramatically

reduced in *nrg2a*$^{mn0237Gt/mn0237Gt}$ compared to *nrg2a*$^{+/mn0237Gt}$ animals. (**E**) Graph showing total number of *TP1*:VenusPEST-positive CMs in *nrg2a*$^{mn0237Gt/mn0237Gt}$ (n=8) and *nrg2a*$^{+/mn0237Gt}$ (n=11). Each dot represents one heart. Data are shown as mean ± SEM. ···$P < 0.001$ by Student's t test. (**F-H**) Confocal images (mid-sagittal sections) of *Tg(TP1:VenusPEST)* larval hearts at 96 hpf. Non-injected larvae show *TP1*:VenusPEST-positive CMs in the compact-layer (F, arrows). *tnnt2a* morphants do not show any *TP1*:VenusPEST-positive CMs (G, Ø). In *tnnt2a* morphants, overexpression of Nrg2a in CMs activates Notch signaling in neighboring CMs (H, arrows). (**I**) Graph showing percentage of *TP1*:VenusPEST-positive CMs at 96 hpf in non-injected larvae (n=18), *tnnt2a* morphants (n=31), and *tnnt2a* morphants overexpressing *nrg2a* in CMs (n=23). V, ventricle; At, atrium; AVC, atrioventricular canal. Scale bars, 20 μm. Modified figure reprinted with permission from Jiménez-Amilburu et al., Cell Reports, 2016 Dec 6;17(10):2687-2699;11.023.

4.1.9 Abrogation of myocardial Notch signaling does not lead to an increase in the number of apical constrictions or trabecular cardiomyocytes, but affects compact wall thickness

My previous results indicate that only compact-layer CMs adjacent to those CMs trabeculating show Notch reporter activity. Therefore, I hypothesized that Notch activity might be preventing cells from entering the trabecular layer. In that case, I reasoned that inhibiting the Notch pathway during trabecular stages would lead to increased trabeculation. To test this hypothesis, I manipulated Notch activity by using two different Notch inhibitors, the γ-secretase inhibitor DAPT (Geling et al., 2002) or the LY411575 inhibitor (Ghaye et al., 2015). Both inhibitors were added at 48 hpf and the heart imaging was performed at 79 hpf, when apical constrictions are easy to observe and readily visible for counting. In order to find the right dosage and to confirm the efficiency of the inhibitors in the myocardium, I tested two different concentrations of DAPT, 50 and 100 μM, and 10 μM LY411575 in *Tg(TP1:VenusPEST);Tg(myl7:MKATE:CAAX)* embryos. DMSO-treated larvae showed Notch expression in some CMs in the compact-layer and in the AVC by 81 hpf (**Figures 14A-A'**). Upon treatment with DAPT (**Figures 14B-B'** and **Figures 14C-C'**) and LY411575 (**Figures 14D-D'**), larval hearts showed a lack of Notch reporter positive CMs in the myocardium as well as in the AVC, confirming the efficiency of the inhibitors. Next, I decided to investigate whether Notch inhibition has consequences in cardiac trabeculation. Then, I treated *Tg(TP1:H2B-mCherry);Tg(-0.2myl7:EGFP-podxl);Tg(myl7-MKATE-CAAX)* embryos with 50 and 100 μM DAPT at 48 and 60 hpf. After treatment, I found that control larvae at 79 hpf showed a normal number of apical constrictions (**Figures 14E-E'**). Interestingly, in DAPT-treated larvae the number of apical constrictions was unaffected (**Figures 14F-F'** and **Figure 14G**). The same results were found when Notch activity was inhibited with 100 μM

DAPT from 60 to 79 hpf (**Figure 14H**). In order to confirm these results, I also quantified the number of apical constrictions per heart after using 10 µM LY411575 or 50 µM DAPT. As observed after administration of 100 µM DAPT, both treatments led to no differences in the number of apical constrictions in between DMSO- and inhibitor-treated larvae (**Figure 14I**).

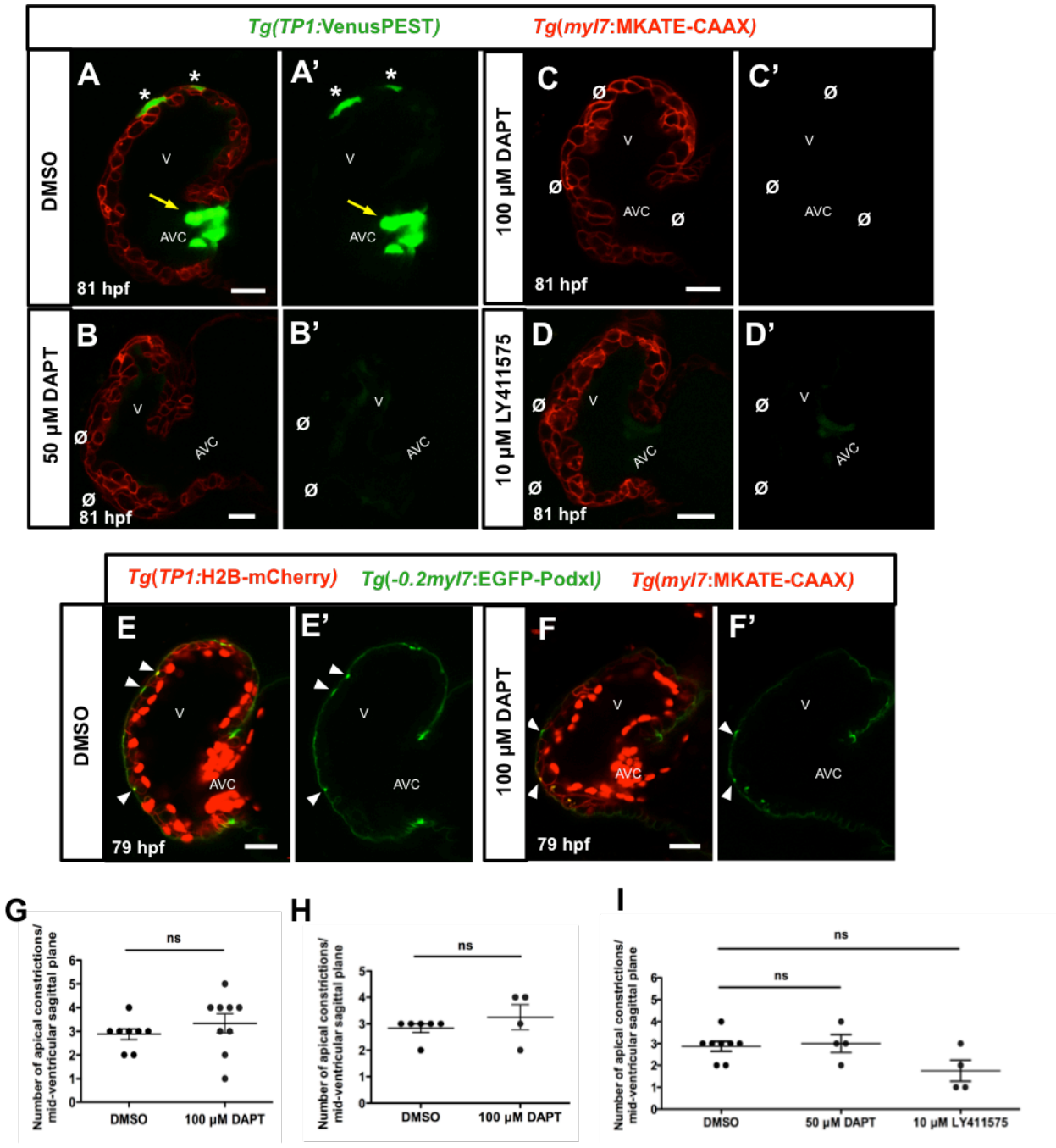

Figure 14. Blocking Notch signaling does not affect apical constriction formation.

(**A-D'**) Confocal images (mid-sagittal sections) of *Tg(TP1:VenusPEST); Tg(myl7:MKATE-CAAX*) 81 hpf larval hearts after DMSO (**A-A'**), 50 μM DAPT (**B-B'**), 100 μM DAPT (**C-C'**), and 10 μM LY411575 (**D-D'**) treatments. Asterisks in A-A' indicates *TP1*:VenusPEST-positive CMs and yellow arrow point to *TP1*:VenusPEST-positive cells in AVC. Lack of Notch activity is represented by Ø. (**E-F'**) Confocal images (mid-sagittal sections) of *Tg(TP1:H2B-mCherry);Tg(−0.2myl7:EGFP-podxl);Tg(myl7:MKATE-CAAX*) 79 hpf larval hearts. Arrowheads point to individual CM apical constrictions. Note that in these images (E-F') there is still some residual mCherry signal, due to the long half-life of this protein. Experiments done with VenusPEST, which half-life of the protein is shorter, confirmed the efficacy of the treatment (B-D'). Graphs showing number of CMs undergoing apical constrictions per ventricle at the mid-sagittal plane after 50 μM (**I**), 100 μM (**G, H**) DAPT treatments, or 10 μM (I) LY411575 treatment. Animals were incubated with DAPT at 48 hpf and imaged at 79 hpf (**G**), or at 60 hpf and imaged at 72 hpf (H). Each dot represents one heart. Data are shown as mean ± SEM. ns, no significant differences by Student's t test. V, ventricle; AVC, atrioventricular canal. Scale bars, 20 μm. Modified figure reprinted with permission from Jiménez-Amilburu et al., Cell Reports, 2016 Dec 6;17(10):2687-2699;11.023.

After Notch inhibitor treatments, I observed an increase in the compact wall thickness of larvae and changes in cardiac morphology. I decided to investigate whether this phenotype was due to an increase in CM delamination. In order to study these changes, I crossed *Tg(−0.2myl7:EGFP-podxl);Tg(myl7:MKATE-CAAX*) line with a CM nuclear line *Tg(-5.1myl7:DsRed2-NLS)*^{f2Tg} line (Mably et al., 2003), hereafter *Tg(myl7:nDsRed2)* and treated these embryos with 100 μM DAPT starting at 48 hpf. These transgenes allow one to distinguish individual CMs and count the number of trabecular CMs. I analyzed 24 stacks around the mid-sagittal region of the ventricle in 79 hpf DMSO- (**Figures 15A-A'**) or DAPT-treated larvae (**Figures 15B-B'**). I observed that CMs in the outer curvature in control larvae display elongated and squamous morphology, and the compact wall is well organized and single layered (**Figure 15A'**). In contrast, DAPT-treated hearts showed CMs with columnar shape, and a tightly packed and disorganized compact-layer (**Figure 15B'**). I have also quantified the percentage of trabecular CMs versus total number of CMs in the set of stacks imaged at 79 hpf and found that the number of trabecular CMs in DAPT-treated larvae did not increase compared to DMSO-treated larvae (**Figures 15C-D**). The quantification was done in two different regions of the outer curvature of the heart (**Figure 15C** and **Figure 15D**). In addition, to explore in more detail the formation of the trabecular network in the cardiac lumen after blocking Notch signaling, I performed 3D maximum projection and surface rendering of the larval ventricles at 79 and 98 hpf after treatment with DMSO and DAPT. While DMSO-treated fish at 79 (**Figures 15E-E'**) and 98 (**Figures 15G-G'**) hpf extend long trabecular ridges in the lumen of the heart, DAPT-treated larvae exhibit short and disorganized

ridges at 79 (**Figures 15F-F')** and 98 (**Figures 15H-H'**) hpf. Altogether, these data suggest that Notch signaling in the myocardium might not be involved directly in CM delamination from the compact to trabecular layers. (Certain lines in this section 4.1.7 have been quoted verbatim from Jiménez-Amilburu et al., Cell reports, 2016; 17(10):2687-2699;11.023).

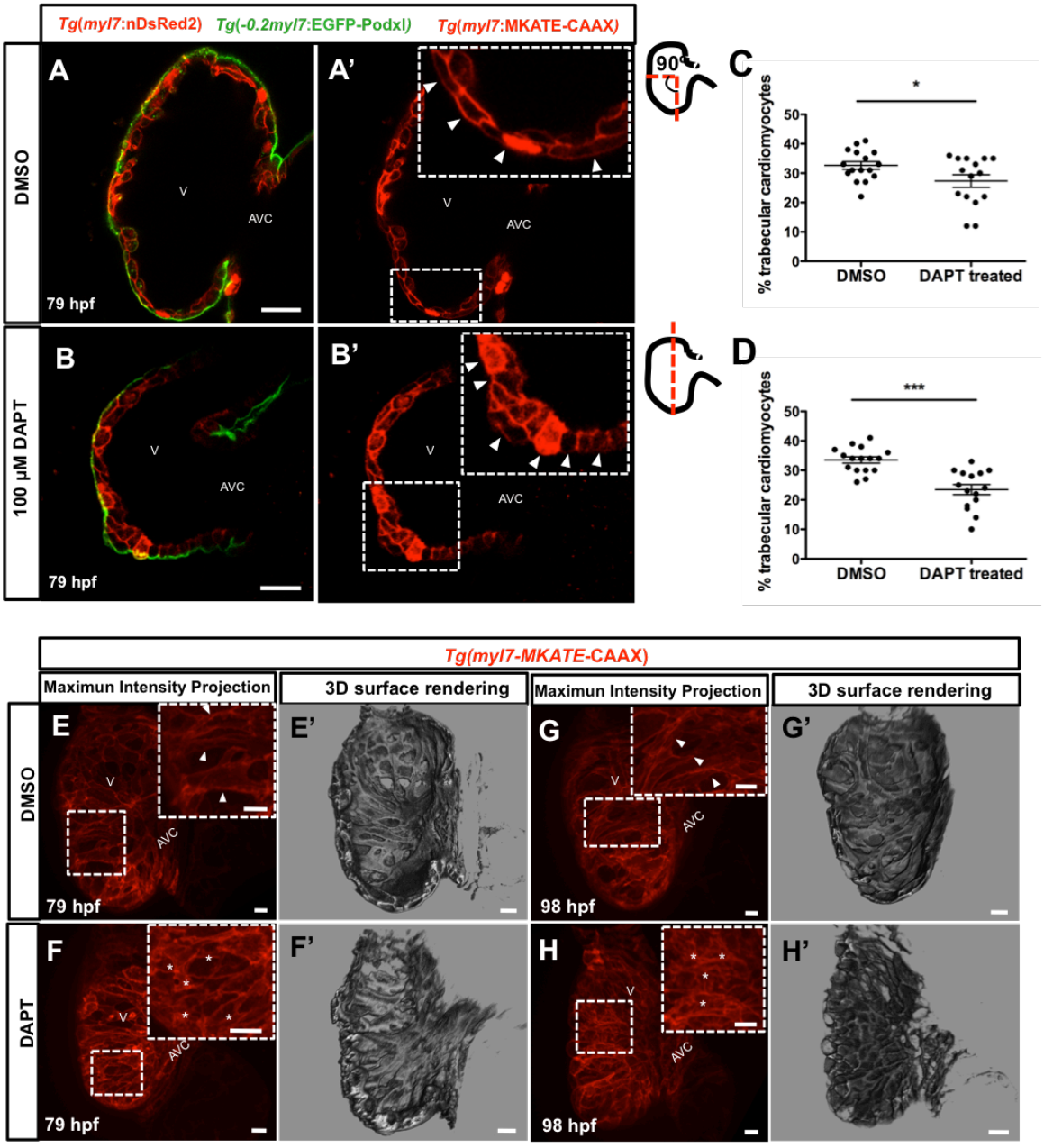

Figure 15. Blocking Notch signaling does not affect the number of trabecular CMs.

(**A-B'**) Confocal images (mid-sagittal sections) of *Tg(myl7:nDsRed2);(−0.2myl7:EGFP-podxl);Tg(myl7:MKATE-CAAX)* 79 hpf larval hearts. After DAPT treatment, larvae exhibit a disorganized compact wall (B-B', arrowheads) compared to DMSO-treated larvae (A-A', arrowheads). (**C-D**) Graphs showing percentage of trabecular CMs in DAPT versus DMSO-treated larvae in two regions of the outer curvature. Each dot represents

one heart. Data are shown as mean ± SEM. $^{*}P < 0.05$ and $^{***}P < 0.001$ by Student's t test. (**E-H'**) 3D maximum projection and surface rendering images of the cardiac lumen of DMSO- and DAPT-treated larvae at 79 (E-E' and F-F', respectively) and 98 (G-G' and H-H', respectively) hpf. Arrowheads in E and G point to trabecular ridges while asterisks in F and H indicate disorganized compact wall. V, ventricle; AVC, atrioventricular canal. Scale bars, 20 μm. Modified figure reprinted with permission from Jiménez-Amilburu et al., Cell Reports, 2016 Dec 6;17(10):2687-2699;11.023.

4.1.10 Blocking Notch activation in the myocardium does not increase cardiomyocyte proliferation

In order to investigate whether the observed heart phenotype after DAPT treatment was due to a dysregulation in CM proliferation, I used a recently generated Fucci line, *Tg(myl7:mVenus-gmnn),* which labels proliferating CMs in green. I crossed the *Tg(myl7:mVenus-gmnn)* line with the *Tg(myl7:nDsRed2)* line and treated embryos with 50 (data not shown) or 100 μM DAPT at 48 hpf (**Figures 16A-A′** and **Figures 16B-B′**) and with 100 μM DAPT at 60 hpf (**Figures 16C-C′** and **Figures 16D-D′**). I did not find any change in the number of proliferating CMs after DAPT treatments compared to DMSO controls (**Figure 16E** and **Figure 16F**). I also counted the total number of CMs per ventricle after DAPT treatments, and no significant differences were found (**Figure 16G** and **Figure 16H**). Altogether, these data show that Notch signaling in embryonic and larval CMs is activated by Nrg2a signaling; however, inhibiting Notch activity has no obvious effect on CM apical constriction, delamination, or proliferation. (Certain lines in this section 4.1.7 have been quoted verbatim from Jiménez-Amilburu et al., Cell reports, 2016; 17(10):2687-2699;11.023).

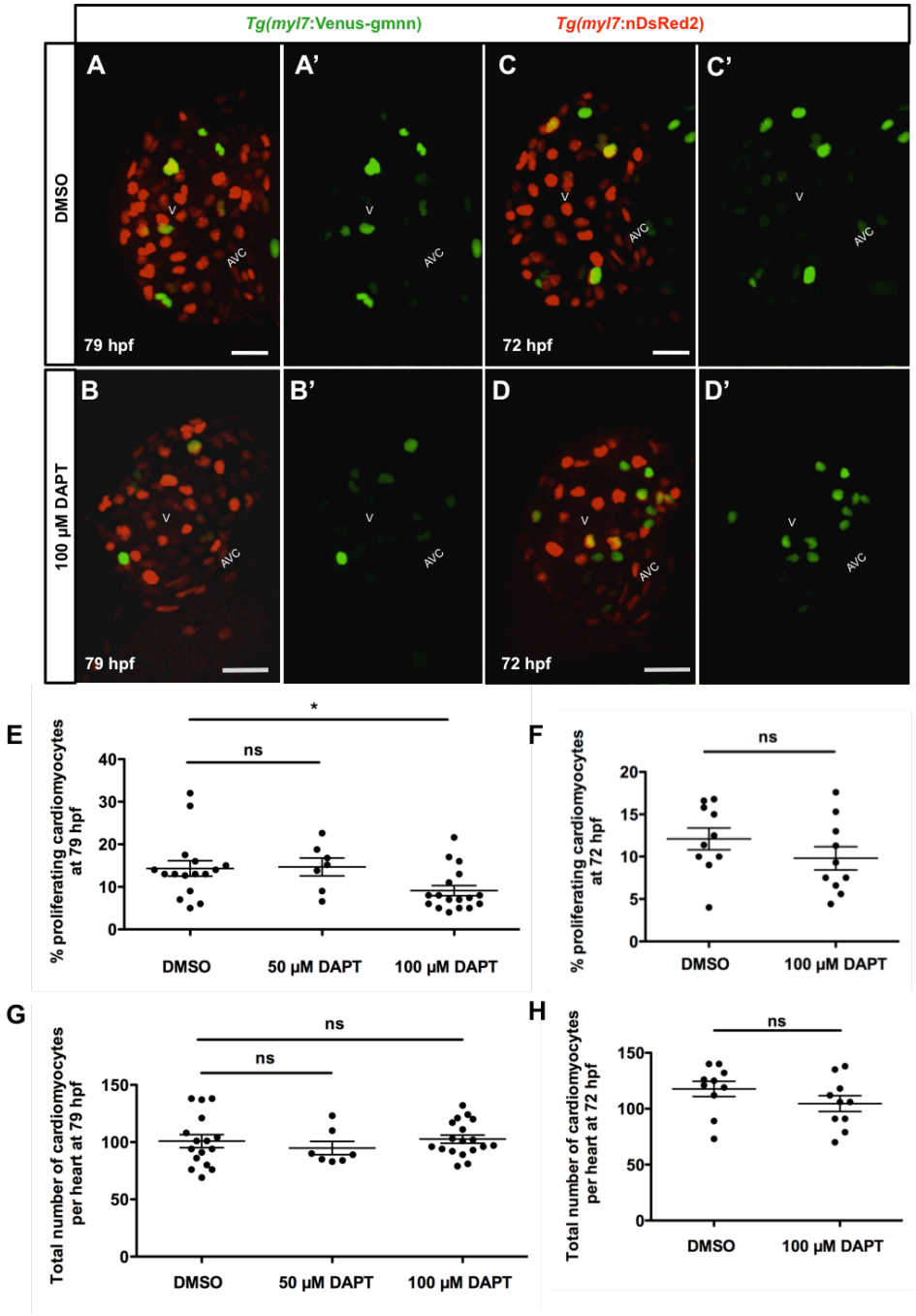

Figure 16. Inhibiting Notch signaling does not increase CM proliferation.

(**A-D'**) 3D spinning disk images at mid-sagittal plane of 79 (A-B') and 72 (**C-D'**) hpf *Tg(myl7:nDsRed2);Tg(myl7:mVenus-gmnn)* zebrafish hearts. DMSO-treated larvae showing *myl7*:mVenus-gmnn-positive CMs at 79 (A-A') and 72 (C-C') hpf. Larvae treated with 100 µM at 48 hpf, showing *myl7*:mVenus-gmnn-positive CMs at 79 (B-B') and 72 (D-D') hpf. Graph showing percentage of proliferating CMs at 79 (**E**) and 72 (**F**) hpf. Graph showing total number of ventricular CMs per heart at 79 (**G**) and 72 (**H**) hpf. Each dot represents one heart. Data are shown as mean ± SEM. ns, no significant differences by Student's t-test. V, ventricle; AVC, atrioventricular canal. Scale bars, 20 µm. Modified figure reprinted with permission from Jiménez-Amilburu et al., Cell Reports, 2016 Dec 6;17(10):2687-2699;11.023.

4.1.11 Proposed model

In this work, I proposed that CMs display apicobasal polarity and that this polarity is dynamically regulated during cardiac trabeculation (**Figure 17**).

1) Compact-layer CMs exhibit apicobasal polarity. Moreover, I establish for the first time that the apical domain of CMs faces the abluminal side of the ventricle.
2) Live imaging reveals that apical constriction precedes CM depolarization during CM delamination, suggesting an EMT-like process during cardiac trabeculation.
3) Nrg/ErbB2 signaling and blood flow/contractility are required for the formation of the apical constriction and CM depolarization
4) Notch signaling is activated in CMs adjacent to those undergoing apical constriction, however blocking Notch signaling does not alter the number of CMs undergoing apical constriction.

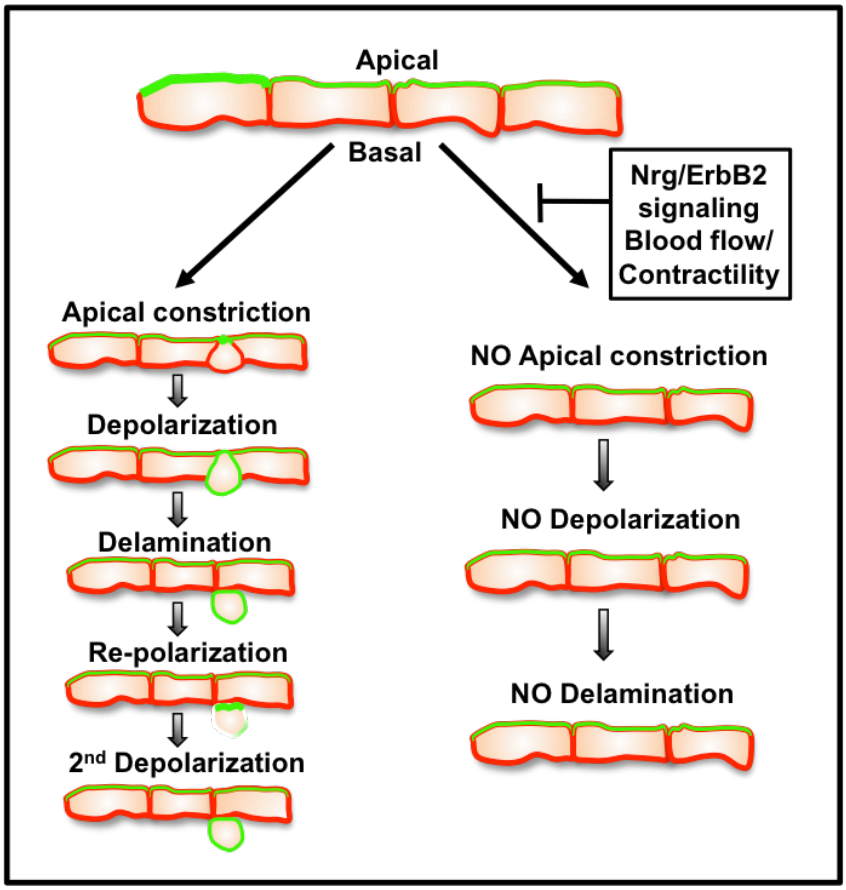

Figure 17. Proposed model (see text).

Modified figure reprinted with permission from Jiménez-Amilburu et al., Cell Reports, 2016 Dec 6;17(10):2687-2699;11.023.

4.2 Role of the polarity complex Crumbs in regulating the junctional rearrangement in cardiomyocytes during cardiac trabeculation in zebrafish

4.2.1 Crb2a localization in cardiomyocytes during apical constriction formation and cardiomyocyte delamination

After observing that CMs display apicobasal polarity and that they experience polarity changes during delamination, I set out to investigate how these changes are regulated.

During EMT, epithelial apicobasal polarity is regulated by the coordination of polarity complexes and cellular rearrangements, where the Crb complex plays a key role. As a consequence of the genome duplication in fish, Crb in zebrafish is present in 5 isoforms. In order to know which of these paralogs is the most relevant during cardiac trabeculation, I first performed a transcriptomic analysis using isolated zebrafish hearts at 52 hpf and 7 dpf, before and after the onset of cardiac trabeculation. These data sets revealed that *crb2a* is the highest crumbs isoform expressed in the heart before trabeculation occurs (**Figure 18**).

Gene	52 hpf	7 dpf
myl7	119046,5	100047,15
crb1	9,56	3,06
crb2a	225,38	90,53
crb2b	83,84	359,50
crb3a	Ø	Ø
crb3b	35,28	33,09

Figure 18. Expression of the five different Crb isoforms in the zebrafish heart.
Values are expressed as arbitrary units. The heart specific *myl7* gene serves as a reference. Ø stands for no detectable expression.

In order to gain understanding on the possible role for *crb2a* during cardiac trabeculation, I first performed Crb2a immunostaining together with ZO-1, a TJs marker, in *Tg(myl7:ras-GFP)* embryonic hearts at different developmental stages (**Figure 19**). At 50 hpf, when trabeculation has not been initiated, I found that Crb2a is highly enriched at the apical junctions in compact-layer CMs (**Figures 19A-A"**). Once trabeculation starts, at 74 hpf, Crb2a homogenously relocalizes to the entire apical membrane (**Figures 19B-B"**). This change of Crb2a

localization was also observed in 3D maximum intensity images at 51 (**Figure 19C**) and 72 hpf (**Figure 19D**). Of great interest is the fact that delaminated CMs were never found immunostained for Crb2a (**Figures 19B'-B"**). To confirm these observations, I also performed Crb2a immunostaining in *Tg(−0.2myl7:EGFP-podxl)* hearts at 50 and 79 hpf (**Figures 19E-F"**). Colocalization with this transgenic line confirmed that Crb2a transitions from a prominently junctional to an apical localization in compact-layer CMs, coinciding with the initiation of cardiac trabeculation.

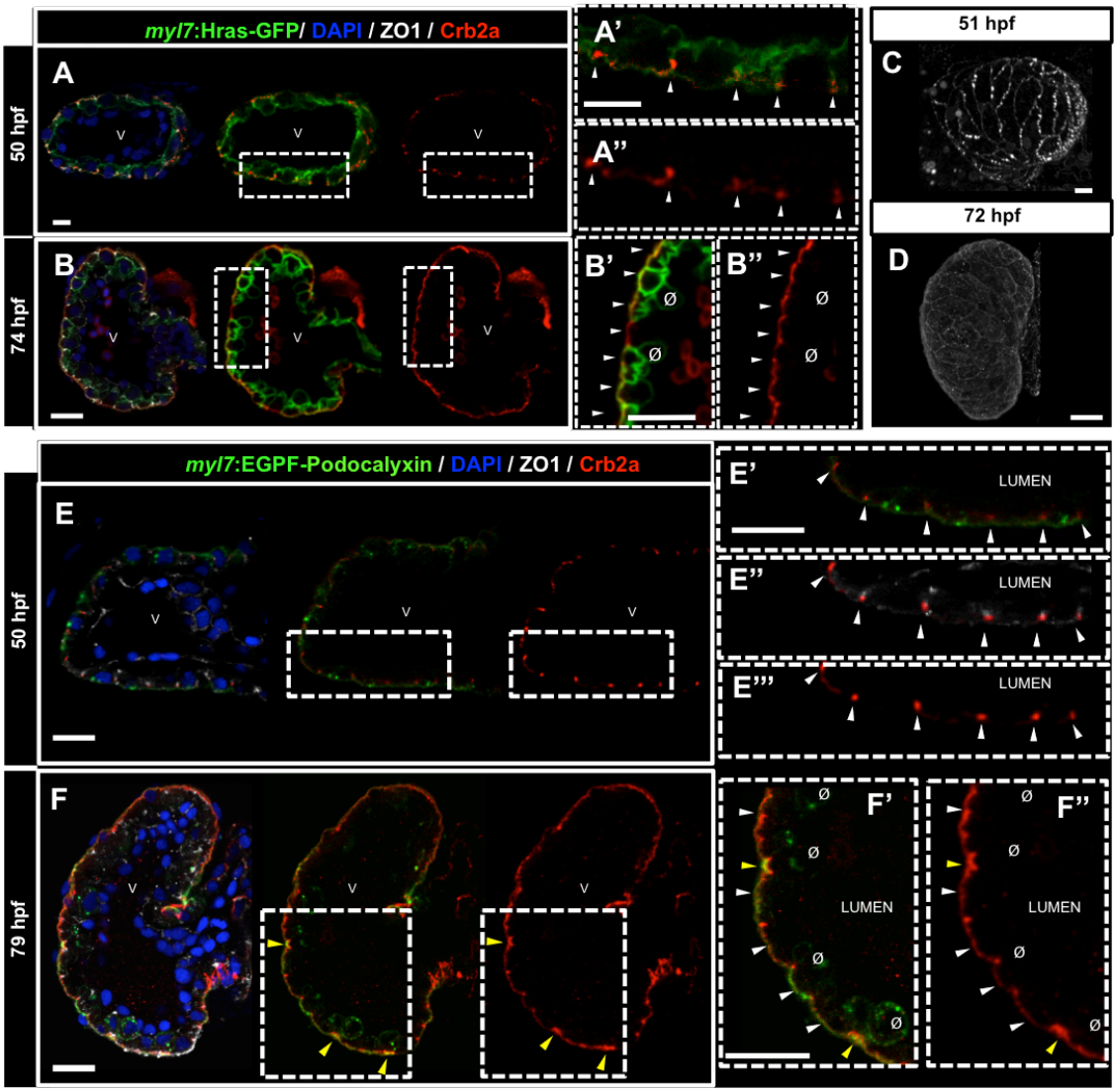

Figure 19. Crb2a localization during cardiac trabeculation in zebrafish.

(**A-B"**) Crb2a immunostaining in *Tg(myl7:Hras-GFP)* hearts at 50 (A-A") and 74 (B-B") hpf. At 50 hpf, Crb2a localizes to the junctions between CMs at the apical side (A'-A", arrowheads). At 74 hpf, Crb2a localization homogenously extends to the whole apical side of CMs (B'-B", arrowheads). (**C-D**) 3D reconstructed ventricles showing Crb2a localization at 51(C) and 72 (D) hpf. (**E-F"**) Crb2a immunostaining in *Tg(−0.2myl7:EGFP-podxl)* hearts at 50 (E-E'") and 79 (F-F") hpf. At 50 hpf, Crb2a localizes to the junctions between CMs at the apical

side, coinciding with ZO-1 (E'-E'", white arrowheads). At 79 hpf, CMs undergo apical constriction (F, yellow arrowheads). Crb2a accumulates to the constricting apical membrane of CMs, coinciding with Podocalyxin localization (F'-F", yellow arrowheads). Moreover, Crb2a expression extends to the apical membrane of compact-layer CMs (F'-F", white arrowheads). Crb2a expression was not observed at 74 (B'-B", Ø) or 79 (F'-F", Ø) hpf in the delaminated CMs. V, ventricle. Scale bars, 20 µm.

4.2.2 ErbB2 signaling and epicardial cues might be involved in the regulation of Crb2a localization

In order to explore whether there is a role for Crb during cardiac trabeculation, I investigated whether ErbB2 signaling regulates Crb2a localization in CMs.

First, I treated *Tg(myl7:Hras-GFP)* 54 hpf embryos, before trabeculation starts, with 10 µM PD168393, an ErbB2 inhibitor, or DMSO as control. Then, I fixed both, DMSO and PD168393-treated larvae at 96 hpf and immunostaining for Crb2a was performed. In the case, of 96 hpf DMSO-treated larvae, Crb2a is localized homogenously in the apical membrane of compact-layer CMs (**FigureS 20A-A"**). Interestingly, in PD168393-treated larvae, at the same stage, Crb2a was found highly enriched at the junctions of compact-layer CMs (**Figures 20B-B"**). Junctional enrichment of Crb2a in PD168393-treated larvae was also quantified (**Figure 20C**).

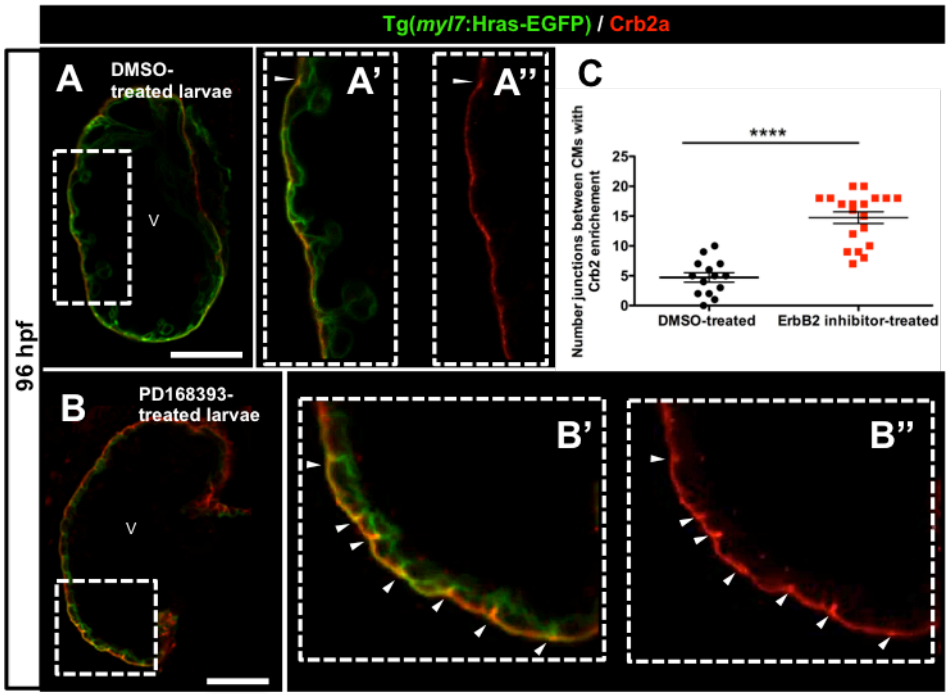

Figure 20. ErbB2 signaling regulates Crb2a localization in CMs.

(**A-B"**) Crb2a immunostaining in *Tg(myl7:Hras-GFP)* hearts treated with DMSO (A-A") or PD168393 (B-B") at 96 hpf. Arrowheads in higher magnification images point to Crb2a enrichment at the junctions between CMs in DMSO (A'-A") and PD168393-treated larvae (B'-B"). (**C**) Quantification of number of junctions between CMs with Crb2a enrichment (DMSO-treated larvae n=14; ErbB2 inhibitor-treated larvae n=19). Each dot represents one heart. Data are shown as mean ± SEM. ****$P < 0.0001$ by Student's t test. v, ventricle.

Then, since it is known that paracrine cues from the epicardium are important for myocardial growth (Braitsch et al., 2013), I wanted to know if epicardial cues might be also affecting Crb2a localization. First I crossed the *Tg(tcf21-mCherry-NTR)*^{pd108} line, hereafter *Tg(tcf21-mCherry-NTR),* for epicardial ablation with *Tg(myl7:Hras-EGFP)* line. Then I selected double positive embryos for mCherry and EGFP and I incubated the embryos with 2 mM metronidazole (MTZ) from 54 to 96 hpf. After MTZ incubation, 96 hpf ventricles did not show any mCherry positive cell in the epicardium, suggesting that the epicardial ablation was complete. At 96 hpf, DMSO-treated larvae show an average of 5 junctions between CMs with Crb2a enrichment (**Figures 21A-A"** and **Figure 21C**), while MTZ-treated larvae exhibit a significant increase in junctions showing Crb2a enrichment (average of 18) (**Figures 21B-B"** and **Figure 21C**). Altogether, these data suggest that both ErbB2 signaling and the epicardium are involved in the regulation of Crb2a localization in CMs.

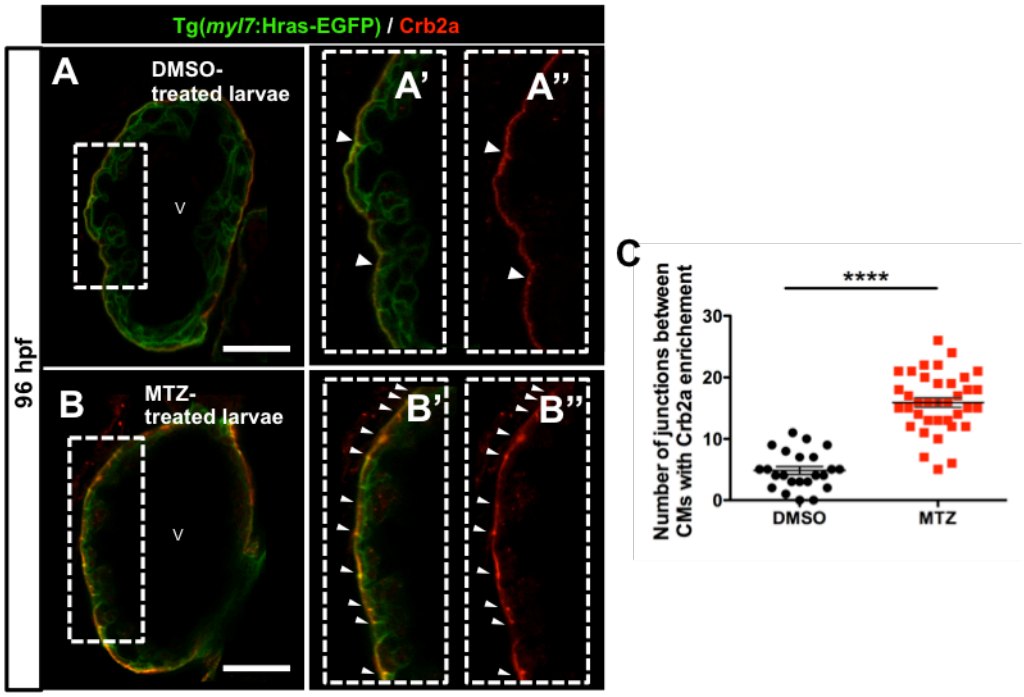

Figure 21. Crb2a relocalizes in CMs upon epicardial ablation.

(**A-B"**) Crb2a immunostaining in *Tg(tcf21:mCherry-NTR);Tg(myl7:Hras-GFP)* hearts treated with DMSO (A-A") or MTZ (B-B") at 96 hpf. Arrowheads in higher magnification images point to Crb2a enrichment at the junctions between CMs in DMSO (A'-A") and MTZ-treated larvae (B'-B"). (**C**) Quantification of number of junctions between CMs with Crb2a enrichment (DMSO-treated larvae n=22; MTZ-treated larvae n=37). Each dot represents one heart. Data are shown as mean ± SEM. $^{****}P < 0.0001$ by Student's t test. v, ventricle.

4.2.3 Analysis of early defects in *crb2a* mutants

To investigate if c*rb2a* is required for early heart development, I studied the *crb2a*$^{m298/m298}$. The zebrafish *crb2a*$^{m298/m298}$ was originally named as *ome* (Malicki et al., 1996). The *ome* locus was first identified in a large-scale ENU screening to find genetic embryogenesis defects in the development of zebrafish retina (Malicki et al., 1996). In that study, they found that the *ome* locus encodes the polarity gene *Crb2a* (Omori and Malicki, 2006). The genetic lesion consists of a point mutation (764A>T;764Arg>STOP) in the exon 8 which leads to a truncated protein where the extracellular domain is affected (Omori and Malicki, 2006).

Then, to understand how early is Crb2a required for heart development, I analyzed maximum intensity projection images of 36-38 hpf embryos (**Figure 22**). *crb2a*$^{m289/m289}$ were crossed into *Tg(−0.2myl7:EGFP-podxl);Tg(myl7:MKATE-CAAX)* lines. Spinning disc confocal images show that all mutants analyzed exhibited either no heart looping (**Figure 22C**) or delay in the looping formation (**Figure 22C'**) when compared to WT or heterozygous embryos (**Figure 22A-B**).

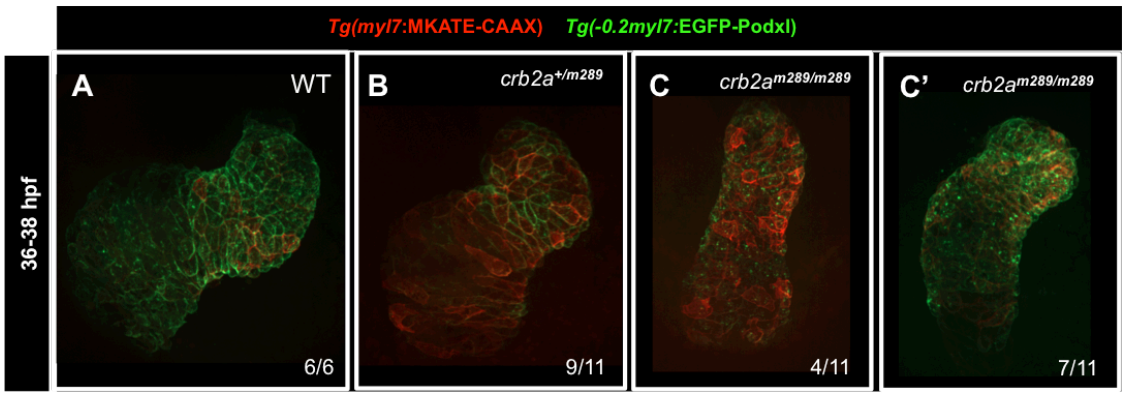

Figure 22. *crb2a*$^{m289/m289}$ exhibit looping defects.

(**A-C'**) 3D Maximum intensity images of *(−0.2myl7:EGFP-podxl);Tg(myl7:MKATE-CAAX)* 36-38 hpf embryonic hearts.

As previously reported, *crb2a* $^{m289/m289}$ display defects in blood flow (Malicki et al., 1996). I found that 40% of the mutants have no or very low number of circulating blood cells while 60% still present normal circulation (**Figure 23D**). In order to be consistent and rule out the possible side effects on the heart due to lack of circulation, for all my experiments I used only mutants displaying normal blood flow/circulation. Next, I examined cardiac performance in *crb2a* $^{m289/m289}$ by studying atrial fractional shortening (FS), which compares diastole and systole measurements during heart contraction (FS= (diastole length-sistole length/diastole length) X 100). I acquired brightfield images of 48 hpf beating hearts using spinning disc, and calculated the atrial FS (**Figures 23A-C'**). In this case I examined *crb2a*$^{+/+}$, *crb2a*$^{+/m289}$ and *crb2a* $^{m289/m289}$ with and without circulation. The results show that *crb2a*$^{m289/m289}$ without circulation display a severe significant decrease in FS compared to WT, while *crb2a* $^{m289/m289}$ with circulation present a slight, but not significant, reduction in FS (**Figure 23E**).

To rule out the possibility that defects in sarcomere structure were causing this slight reduction of FS in *crb2a* $^{m289/m289}$ with circulation, I stained for α-Actinin. CM sarcomeres were analyzed at 80 hpf and found that mutant hearts display normal sarcomere organization compared to WT hearts (**Figures 23F-G'**).

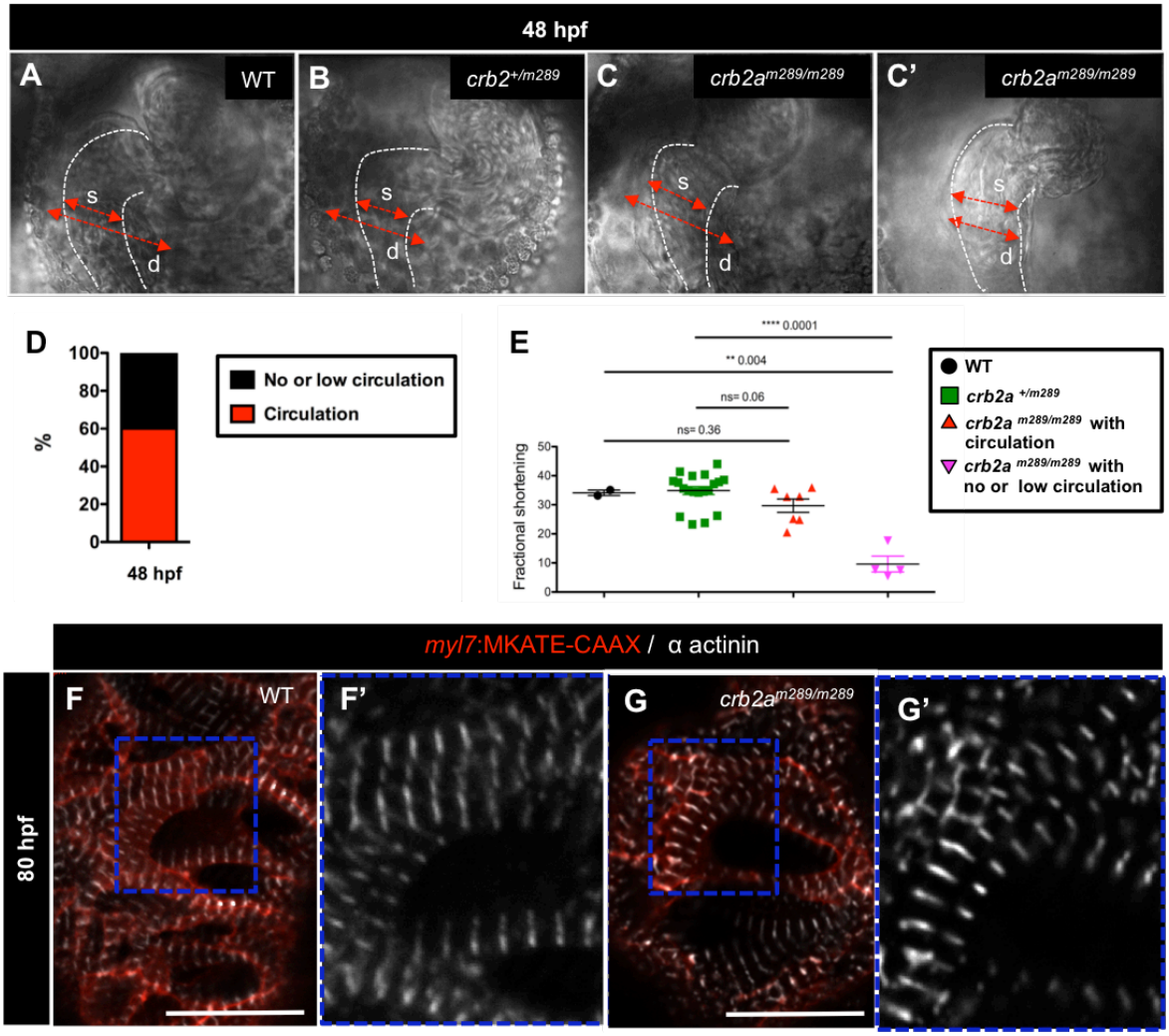

Figure 23. Analyses of FS and CM sarcomere structure in *crb2a*$^{m289/m289}$.

(**A-C'**) Brightfield images of 48 hpf embryonic hearts. Red arrows indicate length of diastole (d) and systole (s). White dashed lines represent the heart shape in systole. (**D**) Graph showing percentage of mutant embryos with normal and with no or low circulation at 48 hpf. The total number of embryos analyzed, 650, total number of mutants analyzed, 124. (**E**) FS measurements in WT, *crb2a*$^{+/m289}$ and *crb2a* $^{m289/m289}$ (with circulation (n=50), low or no circulation (n=74). Data are shown as mean ± SEM. "$P < 0.001$, ""$P < 0.0001$ by Student's t test. (**F-G'**) Confocal images of α-actinin immunostaining in *Tg(myl7:MKATE-CAAX)* 80 hpf larval hearts. Blue boxes show high magnification images of the α-actinin immunostaining in WT (I') and *crb2a* $^{m289/m289}$ (J'). Scale bars, 20 μm.

4.2.4 *crb2a*$^{m289/m289}$ exhibit a disorganized compact wall, fail to form trabeculae and display altered cardiomyocyte polarity

To further investigate whether the polarity complex Crb has a role during cardiac trabeculation, I set out to study the *ome* mutant, hereafter referred as *crb2a* $^{m289/m289}$. To be able to carefully characterize CM morphology during development and specially trabeculation, I crossed *crb2a*$^{+/m289}$ with the CM membrane reporter line *Tg(myl7:MKATE-CAAX)*. I imaged

crb2a $^{m289/m289}$ after the onset of trabeculation and found that *crb2a* $^{m289/m289}$ fish exhibit a smaller and more rounded heart compared to WTs (**Figure 24A** and **Figure 24B**). Next, I analyzed trabeculation at 80 hpf and found that, while WT hearts display a compact wall composed of a single layer of CMs and few delaminated CMs, the mutant ventricular compact wall is composed by two layers of CMs and appears disorganized (**Figures 24A'-A", Figures 24B'-B"** and **Figures 24E-E'**). Interestingly, CMs in the compact-layer of *crb2a* mutants seem to be more elongated that WT CMs. Moreover, I imaged the same larvae over time until 98 hpf and observed that while WT hearts display a complex network of trabeculae in the lumen of the ventricle, mutants do not exhibit myocardial protrusions and fail to form trabeculae (**Figures 24C-C'** and **Figures 24D-D'**). In conclusion, *crb2a* $^{m289/m289}$ display a disorganized compact wall and fail to form and extend trabeculae.

To gain insight into the polarization of mutant CMs, I crossed *crb2a*$^{+/m289}$ into *Tg(-0.2myl7:EGFP-podxl); Tg(myl7:MKATE-CAAX)* lines. As shown before, EGFP-Podocalyxin it WT ventricles at 80 hpf could be observed apically in compact-layer CMs and all around the membrane of those delaminating (**Figures 24F-F'**). Conversely, mutant ventricles presented a bi-layered compact wall with CMs in both layers displaying apical localization of EGFP-Podocalyxin (**Figures 24G-G'**).

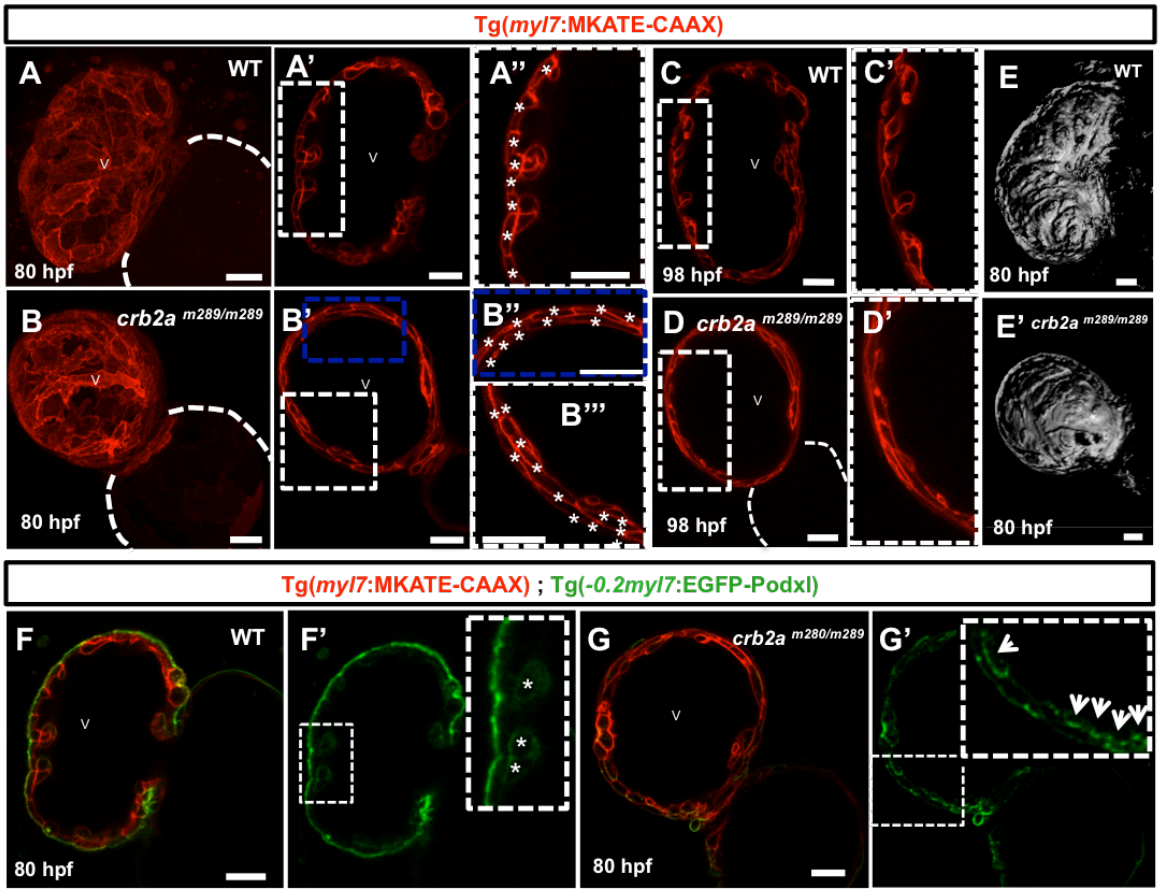

Figure 24. *crb2a*$^{m289/m289}$ hearts exhibit a disorganized compact wall, fail to form trabeculae and CM polarity is affected.

(**A-B**) Confocal images (Maximum intensity projections) of *Tg(myl7:MKATE-CAAX)* ***crb2a***$^{m289/m289}$ (A) and WT (B) hearts at 80 hpf. (**A'-D'**) Confocal images (mid-sagittal sections) of *Tg(myl7:MKATE-CAAX)* hearts of WT (A-A" and C-C') and *crb2a*$^{m289/m289}$ (B-B" and D-D') at 80 and 98 hpf respectively. (**E-E'**) 3D surface rendering images of WT (E) and mutant (E') ventricles at 80 hpf. Asterisks in A" and B" mark individual CMs. (**F-G'**) Confocal images (mid-sagittal sections) of *Tg(−0.2myl7:EGFP-podxl);Tg(myl7:MKATE-CAAX)* hearts of WT (F-F') and *crb2a*$^{m289/m289}$ (G-G') at 80 hpf. Asterisks in F' show delaminated CMs and arrows in G' point to polarized CMs. V, ventricle. Scale bars, 20 µm.

To further confirm whether the second layer of CMs in *crb2a*$^{m289/m289}$ have trabecular identity, I stopped cardiac contraction by injecting *tnnt2a* MO into in mutant embryos at one-cell stage. As previously described, lack of blood flow/contractility prevents cardiac trabeculation. Thus, *crb2a*$^{+/m289}$ larvae injected with *tnnt2a* MO show a single layer of CMs and no trabeculae (**Figures 25A-B**). It was interest to notice that after *tnnt2a* MO injection in *crb2a*$^{m289/m289}$ I was not able to rescue the multilayer heart phenotype (**Figures 25C-D**). These data support that the second layer of compact CMs in *crb2a*$^{m289/m289}$ are not trabecular. However, it remains to be clarified whether still some of the CMs observed in this second layer have previously

delaminated. Careful analysis and quantification of apical contractions and CM depolarization will be required. Taken together, these data show that Crb2a plays a role during cardiac trabeculation.

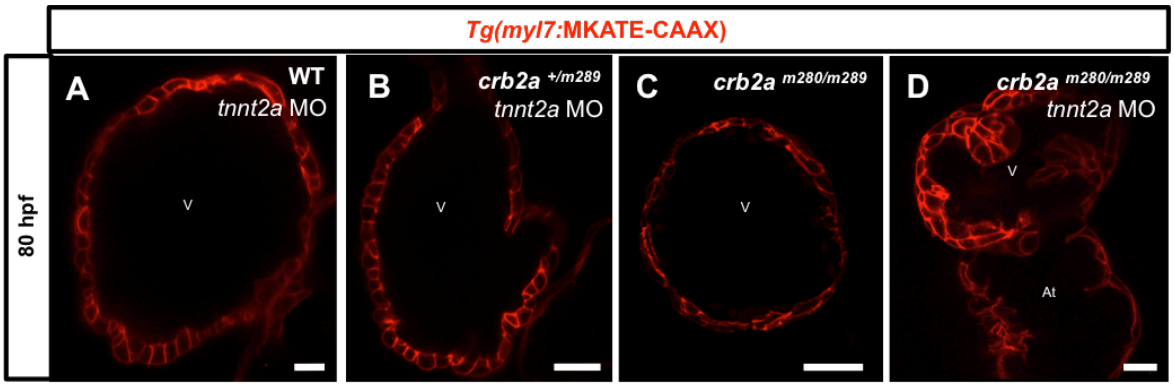

Figure 25. Multilayering phenotype in *crb2a*$^{m289/m289}$ hearts cannot be rescued by blocking contractility. (**A-D**) Confocal images (mid-sagittal sections) of *Tg(myl7:MKATE-CAAX)* hearts of WT, *crb2a*$^{+/m289}$, *crb2a*$^{m289/m289}$ hearts after *tnnt2a* MO injection at 80 hpf. (**A-B**) WT and *crb2a*$^{+/m289}$ embryos display a single layer of CMs. (**C**) Uninjected *crb2a*$^{m289/m289}$ display multilayering in the ventricle. (**D**) Injection of *tnnt2a* MO in *crb2a*$^{m289/m289}$ does not rescue the multilayering phenotype. V, ventricle; At, atrium. Scale bars, 20 µm.

Cardiac jelly is necessary for the correct endocardium-myocardium crosstalk that regulates developmental cardiac morphogenesis, and its degradation coincides with the onset of trabeculation (Del Monte et al., 2007; Rasouli and Stainier, 2017). Thus, I reasoned that *crb2a*$^{m289/m289}$ could present alterations in cardiac jelly thickness. In order to be able to visualize *in vivo* cardiac jelly thickness (delimited by both endocardial and myocardial layers), I crossed *crb2a*$^{m289/m289}$ into the *Tg(kdrl:EGFP)*^{s843} (Jin et al., 2005), hereafter *Tg(kdrl:EGFP)* and *(myl7:MKATE-CAAX)* lines. Analysis of larval hearts at 80 and 100 hpf revealed no differences in cardiac jelly thickness between WT and mutants animals (**Figure 26**).

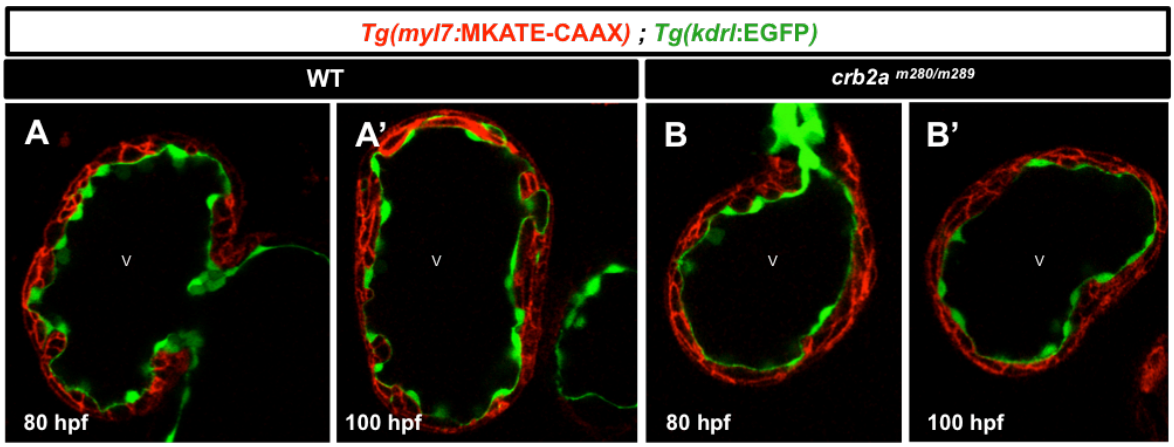

Figure 26. Cardiac jelly reduction is not affected in *crb2a*$^{m289/m289}$.

(**A-B'**) Confocal images (Maximum intensity projections) of *Tg(myl7:MKATE-CAAX);Tg(kdrl:EGFP)* hearts at 80 (A-A') and 100 (B-B') hpf. V, ventricle. Scale bars, 20 μm.

4.2.5 Increased number of cardiomyocytes in *crb2a*$^{m289/m289}$ ventricles

Crb is involved in tissue growth, and cell proliferation and survival. Thus, disrupting polarity might cause overgrowth, excessive and uncontrolled proliferation, and apoptosis (Genevet and Tapon, 2011; Kolahgar et al., 2011; Laprise, 2011). To understand if the *crb2a*$^{m289/m289}$ heart phenotype was due to and excess of CM proliferation, I quantified at 80 hpf the total number of CMs in WT and mutants *Tg(myl7:MKATE-CAAX)* ventricles stained for DAPI (**Figure 27A** and **Figure 27B**). I imaged the whole ventricle and quantified the number of DAPI+ CMs in both compact and trabecular layers. I measured 10 different ventricular planes, each plane every 5 μm. I found that *crb2a*$^{m289/m289}$ hearts showed an increased number of CMs in the ventricle compared to WT hearts (**Figure 27C**). In order to confirm whether this increase in number of CMs is due to proliferation in *crb2a*$^{m289/m289}$, further experiments assessing CM proliferation in these mutants will be performed.

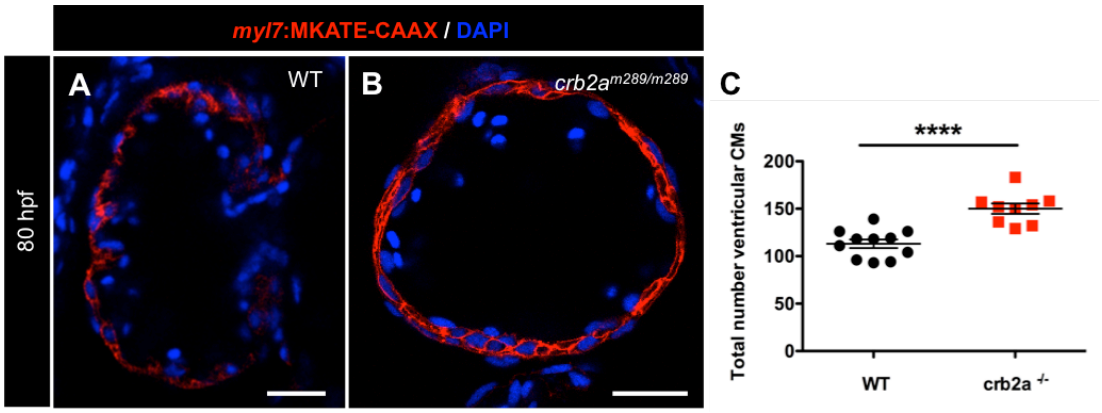

Figure 27. Increase number of CM in *crb2a*$^{m289/m289}$ ventricles.

(A-B) Confocal images (mid-sagittal sections) of *Tg(myl7:MKATE-CAAX)* hearts of WT (A) and ***crb2a***$^{m289/m289}$ (B) immunostained with DAPT at 80 hpf. (**C**) Graph showing quantification of DAPI+ CMs in WT and mutant ventricles. Each dot represents one heart. Data are shown as mean ± SEM. ****$P < 0.0001$ by Student's t test. Scale bars, 20 μm.

4.2.6 Tight and adherens junctions are mislocalized in the compact wall cardiomyocytes of *crb2a*$^{m289/m289}$

Tissue integrity, cell shape changes, apicobasal polarity organization, and cell-cell contacts are essential features to ensure the correct migration of epithelial cells during morphogenesis and oncogenesis (Paluch and Heisenberg, 2009; Pilot and Lecuit, 2005; Wang et al., 2011). Crb

complex, TJs, and AJs are closely inter-linked in the apico-lateral domain of epithelial cells (Assémat et al., 2008; Médina et al., 2012). Disruption of this polarity complex has been shown to cause ZO-1 and N-Cadherin disruption in cells in *Drosophila* (Grawe et al., 1996; Izaddoost et al., 2002). To further study the role of TJs and AJs and its possible regulation by *crb2a* during cardiac trabeculation, I performed immunostaining for Crb2a and ZO-1 in the *TgBAC(cdh2:cdh2-EGFP,crybb1:ECFP)*^{zf517} line, hereafter *TgBAC(cdh2:cdh2-EGFP)* that labels the adherens junction protein N-Cadherin (Cdh2) (Revenu et al., 2014). At 54 hpf (**Figures 28A-A'**), ZO-1 localizes to the junctions but also apically in the CM membrane, contrary Crb2a is highly enriched at the junctions, as shown before, overlapping with ZO-1. N-Cadherin localizes laterally in the membrane of compact-layer CMs (Cherian et al., 2016) and Crb2a and N-Cadherin do not colocalize in CMs at this stage. Later at 80 hpf (**Figures 28B-B'**), ZO-1 becomes restricted at the junctions between CMs, Crb2a localizes apically in compact-layer CMs, and then Crb2a and ZO-1 do not colocalize anymore at the junctions. Now, N-Cadherin localizes baso-laterally in CMs (Cherian et al., 2016).

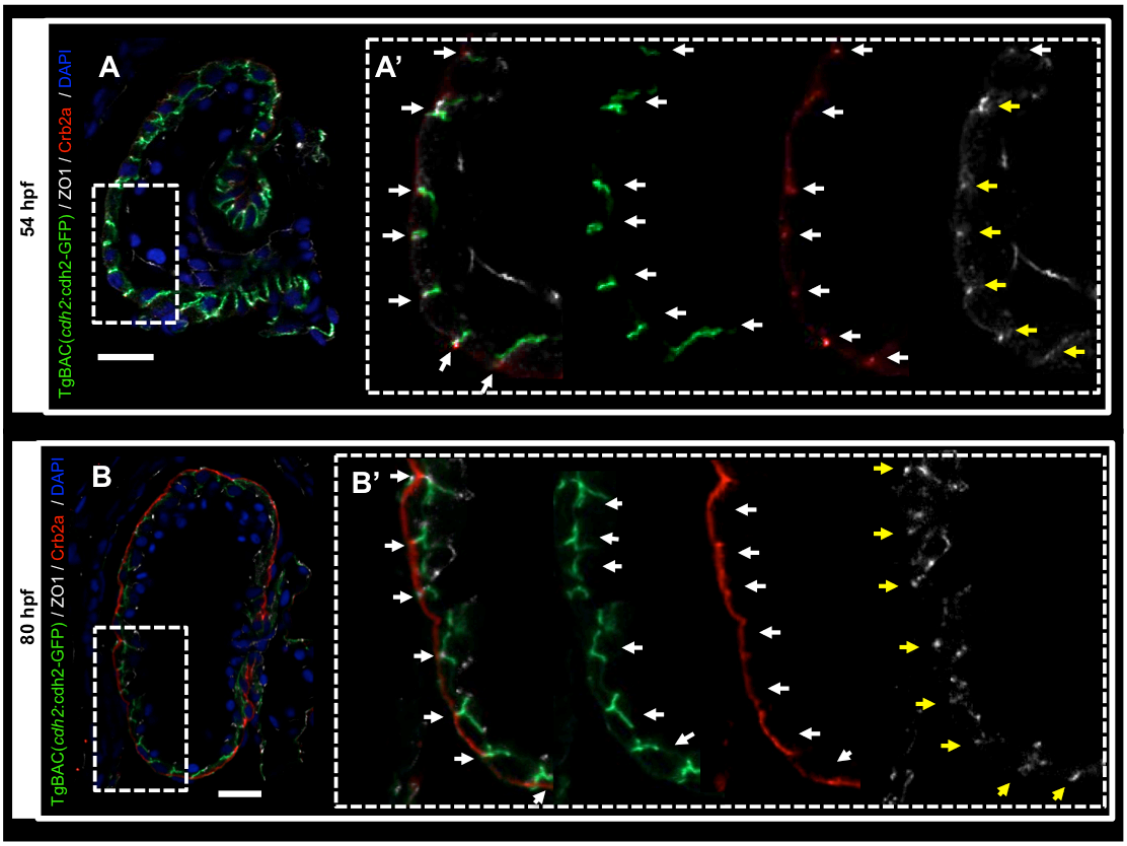

Figure 28. Localization of TJs, AJs, and Crb2a in CMs during cardiac trabeculation.

Crb2a and ZO-1 immunostainings in *TgBAC(cdh2:cdh2-GFP)* hearts at 54 (A-A') and 80 (B-B') hpf. White arrows point to N-Cadherin and Crb2a localization and yellow arrows point to ZO-1 staining in A' and B'. Scale bars, 20 μm.

Cardiac wall structure and CM morphology are also crucial for the correct CM delamination and formation of trabeculae in zebrafish (Lai et al., 2018; Liu et al., 2010). In order to understand the multilayering phenotype in *crb2a* $^{m289/m289}$, I set out to investigate TJs and AJs in CMs by immunostaining in these mutants. Maximum intensity projection images revealed that while ZO-1 is localized at the junctions in WT CMs at 79 hpf (**Figures 29A-A'**), *crb2a* $^{m289/m289}$ ventricles exhibit mislocalized distribution of ZO-1 (**Figures 29B-B'**). Similar to our observation with the *TgBAC(cdh2:cdh2-EGFP)* line, I confirmed by immunostaining that N-Cadherin is localized laterally at 79 hpf in WT CMs (**Figures 29C-C''**). However, analysis of maximun intensity projection images of *crb2a* $^{m289/m289}$ ventricles at this stage show that the N-Cadherin pattern is lost in CMs (**Figures 29D-D'**). In more detail, single plane images of the *crb2a* $^{m289/m289}$ hearts show N-Cadherin distributed as a punctate in both apical and basal CM membranes (**Figure 29D''**).

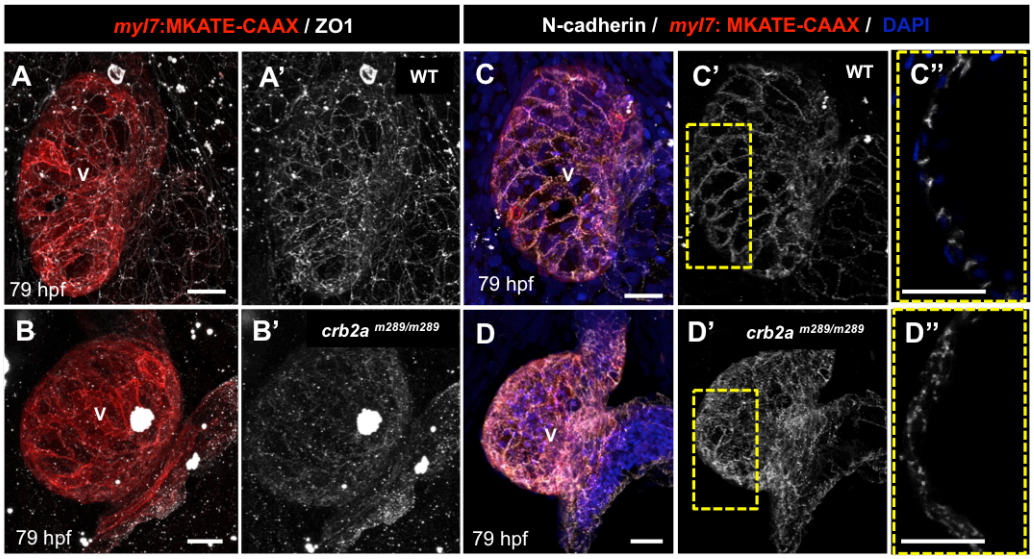

Figure 29. TJs and AJs are mislocalized in *crb2a*$^{m289/m289}$.

(**A-B'**) ZO-1 immunostaining in *Tg(myl7:MKATE-CAAX)* hearts at 79 hpf. Maximum intensity projection images show that ZO-1 localizes to the junctions between CMs in WT (A'), while are mislocalized in *crb2a*$^{m289/m289}$ (B'). (**C'-D'**) N-Cadherin immunostaining and DAPI in *Tg(myl7:MKATE-CAAX)* hearts at 79 hpf. Maximum intensity projection images show that N-Cadherin localizes at the junctions between CMs in WT embryos (C') but is mislocalized at the junctions of CMs in *crb2a*$^{m289/m289}$ (D'). (**C"-D"**) Confocal images (mid-sagittal sections) of *Tg(myl7:MKATE-CAAX)* hearts. High magnifications of single plane images show the lateral localization of N-Cadherin between CMs in WTs (C"), while in *crb2a*$^{m289/m289}$ N-Cadherin appears mislocalized and disorganized in compact-layer CMs (D"). V= ventricle. Scale bars, 20 μm.

4.2.7 Crb2a might drive the fate of trabecular cardiomyocytes

Lastly, I wanted to test whether Crb2a has a role in CMs during cardiac trabeculation. To answer this question, I generated chimeric embryos by transplanting *crb2a*$^{m289/m289}$ *Tg(myl7:MKATE-CAAX)* CMs at mid-blastula stage into WT *Tg(myl7:Hras-GFP)* animals. After transplantation, larvae were imaged at 100 hpf and later genotyped. Interestingly, I found that while WT and *crb2a*$^{+/m289}$ CMs transplanted into WT ventricles localized in both compact and trabecular layer, transplanted *crb2a*$^{m289/m289}$ CMs where always found trabecular (**Figures 30A-C**). To confirm these observations I quantified the number of transplanted CMs in both compact and trabecular layers in chimeric larvae at 100 hpf. Indeed, I was able to confirm that *crb2a*$^{m289/m289}$ CMs populate the trabecular layer of WT transplanted ventricles (**Figure 30D**). These data show that Crb2a functions cell-autonomously in CMs and suggest a possible role for Crb2a in driving the fate of trabecular CMs during cardiac trabeculation.

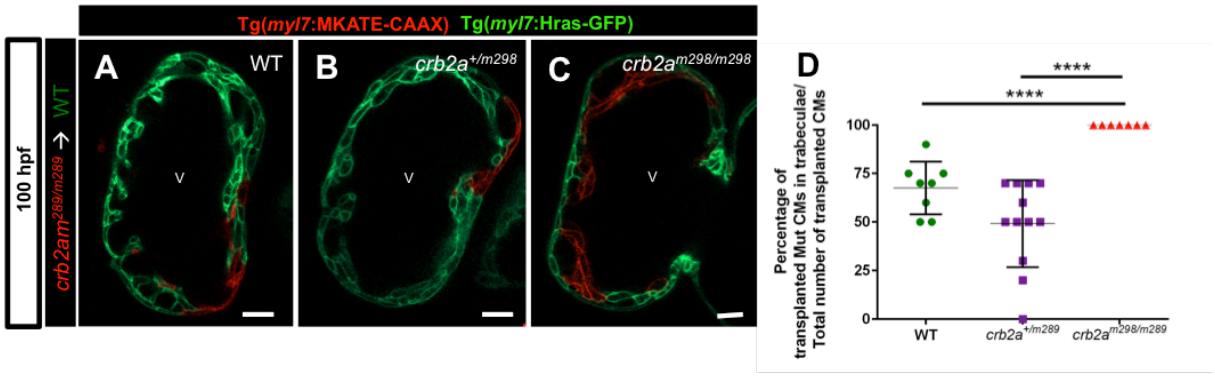

Figure 30. Crb2a might drive fate of trabecular CMs.

(**A-C**) Confocal images (mid-sagittal sections) of mosaic WT *Tg(myl7:Hras-GFP)* hearts at 100 hpf transplanted with *Tg(myl7:MKATE-CAAX)* mutant CMs. (**D**) Graph showing the percentage of transplanted mutant hearts in trabeculae versus compact-layer. Each dot represents one heart. Data are shown as mean ± SEM. ****$P <$ 0.0001 by Student's t test. Scale bars, 20 μm.

4.2.8 Proposed model

I proposed that Crumbs has a role in coordinating CM polarity and junctional rearrangements during cardiac trabeculation in zebrafish (**Figure 31**).

1) Crb2a is enriched at the junctions in compact-layer CMs and relocalizes to the entire apical membrane during the onset of trabeculation. Blocking Nrg/Erbb2 signaling or epicardial ablation lead to an increase in junctional Crb2a between CMs at 96 hpf.
2) *crb2a* $^{m289/m289}$ display a bilayer of disorganized CMs in the compact wall and fail to form trabeculae.
3) TJ reorganization in CMs is likely to play a role during CM delamination. Moreover, *crb2a* $^{m289/m289}$ exhibit mislocalization of both TJs and AJs.
4) Crb2a might be involved in regulating TJs and AJs, and driving the fate of trabecular CMs during cardiac trabeculation.

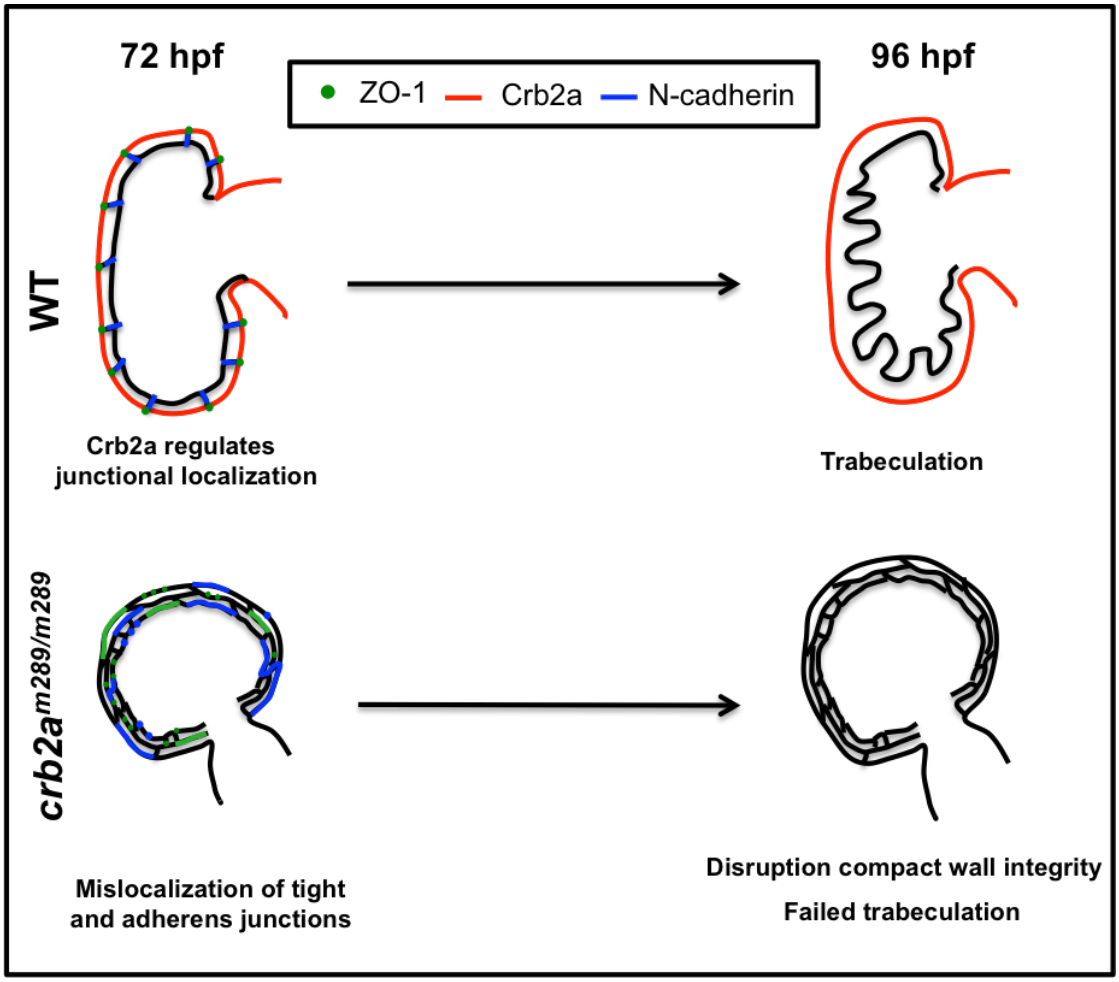

Figure 31. Proposed model (see text).

5. Discussion

5.1 Establishment of apicobasal polarity in cardiomyocytes and its regulation during cardiac trabeculation in zebrafish

Trabeculation is a highly dynamic and regulated process where clusters of ventricular CMs delaminate and expand into the cardiac jelly to form sheet-like projections in the developing heart. Alterations during development affecting this process lead to congenital embryonic malformations (Gassmann et al., 1995; Lee et al., 1995; Meyer and Birchmeier, 1995; Jenni et al., 2007; Liu et al., 2010; Zhang et al., 2013). Although great efforts have been done over years to elucidate developmental and mechanistic drivers of heart trabeculation, still many aspects remain poorly understood. How changes in polarity are regulated in order for CMs to achieve successful delamination and subsequent expansion during cardiac trabeculation is one of these unknown aspects. It has been assumed for many years that, like epithelial cells, CMs display apicobasal polarity. However, there is no experimental evidence supporting this hypothesis. In this study, I show for the first time that CMs display apicobasal polarity. Moreover, live imaging at single cell resolution reveals that CMs experience changes in apicobasal polarity, undergo apical constriction, and depolarize prior to delaminate into the trabecular layer. Together, my data support the idea that cardiac trabeculation is an EMT-like process.

5.1.1 Cardiomyocytes display apicobasal polarity

CM polarity has been poorly investigated. Studies in *Drosophila* cardiac tube formation suggested that CBs are polarized based on α-spectrin expression, which is a basolateral membrane marker (Fremion et al., 1999). However, these results remain controversial as other studies failed to detect by immunostaining expression of classical polarity markers in these cells (Tepass et al., 1990; Qian et al., 2005). In zebrafish, during early stages of cardiac morphogenesis, junctional localization of proteins such us, α-Catenin, ZO-1 and Prkci, indicate that CMs might display epithelial features (Le and Stainier, 2004; Le et al., 2005; Rohr et al., 2006). Indeed, *nok* and *prcki* morphants show disrupted myocardium and lost of junctional localization of the previous markers, suggesting a role for *has/prkci* and *nok/mpp5* during heart cone tilting (Rohr et al., 2006). Despite some studies suggesting the myocardium as a polarized epithelium at early developmental stages, no specific polarity markers have been generated to establish and visualize CM polarity *in vivo*.

Epithelial cells are characterized by their plasticity during processes like EMT, where they have to lose apicobasal polarity and adhesion with contiguous cells, change in shape, and become more migratory (Lee et al., 2006). CMs have never been studied as classical epithelial cells. However, previous data have shown that selected CMs ingress in the trabecular network by a process called delamination. During this process, compact-layer CMs change their shape from their characteristic cobblestone epithelial morphology to that of a mesenchymal motile cell (Staudt et al., 2014, Liu et al., 2010). E- and N-Cadherin, are in many cases considered as inducers of EMT (Kim et al., 2000). During cardiac trabeculation, N-Cadherin has been found to change its location very dynamically (Cherian et al, 2016).

As part of my studies, I have shown that compact-layer CMs display clear apicobasal polarity. By engineering two different transgenes, *podocalyxin* and *mark3a*, I was able to label *in vivo* CM apical and basolateral membranes respectively and visualize dynamic changes in apicobasal polarity during cardiac trabeculation. Our data are consistent with previous evidences showing that epithelial cells lose apicobasal polarity and change their shape during EMT (Royer and Lu, 2011; Thiery et al., 2009). Here, I have established that "apical" faces the abluminal side of CMs and "basal" faces the lumen of the ventricle in the heart, and is attached to the cardiac jelly that separates endocardium and myocardium. Furthermore, I showed that the apical marker PRKCI localizes in the abluminal side in the developing mouse heart, indicating that apicobasal polarity is conserved during cardiac development among vertebrates. Altogether, these data support the notion of cardiac trabeculation as an EMT-like process. (Certain lines have been quoted verbatim from Jiménez-Amilburu et al., Cell reports, 2016 Dec 6;17(10):2687-2699).

5.1.2 Cardiomyocytes undergo apical constriction and depolarization prior to delaminate

My live imaging of the beating heart revealed that similar to epithelial cells, CMs acquire a wedge shape in their apical membrane while undergoing apical constriction in the compact-layer prior to delamination. In addition, I have shown that CMs depolarize while still in the compact wall, and subsequently delaminate towards the lumen in order to populate the trabecular layer. Similar to my findings during CM trabeculation, cells undergoing apical constriction have been observed during organ morphogenesis in other models like in *Drosophila* trachea and salivary gland formation (Brodu and Casanova, 2006; Nikolaidou and

Barrett, 2004), *Drosophila* ventral furrow (Costa et al., 1994; Sweeton et al., 1991), *C.elegans* endoderm internalization (Anderson et al., 2008; Nance and Priess, 2002), or in neural tube formation in vertebrates (Haigo et al., 2003; Schoenwolf and Smith, 1990). However, mechanisms driving apical constriction in CMs remain to be elucidated. One possibility is that F-actin associated motor myosin II cable in CMs generates contractions and destabilizations that actively promote invagination of the cell, like in *Drosophila* amnioserosa cells (David et al., 2010; Kiehart et al., 2000; Martin et al., 2009). Another possibility is that CMs delaminate passively as a consequence of the morphological changes and junctional rearrangements of neighboring myocytes (Sawyer et al., 2010). Lastly, it is possible that a combination of both active and passive movements in the tissue regulate the formation of apical constriction as it has been reported in *Drosophila* dorsal closure or wound healing (Antunes et al., 2013; Franke et al., 2010; Kiehart et al., 2000). Furthermore, I found that once in the trabecular layer some CMs have the ability to repolarize and subsequently depolarize again. Similarly, data in *Drosophila* indicate that embryonic neuroblasts repolarize after ingression, preceding repeated asymmetric cell divisions (Prehoda, 2009; Yu et al., 2000). In addition to these observations, I found that several mesenchymal markers (such us, *snail1a*, *snail2*, *twist1a* and *twist1b*) are downregulated in the embryonic zebrafish heart after blocking trabeculation, further supporting trabeculation as an EMT-like process.

Nrg/ErbB2 signaling and mechanical forces such us blood flow and contractility are known to be required for the proper formation of trabeculae in the cardiac lumen Gassmann et al., 1995; Lee et al., 1995; Meyer and Birchmeier, 1995; Liu et al 2010; Rasouli and Stainier, 2017) Peshkovsky et al., 2011; Samsa et al 2015; Cherian et al 2016). To test whether Nrg/ErbB2 signaling is regulating apicobasal polarity during cardiac trabeculation, I used different reagents to disrupt this signalling pathway *in vivo*. I blocked Nrg/ErbB2 signaling by using 1) a Nrg2a gene trap zebrafish mutant or 2) an ErbB2 inhibitor. In both cases I found no apical constricion formation or depolarized CMs in the compact wall. These results are in line with previous studies in breast epithelial cells showing that ErbB2 is necessary in cancer cells to disrupt cellular apicobasal polarity in order to migrate during metastatic invasion (Aranda et al., 2006). Based on these data, I hypothesyze that similar to breast cancer cells, CMs require ErbB2 signaling to disrupt apicobasal polarity and then delaminate during cardiac trabeculation. Moreover, after using BDM, tricaine, and *tnnt2a* MO to block blood flow and contractility I observed similar results, apicobasal polarity was affected and CMs did not

undergo constriction. Overall, these data suport a role for both Nrg/ErbB2 signaling and blood flow and contractility in apical constriction formation and CM depolarization. (Certain lines have been quoted verbatim from Jiménez-Amilburu et al., Cell reports, 2016 Dec 6;17(10):2687-2699).

5.1.3 Myocardial Notch activation does not regulate seeding or expansion of trabecular CMs in zebrafish

Several studies have described the importance of Notch activation in the endocardium to trigger different signaling during cardiac trabeculation (D'Amato et al., 2016; Del Monte et al., 2007; Grego-Bessa et al., 2007; VanDusen et al., 2014). However, a role for Notch signaling in the myocardium has not been elucidated yet. Here, using lineage tracing experiments, I identified a sub-population of compact-layer CMs that activate Notch. Moreover, I found that Notch is activated only in those compact-layer CMs contacting a CM undergoing apical constriction. Previous studies have shown that both Nrg/ErbB2 and Notch signaling pathways converge in the regulation of cell cycle, migration, and apoptosis during tumorigenesis (Lindsay et al., 2008). Since Nrg/ErbB2 signaling is key to cardiac trabeculation, I tested whether this pathway regulates myocardial Notch activation. Indeed, using the *nrg2a* mutant crossed into a Notch reporter line, I found that Nrg/ErbB2 signaling positively regulates Notch in compact-layer CMs and activate only compact-layer CMs adjacent to those undergoing apical constriction or delaminated. In view of these results, I speculate that Notch in the myocardium might have a cell-autonomous role in preventing CMs to enter the trabecular layer via classical lateral inhibition. Then, blocking Notch signaling should lead to an increase of CMs forming the trabecular layer. To test this hypothesis, I manipulated Notch signaling during myocardial activation (from 48 hpf) and observed that after blocking the pathway, number of apical constrictions, depolarized CMs, and proliferating CMs remain unchanged. Chemical inhibition of this pathway affected severely the morphology of the developing heart. As a result, I found that Notch inhibition causes ventricle collapse rather than a "hypertrabeculated" phenotype, as recently reported (Han et al., 2016). Moreover, blocking Notch signaling by using DAPT, disrupts apicobasal polarity and intercellular junctions in zebrafish neuroepithelium, suggesting a role for Notch signaling in maintaining neuroepithelial polarity (Ohata et al., 2011). In view of these data, is tempting to speculate that Notch signaling in the myocardium might be playing a role in reinforcing CM apicobasal polarity in compact-layer CMs. Importantly, my observations highlight the importance of using the right tools to follow developmental processes at single cell resolution. In an effort

to rigorously analyze cardiac trabeculation at high resolution, during my PhD studies I have developed a number of reagents that will serve as a toolbox for others in the field. Importantly, some of the lines I generated allow to discriminate between confounding factors like multilayering or aberrant ventricular morphology, and hypertrabeculation phenotypes. Overall, I speculate that Notch signaling in the myocardium might have a role in maintaining shape of compact-layer CMs rather than a role in regulating the seeding and expansion of the trabecular layer. (Certain lines have been quoted verbatim from Jiménez-Amilburu et al., Cell reports, 2016 Dec 6;17(10):2687-2699).

5.2 Role of the polarity complex Crumbs in regulating junctional rearrangement in cardiomyocytes during cardiac trabeculation in zebrafish

During EMT, epithelial apicobasal polarity is regulated by the coordination of different polarity proteins and cellular rearrangements (Hurd et al., 2003; Kempkens et al., 2006). Polarity complexes including PAR, Scribble, and Crumbs, are known to interact in order to maintain apicobasal identity, cell shape, and tissue integrity. A recent study has shown that *Prkci* mouse mutants show trabeculation defects (Passer et al., 2016), further supporting the involvement of polarity complexes during cardiac trabeculation. In order to explore deeper into the role and regulation of polarity in CMs during cardiac trabeculation, I set out to study the Crumbs complex. Crb has a well conserved role in different tissues and organisms, regulating apicobasal polarity and maintaining junctional integrity during morphogenetic processes (Grawe et al., 1996; Izaddoost et al., 2002). However, Crb has never been studied *in vivo* in the context of heart development. Here, I found that *crb2a* is the highest *crb* isoform expressed in the embryonic zebrafish heart and that during the onset of trabeculation Crb2a is very dynamic, changing its localization from junctional to apical in compact-layer CMs. Moreover, I present experimental evidence that suggest a key role for Crb2a in maintaining CM apicobasal polarity and CM junctional rearrangements during cardiac trabeculation in zebrafish.

5.2.1 Crb2a localization in cardiomyocytes changes during cardiac trabeculation

Similar to epithelial cells during morphogenetic processes, also CMs experience changes in cell shape as well as junctional and cytoskeletal rearrangements prior and during cardiac trabeculation (Staudt et al., 2014, Liu et al., 2010). The wide range of changes that CMs

undergo during this process implies great cellular plasticity and is similar to changes in cell shape observed during follicular morphogenesis in *Drosophila* (Wu et al., 2008). Xiaodong and co-workers showed that during the formation of the follicular epithelium, cells change their shape from columnar to cuboidal, and finally to squamous morphology. In addition, they show that changes in cell shape imply not only remodeling of junctions and membrane domains but also changes in the localization of the transmembrane protein Crumbs (Sherrard and Fehon, 2015). Here, I found that during the onset of trabeculation Crb2a shifts its localization in CMs from junctional to apical. These observations suggest that at early developmental stages Crb2a is required as a junctional protein in CMs in order to maintain adhesion with contiguous CMs within the myocardium, and in turn maintains the epithelial-like shape in individual CMs. Once trabeculation initiates, Crb2a might not be longer needed to undergo homophilic adhesions in CMs, becoming apical to function solely as a determinant of apical identity in CMs. My results indicate that similar to the changes observed in *Drosophila*, changes in Crb2a localization in CMs are associated to profound cellular rearrangements. Initially, Crb2a localizes between compact-layer CMs with epithelial-like shape, overlapping with tight junctions. Later, during trabeculation, Crb2a has relocalized at the apical surface of compact-layer CMs. At that time, selected CMs undergoing apical constriction and surrounding CMs need to adapt to changes in shape and cellular rearrangements. However, in *Drosophila* Crb at later stages in follicular morphogenesis, returns to the marginal zone before the flattening of the follicle cell with squamous morphology. Interestingly, in the heart, Crb2a was never observed in delaminated CMs that loss the cobblestone epithelial morphology. Moreover, I found that at 96 hpf, after blocking Nrg/ErbB2 signaling and/or ablating the epicardium, Crb2a becomes highly enriched at the junctions of compact-layer CMs, while in control animals it remains apical. Similarly, previous data in D*rosophila* epithelia show that Moe promotes Crb stability, and that while in WT conditions Crb is localized apically, after Moe depletion Crb becomes junctional (Sherrard and Fehon, 2015). Based on these data, I speculate that Crb2a shift in localization might be 1) associated to CM phenotypic plasticity and 2) involved in selecting which CMs delaminate and which will remain in the compact-layer CMs. However, it still remains unclear whether the switch of Crb2a localization in CMs from junctional to apical is directly regulating cardiac trabeculation. Further studies will be needed to understand mechanistically how this change in Crb2a localization is regulated and its implications in trabecular fate.

5.2.2 Crb2a is required for compact wall integrity and trabeculation

During gastrulation, CRB2 together with Myosin IIB promote cell ingression during EMT in the mouse embryo (Ramkumar et al., 2016). During cardiac trabeculation, from the single layer of compact-wall CMs, selected CMs undergo first a process of migration called delamination in order to settle the trabecular layer (Staudt et al., 2014). I found that in *crb2a* mutants the compact ventricular wall is composed of two layers of cells instead of one. Moreover, the cardiac morphology in these mutants is affected, displaying smaller and rounder ventricles. As a possible undelaying cause for these alterations, I found that mutant CMs are elongated and arranged in a more random fashion than those in WT animals. These observations suggest a role for Crb2a in maintaining CM shape prior to delaminate.

Interestingly, following the development of mutant hearts over time, I observed that they never extend myocardial protrusions into the lumen, failing to form the extensive network of trabecular ridges in the ventricle observed in WTs. Right orientation of the mitotic spindle is necessary for proper symmetric cell division during animal development (Morin and Bellaïche, 2011). It has been reported that both delamination and oriented cell division take place during trabeculae formation in both mouse (Li et al., 2016) and zebrafish (Uribe et al., unpublished). Additionally, apical polarity in these mutants was affected, since CMs in the second layer of the ventricular compact wall were strongly polarized. However, the origin and identity of the second layer of CMs observed in the *crb2a* mutants remains to be clarified. Future experiments should include, careful observation and quantification of apical constrictions and CM proliferation in mutant hearts. These analyses will help to understand if these are trabecular CMs, or whether instead the mutant phenotype is caused by excessive CM proliferation. In addition, high resolution imaging of the mutant hearts at later developmental stages will also be needed.

In summary, these results suggest a role for Crb2a in controlling apicobasal polarity in CMs during cardiac trabeculation and maintaining tissue integrity.

5.2.3 Lack of Crb2a causes disruption of tight and adherens junctions in cardiomyocytes

During epithelial morphogenesis, changes in cell shape and localization require a tight regulation of the connection between junctional proteins and cytoskeleton (Costa et al., 1998; Martin et al., 2010; Raich et al., 1999). It is well established in different processes that loss of

Crb causes defects in cell-cell adhesion and results in loss of tissue integrity (Flores-Benitez and Knust, 2015; Grawe et al., 1996; Letizia et al., 2013; Tepaß and Knust, 1990; van de Pavert et al., 2004). Different members of the Cadherin family and TJs have been reported to interact with Crb (Grawe et al., 1996; Malicki and Driever, 1999; Tilston-Lünel et al., 2016). Here, I observed that the the loss of *crb2a*, caused defects in cell-cell adhesion as TJs and AJs in CMs appear mislocalized in *crb2a* mutants.

The beating of the heart takes place in a very contractile and dynamic environment, being plasticity an essential feature for CMs that have to adapt to a high pumping demand. CM architecture then consists of different structures including the actomyosin cytoskeleton and junctional proteins, all pivotal for changes in cell shape. *crb2a* mutants display defects in the localization of the TJs (ZO-1) and AJs (N-Cadherin) in CMs. Similarly, during dorsal closure of amninoserosa cells in *Drosophila*, the role of Crb is to mediate the interaction between cell membrane and cytoskeleton. Thus, lack of Crb cause over-activity of the actomyosin cytoskeleton, resulting in uncontrolled contractions of the amninoserosa cells, defects in cell-cell adhesion, and failure in the closure (Flores-Benitez and Knust, 2015). Future experiments should focus on the understanding of the actomyosin cytoskeleton in *crb2a* mutant CMs and the interaction with TJs and AJs. Moreover, it was shown in MDCK cells that E-Cadherin plays an instructive role in directing mitotic spindle orientation, suggesting that cell division orientation is coupled to cell-cell adhesion (Gloerich et al., 2017). Based on these data, I hypothesize that lack of Crb2a in CMs causes loss in cell-cell adhesion and, in consequence, disrupts the orientation of cell division towards the lumen of the heart during trabeculation causing the observed phenotype. Additionally, to understand the role of Crb2a in the regulation of junction formation in CMs, immunostaining or live imaging of TJs and AJs should be performed at early time points during heart development (i.e. 24, 36 or 40 hpf).
Taken together, these data suggest that Crb2a regulates trabeculation, at least in part, via mediating junctional interactions between CMs.

5.2.4 A cell-autonomous role for Crb2a in cardiomyocytes during cardiac trabeculation

In order to understand whether Crb2a plays a cell-autonomous role in CMs during cardiac trabeculation, I performed several CM transplantation experiments. Firstly, I generated chimeric hearts by CM transplantation at the mid-blastula stage of mutant cells into WT

animals. The images revealed that while WT and heterozygous CMs were able to populate both compact and trabecular layer, *crb2a* mutant CMs were exclusively localized in the trabecular layer, and never being part of the compact-layer. These data indicate that Crb2a functions cell-autonomously in CMs. Strikingly, the fact that *crb2a* mutant CMs were found only in the trabecular layer at 96 hpf, suggests that Crb2a is a key determinant of the trabecular fate. These results are in line with previous data in mouse gastrulation, and tubulogenesis of *Drosophila* salivary glands showing an anisotropic distribution of Crb in the distinct cells within the epithelium (Ramkumar et al., 2016; Röper, 2012). In these studies, it was demonstrated that cells with low levels of Crb, downregulate aPKC and activate Rho kinases, accumulating apical Myosin II that in turn contributes to the actomyosin cable formation and further delamination. Whether in our model low levels of Crb2a can be used as readout to predict CMs that will undergo apical constriction and delamination, remains to be investigated.

6. Conclusion

Cardiac trabeculation is key to cardiac wall maturation during heart development. Lack or excessive trabeculation leads to embryonic congenital heart diseases. Although, efforts in the field have contributed to identify key regulators of different steps of cardiac development, still which mechanisms/factors govern trabeculation remain largely unknown. Cell polarity is a fundamental feature of some cell types that has never been studied in CMs. It is involved in developmental processes such us proliferation, morphogenesis or migration, all these being recapitulated during trabecular development. Therefore, I decided to study CM apicobasal polarity during cardiac trabeculation.

6.1 Establishment of apicobasal polarity in cardiomyocytes and its regulation during cardiac trabeculation in zebrafish

Our studies show for the first time apicobasal polarity in CMs. After some reports give confusing information about this issue, I have precisely established that the apical domain of CMs faces the abluminal side and basal faces the lumen of the ventricle in the heart, and is attached to the cardiac jelly that separates endocardium and myocardium. Moreover, *in vivo* imaging revealed that similar to epithelial cells, CMs undergo apical constriction in the compact-layer followed by depolarization prior to delaminate. These observations together with previous data allow me to suggest that cardiac trabeculation is an EMT-like process. Moreover, I found that Nrg/ErbB2 signaling and blood flow/contractility are regulating apical constriction formation and CM depolarization. Although, many studies have focused on endocardial Notch during cardiac trabeculation, not much is known about the possible role of Notch in the myocardium. Here, a new subpopulation of compact-layer CMs that activate Notch has been identified. Interestingly, Notch is activated only in those compact-layer CMs neighboring others undergoing apical constriction, suggesting a possible role for myocardial Notch in preventing CMs to enter the trabecular layer. However, blocking myocardial Notch signaling does not affect apical constriction formation or CM delamination. I propose that myocardial Notch has a role in maintaining compact-layer CM shape rather than in regulating cardiac trabeculation.

6.2 Role of the polarity complex Crumbs in regulating junctional rearrangement in cardiomyocytes during cardiac trabeculation in zebrafish

Our findings identify a new role in the heart for Crb2a, a member of the Crumbs polarity complex, during cardiac trabeculation in zebrafish. Crb2a is very dynamic and it has been found to change its localization within the cell during morphogenetic processes. Interestingly, Crb2a localization changes in compact-layer CMs from junctional to apical coinciding with the onset of trabeculation. Crb2a has also been involved not only in apicobasal polarity but also in regulating cellular rearrangement to maintain tissue integrity. I found that in *crb2a* mutants the arrangement and morphology of ventricular CMs is severely affected. Additionally, mutant CMs display mislocalization of both tight and adherens junctions what might cause the disruption of compact wall integrity, where Crb2a is expressed. Moreover, mutant CMs transplanted into WT animals were only found in the trabecular layer. These data suggest that, the compromised ability of mutant CMs to integrate the WT compact-layer, caused by the mislocalization of their functional complexes, might make them more prone to delaminate. Altogether, I proposed a new role for Crb2a in driving the fate of trabecular CMs, potentially by regulating junctional proteins in CMs prior and during cardiac trabeculation.

These studies performed *in vivo* provide new insight into the polarization of CMs during cardiac trabeculation, contributing to better understand the complex mechanisms underlying ventricular morphogenesis and maturation, and will provide new clues on the sequence of events that take place during cardiac trabeculation.

1. Einleitung

Das menschliche Herz ist das erste sich entwickelnde Organ. Während der Entwicklung erfährt das embryonale Herz zahlreiche Veränderungen, um zu einem pumpenden Organ zu werden (Sedmera et al., 2000; Moorman and Christoffels 2003). In den letzten Jahren wurde der Zebrafisch zu einem wertvollen Modell um kardiovaskuläre Erkrankungen zu erforschen. Auch wenn das Zebrafisch Herz verglichen mit anderen Vertebraten einfacher aufgebaut ist, sind viele Prozesse der Herzentwicklung stark konserviert (Bakkers, 2011).

Trabekulation ist einer der wichtigsten Prozesse zur Bildung einer funktionierenden ventrikulären Wand, während der Gruppen ventrikulärer Kardiomyozyten (KMs) aus einer Einzelschicht delaminieren und in die Herzgallerte expandieren um Blattartige Projektionen im sich entwickelnden Herz zu bilden (Samsa et al., 2013; Sedmera et al., 2000). Viele angeborene Herzkrankheiten sind mit Defekten in der Bildung dieser Trabekel verbunden und führen zum Tod des Embryos (Jenni et al., 1999; Zhang et al., 2013; Jenni et al., 2001; Towbin 2010). Es wurde experimentell gezeigt, dass das Fehlen von Nrg1/ErbB2/ErbB4, Angiopoetin1/Tie2, EphrinB2/B4, BMP10 oder jeglicher Komponenten des Notch Signalweges zu einer defekten Trabekulation führen können. Zudem können Veränderungen im Blutfluss und/oder der Kontraktilität die Trabekulation beeinflussen (Samsa et al., 2013). Zusammengenommen zeigen diese Beobachtungen, dass die Trabekulation ein hochgradig dynamischer und regulierter Prozess ist.

Trabekulation ist ein morphogener Prozess, der Kontrolle über die Zellform und zelluläre Umgestaltungen voraussetzt, ähnlich den Prozessen, die während der epithelialen zu mesenchymalen Transition (EMT) beobachtet werden. Epithelzellen in einer Epithelschicht sind polarisiert und etablieren Zell-Zell Verbindungen mit Nachbarzellen (Ikenouchi et al., 2003; Ferrer-vaquer et al., 2010). Daher ist die epitheliale Zellpolarität eine wichtige Eigenschaft, die die Zellform und Gewebestruktur erhält. Während Entwicklungsprozessen wie zellulärer Migration und Zellteilung oder im Verlaufe verschiedener Krankheiten kann die Epithelpolarität gestört sein. In Konsequenz dieser Veränderung verlieren die Zellen ihre engen Zell-Zell-Verbindungen, modifizieren ihr Zytoskelett, ändern ihre Form und erlangen die Fähigkeit zur Migration, um mesenchymale Zellen zu werden (Micalizzi et al., 2010). In Epithelzellen wird die apikal-basale Polarität durch eine Reihe konservierter Schlüsselkomplexe gebildet, zu denen die PAR, Scribble und Crumbs Komplexe zählen

(Kemphues et al., 1988; Bilder and Perrimon 2000; Teppas et al., 1984). Die Polaritätsproteine in diesen Komplexen interagieren gut organisiert und koordiniert um die molekulare Asymmetrie entlang der apikal-basalen Achse der Zelle zu erzeugen. Dieser Crosstalk reguliert wiederum die Reifung und Stabilisierung der Verbindungen zwischen Zellen und Zytoskeletten um die Zellpolarität zu stärken (Roignot et al., 2013).

Unter den verschiedenen Polaritätskomplexen ist Crumbs ein Schlüsselregulator der apikal-basalen Polarität während der Entwicklung von Vertebraten und Invertebraten (Hurd et al., 2003; Tepass et al., 1990). Crumbs war das erste Polaritätsprotein, das 1990 von Tepass et al. in *D. melanogaster* entdeckt wurde. Das apikale Polaritätsprotein Crumbs ist ein Transmembranprotein mit einer kurzen intrazellulären und einer langen extrazellulären Domäne (Bulgakova and Knust, 2009). Das intrazelluläre Ende von Crumbs ist an der Regulierung der apikalen Identität beteiligt. In ihr interagieren die PDZ und die 4.1/Ezrin/Radixin/Moesin (FERM)-Bindedomänen direkt oder indirekt mit Zytoskelett-Proteinen und Komponenten des PAR-Komplexes, insbesondere mit Par6 und der atypischen Proteinkinase C (aPKC) (Polesello et al., 2002; Kempkens et al., 2006). Andererseits wurde kürzlich herausgefunden, dass die extrazelluläre Domäne an der homophilen Crb-Crb-Interaktion beteiligt ist, die die Interaktion zwischen Zellen mediiert (Thompson et al., 2013). In *Drosophila* und *C. elegans* gibt es nur ein *crumbs (crb)*, während es in Säugetieren drei (*Crb1*, *Crb2* and *Crb3*) und in Zebrafischen fünf (*crb1*, *crb2a, crb2b*, *crb3a* and *Crb3b*) verschiedene Paraloge gibt (Omori and Malicki, 2006).

In *Drosophila* verursachen Mutationen in *crb* ein Versagen der Positionierung und Aufrechterhaltung von Adhäsionskontakten und Barrierekontakten, was zu einem Verlust der apikal-basalen Polarität und der Störung der Gewebeintegrität führt (Grawe et al., 1996; Wodarz et al., 1993). Die Überexpression von *crb* in *Drosophila* und *crb3* in *Xenopus* führt jedoch gleichermaßen zu einer Expansion der apikalen Membrandomäne („Apikalisierung“) und induziert den Übergang von einem einschichtigen zu einem mehrschichtigen Epithel (LaPrise et al., 2010; Klebes and Knust, 2000; Chalmers et al., 2005). Im Zebrafisch wurden *crb1*, *crb2a (ome)* und *crb2b* im Zentralnervensystem (ZNS) einschließlich der Retina und Fotorezeptoren untersucht. Mutationen in *crb2a* verursachen den Verlust der apikal-basalen Polarität im Neuroepithel und eine gestörte Musterbildung in der Retina (Malicki and Driever 1999; Wei and Malicki, 2002). Zusammenfassend bestätigen diese Studien die Rolle von Crumbs in der

Spezifizierung der apikalen Domäne der Epithelzellen und der Erhaltung der Organisation von Zellkontakten. Die Rolle von Crumbs in der Trabekulation bleibt jedoch unerforscht.

Hier nutze ich die Vorteile des Zebrafischmodelles, um die Veränderungen der apikal-basalen Polarität von KMs während der Trabekulation *in vivo* mit Einzelzell-Auflösung zu studieren. Außerdem zeige ich, welche Faktoren die apikal-basale Polarität der KMs während dieses Prozesses regulieren. Zusätzlich analysiere ich die Rolle des Polaritätskomplexes Crumbs in der Regulierung von Veränderung von Kontakten zwischen KMs und der Ausbildung von Trabekel-Netzwerken.

2. Ergebnisse und Diskussion

2.1 Etablierung der apikal-basalen Polarität in KMs und ihre Regulierung während der Herz-Trabekulation im Zebrafisch

KMs ändern ihre Form während der Delaminierung vom charakteristischen pflastersteinartigen Epithelphänotyp in den beweglichen mesenchymalen Zellphänotyp (Staudt et al., 2014; Liu et al., 2010). Außerdem ändert sich die N-Cadherin Lokalisierung sehr dynamisch während der Herz-Trabekulation (Cherian et al., 2016). Trotzdem wurden KMs bislang nicht als klassische Epithelzellen betrachtet und KM-Polarität im Kontext der Herz-Trabekulation nicht erforscht.

Um die apikal-basale Polarität in KMs während der Herz-Trabekulation zu studieren, habe ich zwei neue transgene Linien mit den Transgenen Podocalyxin und Mark3a generiert. Durch die Verwendung dieser Tiere war ich in der Lage, die apikalen und basolateralen Membranen der KMs jeweils spezifisch *in vivo* zu markieren. Dann analysierte ich *Tg(−0.2myl7:EGFP-podxl)*;*Tg(myl7:MKATE-CAAX*) und *Tg(−0.2myl7:mark3a-TagRFP-T); Tg(myl7:ras-GFP)* Herzen vor (54 hpf) und nach (82 hpf) dem Beginn der Trabekulation im Zebrafisch. 54 hpf erscheinen die KMs im kompakten Myokard polarisiert, erkennbar an der apikalen Lokalisierung des EGFP-Podokalyxin Markers und der basolateralen Lokalisierung des Mark3a-TagRFP-T Markers (**Abbildung 1A-A"** und **Abbildung 2A-A").** Später, 82 hpf, fand ich heraus, dass delaminierte KMs depolarisiert waren, erkennbar durch die Lokalisierung von EGFP-Podocalyxin und Mark3a-TagRFP-T in der gesamten Zellmembran (**Abbildung 1B-B"** und **Abbildung 2B-B"**). Interessanterweise bleiben KMs im kompakten Myokard polarisiert (**Abbildung 1B-B"** und **Abbildung 2B-B"**). In dieser Studie habe ich gezeigt, dass

KMs im kompakten Myokard apikal-basal polarisiert sind. Außerdem habe ich herausgefunden, dass die apikale Membran sich auf der abluminalen Seite der KMs befindet und die basale Oberfläche dem Lumen des Herzventrikels zugewandt und an der Herzgallerte befestigt ist, die das Endokard und das Myokard separiert.

Um die verschiedenen Veränderungen in der KM-Polarität während der Herz-Trabekulation zu erforschen, habe ich Videos von *Tg(−0.2myl7:EGFP-podxl)*;*Tg(myl7:MKATE-CAAX)* Larven mit Live-Bildgebung in Einzelzell-Auflösung untersucht. Spinning Disc Zeitraffer-Videos zeigten, dass KMs eine apikale Konstriktion durchlaufen, die sich durch eine Akkumulation von EGFP-Podokalyxin auf der apikalen Seite zeigt (**Abbildung 5A**). Dann ziehen sich die KMs im kompakten Myokard zusammen und durchlaufen eine Depolarisation bevor sie delaminieren, sichtbar durch die Neu-Lokalisierung des EGFP-Podocalyxin in der gesamten Plasmamembran (**Abbildung 5B**). Nach der Depolarisation delaminieren die und besiedeln die Trabekel-Schicht. Sobald sich KMs in der Trabekel-Schicht befinden, beobachtete ich, dass sich eine Teilmenge der Zellen wieder polarisiert (**Abbildung 5C**) und mit der Zeit eine zweite Welle der Depolarisierung erfährt (**Abbildung 5D**). Diese Daten sind vereinbar mit vorherigen Studien, die die Neu-Polarisierung von *Drosophila* Neuroblasten zeigen, bevor sie sich einer asymmetrischen Zellteilung unterziehen (Yu et al., 2000; Prehoda, 2009). Hier beschreibe ich, dass KMs sich einer apikalen Konstriktion und Depolarisierung vor der Delaminierung unterziehen, was nahelegt, dass Herz-Trabekulation ein EMT-ähnlicher Prozess ist.

Anschließend wollte ich verstehen, ob die Nrg und ErbB2 Signalwege oder Blutfluss und Kontraktilität Einfluss auf die Bildung apikaler Konstriktionen und KM Depolarisierung haben. Zuerst behandelte ich *Tg(−0.2myl7:EGFP-podxl)*;*Tg(myl7:MKATE-CAAX)* Embryonen 56 hpf mit dem ErbB2 Inhibitor PD16839 und fand heraus, dass die Larven 100 hpf keine apikalen Konstriktionen und depolarisierte KMs aufweisen (**Abbildung 7**). Anschließend nutzte ich die Nrg2a Enhancer Trap Mutante (Westcot et al., 2015), um die Rolle von NRG zu untersuchen. 82 hpf sah ich, dass *nrg2a*-/- eine signifikante Reduktion der Anzahl apikaler Konstriktionen verglichen mit *nrg2a*+/- aufwies (**Abbildung 8A-B'** und **Abbildung 8E**). 100 hpf zeigt *nrg2a*-/- ebenfalls eine signifikante Reduktion der Anzahl delaminierter KMs (**Abbildung 8C-D'** und **Abbildung 8F**). Außerdem analysierte ich *Tg(−0.2myl7:EGFP-podxl)*;*Tg(myl7:MKATE-CAAX)* nach Aussetzung des Blutflusses und der

Kontraktilität durch MS-222 (Tricaine), 2,3-Butandionmonoxim (BDM), oder einen *tnnt2a* Morpholino. Larven, die mit Tricaine und BDM behandelt wurden zeigten ausnahmslos keine apikale Konstriktionen oder depolarisierte KMs (**Abbildung 9A-C"** und **Abbildung 10**). Zusätzlich injizierte ich den *tnnt2a* Morpholino in *Tg(−0.2myl7:EGFP-podxl)*;*Tg(myl7:MKATE-CAAX*) Embryonen im ein-Zell-Stadium. 100 hpf zeigten die *tnnt2a* Morphanten keine apikalen Konstriktionen oder depolarisierte KMs. Diese Daten zeigen, dass sowohl Nrg/ErbB2 – Signaltransduktion als auch Blutfluss und Kontraktilität nicht nur für die die Herz-Trabekulation sondern auch für die Ausbildung apikaler Konstriktionen und KM Depolarisation notwendig sind.

Die Aktivierung des Notch Signalweges im Endokard ist wichtig für die korrekte Bildung der Trabekel im Herzen. Eine mögliche Funktion für Notch im Myokard wurde jedoch nie aufgeklärt (Grego-Bessa et al., 2007; Luxán et al., 2016). Um herauszufinden, ob Notch Signaltransduktion im Myokard eine Rolle während der Trabekulation spielt, nutzte ich die *Tg(TP1:Venus-PEST)* Linie, die destabilisiertes YFP in Zellen exprimiert, in denen Notch aktiv ist. Während aller analysierten Stadien fand ich *TP1:Venus-PEST*-positive KMs nur im kompakten Myokard und niemals in der Trabekel-Schicht (**Abbildung 11**). Diese Beobachtungen wurden durch Abstammungsverfolgung („Lineage Tracing") bestätigt (**Abbildung 11D-F**). Außerdem beobachtete ich, dass KMs in direkter Nachbarschaft zu einer KM, die eine apikale Konstriktion durchläuft Notch-positiv ist, nicht jedoch die sich zusammenziehende KM selbst (**Abbildung 12**). Auch wenn Nrg/ErbB2 und Notch Signalwege bereits zuvor während der Herz-Trabekulation untersucht wurden, wurde ihre Interaktion nie vollständig aufgeklärt (Samsa et al., 2015; Han et al., 2016). Hier analysiere ich die Notch Expression in *nrg2a* Mutanten und fand heraus, dass Nrg2a für die Aktivierung von Notch im Myokard benötigt wird (**Abbildung 13**). Diese Daten zeigen, dass eine interessante Subpopulation Notch-positiver KMs identifizierbar ist und legen eine Funktion für Notch im Myokard in der Auswahl der KMs nahe, die in die Trabekel-Schicht vordringen. Um zu testen ob Notch verhindert, dass KMs in die Trabekel-Schicht migrieren, blockierte ich die Notch-Signaltransduktion unter Verwendung der Inhibitoren DAPT und LY411575, vor dem Beginn der Trabekulation. Allerdings beobachtete ich keinen Anstieg in der Anzahl apikaler Konstriktionen (**Abbildung 14**), delaminierender (**Abbildung 15**) oder proliferierender KMs (**Abbildung 16**). Zusammengenommen legen diese Daten nahe, dass die apikal-basale

Polarität durch Nrg/ErbB2-Signalwege, Blutfluss und Kontraktilität, nicht aber durch Notch-Signalwege reguliert wird.

2.2 Rolle des Polarität-Komplexes Crumbs in der Regulierung der Umordnung von Zell-Verbindungen in KMs während der Herz-Trabekulation im Zebrafisch

Während EMT wird die apikal-basale Polarität durch die Koordination von Polaritätskomplexen und zellulären Umordnungen reguliert, in denen der Crumbs Komplex eine Schlüsselrolle spielt (Hurd et al., 2003; Kempkens et al., 2006). Um zu untersuchen, welche Crumbs Gene im sich entwickelnden Zebrafisch Herzen exprimiert sind, führte ich eine Transkriptomanalyse isolierter, embryonaler Zebrafischherzen bei 52 hpf und 7 dpf durch. Diese Analysen zeigten, dass *crb2a* das am höchsten exprimierte Crumbs Gen in frühen Stadien ist (**Abbildung 18**). Um zu verstehen, ob crb2a eine Funktion in der Herz-Trabekulation hat, nahm ich Crb2a Immunfärbungen im embryonalen Zebrafischherzen zu verschiedenen Entwicklungszeitpunkten vor. Ich fand heraus, dass Crb2a vor Beginn der Trabekulation (50 hpf) stark in den Verbindungen zwischen KMs im kompakten Myokard angereichert ist und dass es sobald die Trabekulation beginnt (80 hpf) homogen in der apikalen Membran aller KMs im kompakten Myokard lokalisiert ist (**Abbildung 19**). Interessanterweise überschneiden sich diese Veränderungen in der Crb2a-Lokalisierung mit dem Beginn der Herz-Trabekulation. Deshalb nehme ich an, dass Crb2a vor Beginn der Trabekulation als Zelladhäsionsprotein benötigt wird, indem es homophile Crumbs-Crumbs Interaktionen zwischen KMs im kompakten Myokard eingeht. Ich spekuliere jedoch, dass nach Beginn der Trabekulation Crb2a nicht mehr für homophile Interaktionen in den Zellkontakten benötigt wird und sich apikal lokalisiert um ausschließlich als eine apikale Determinante der apikalen KM Membranidentität zu dienen. Ähnliche Beobachtungen, die ebenfalls eine Rolle für Crumbs in der Mediierung der Zell-Zell Adhäsion nahelegen, wurden kürzlich in der Zebrafisch Retina (Wei and Malicki, 2002) und den Speicheldrüsen von *Drosophila* (Katja Roper, 2012) gemacht.

Um die mögliche Funktion von Crb2a während der Herz-Trabekulation zu überprüfen, untersuchte ich *crb2a* Mutanten (Malicki et al., 1996). 36 hpf, zeigten *crb2a*-/- Mutanten Defekte in der Krümmung des Herzschlauches (**Abbildung 22A-C'**). 48 hpf zeigten die Mutanten eine leichte Reduktion der Ausstoß-Fraktion im Atrium (**Abbildung 22A-C'** und **Abbildung 22E**), 40% hatten zudem keinen Blutfluss (**Abbildung 22D**). Außerdem

überprüfte ich, ob Defekte in der Ausstoß-Fraktion durch Defekte in den Sarkomeren des Myokards hervorgerufen werden, indem ich α-Aktinin in *crb2a-/-* anfärbte. Ich fand verglichen mit dem Wildtype (WT) keine Unterschiede in den Strukturen der Myofibrillen (**Abbildung 23F-G'**). Als nächstes analysierte ich diese Mutanten nach Beginn der Trabekulation. 80 hpf haben WT Larven eine einzelne Schicht von KMs im kompakten Myokard, während die Herzen von *crb2a-/-* kleiner und runder sind und eine unorganisiertere, mehrschichtige kompakte Myokardwand mit elongierten KMs aufweisen (**Abbildung 24A-B'"**). 100 hpf beobachtete ich, dass *crb2a-/-* keine Trabekel bildet (**Abbildung 24C-E'**). Zusätzlich fand ich auch heraus, dass die KM Polarität in *crb2a-/-* ebenfalls beeinträchtigt ist (**Abbildung 24F-G'**).

Angesichts der Rolle des Polaritätskomplexes Crumbs in der Regulierung von Barrierenkontakten und Adhäsions-Verbindungen (Flores-Benitez and Knust, 2015), entschied ich mich dazu, die Umordnungen von Zellkontakten in *crb2a-/-* zu untersuchen. 79 hpf Larven mit Immunfärbungen für N-Cadherin und ZO-1 zeigten, dass die Lokalisierung beider Proteine in den KMs der Mutanten gestört ist (**Abbildung 29**). Alles in allem legen meine Daten nahe, dass Crb2a eine Rolle in der Regulation der KM Polarität und der Umorganisation von Zellverbindungen während der Herz-Trabekulation im Zebrafisch spielt.

Zuletzt führte ich mehrere KM-Transplantationsexperimente durch, um zu prüfen ob die Funktion von Crb2a während der Herz-Trabekulation zellautonom ist. Als Erstes generierte ich chimäre Herzen durch die Transplantation von Zellen im Blastula-Stadium. Wenn mutierte KMs in WT Herzen transplantiert wurden, wurden mutierte KMs nur in der Trabekel-Schicht beobachtet, währen heterozygote oder WT KMs sowohl im kompakten Myokard als auch in der Trabekel-Schicht beobachtet wurden (**Abbildung 30**). Diese Ergebnisse legen eine zellautonome Rolle für Crb2a in KM während der Herz-Trabekulation nahe.

Fazit

Zusammenfassend habe ich die apikal-basale Polarität in KMs zum ersten Mal *in vivo* charakterisiert und argumentiere nun, dass Herz-Trabekulation ein EMT-ähnlicher Prozess ist. Ich habe beschrieben, dass die Nrg/ErbB2 – Signalwege sowie Blutfluss und Kontraktilität die KM Polarität während der Trabekulation des Myokards regulieren. Außerdem deuten

meine Resultate an, dass der Notch-Signalweg im Myokard die Induktion und Expansion der Trabekel-Schicht nicht reguliert, dass er jedoch an der Erhaltung der Zellform von KMs im kompakten Myokard nach Aktivierung von Nrg/ErbB2 beteiligt sein könnte. Zusätzlich dazu identifizierte ich eine neue Funktion für Crb2a in der Regulierung der korrekten Etablierung von Adhäsionskontakten und Barrierekontakten in KMs, die essentiell für die korrekte Ausbildung der Trabekel-Balken während der Herzentwicklung sind.

1. Introduction

The human heart is the first organ to develop. During development, the embryonic heart experiences numerous modifications in order to become a capable pumping organ (Sedmera et al., 2000; Moorman and Christoffels, 2003). In the last years, zebrafish has emerged as a valuable model organism to study cardiovascular diseases. Even though the zebrafish heart is simpler in structure compared to other vertebrates, many processes during heart development are highly conserved (Bakkers 2011).

Cardiac trabeculation is one of the essential processes required for the formation of a competent ventricular wall, whereby clusters of ventricular cardiomyocytes (CMs) from a single layer delaminate and expand into the cardiac jelly to form sheet-like projections in the developing heart (Samsa et al., 2013). Several congenital heart diseases are associated with defects in the formation of these trabeculae and lead to embryonic lethality (Jenni et al., 1999; Zhang et al., 2013, Jenni et al., 2001; Towbin 2010). It has been experimentally shown that lack of Nrg1/ErbB2/ErbB4, Angipoetin1/Tie2, EphrinB2/B4, BMP10, or any component of the Notch signaling pathway can cause defective trabeculation. Moreover, changes in blood flow and/or contractility can also affect trabeculation (Samsa et al., 2013). Together, these observations demonstrate that cardiac trabeculation is a highly dynamic and regulated process.

Trabeculation is a morphogenetic process that requires control over cell shape changes and rearrangements, similar to those observed during EMT. Epithelial cells within an epithelium are polarized and establish cell-cell junctions with the neighboring cells (Ikenouchi et al., 2003; Ferrer-vaquer et al., 2010), thus epithelial cell polarity is an important feature to maintain cell shape and tissue structure. During developmental processes such as cell migration and cell division or in disease states epithelial polarity might be disrupted. As a consequence of this alteration, cells lose their tight cell-cell adhesions, undergo cytoskeletal rearrangements, change their shape and gain migratory properties becoming mesenchymal cells (Micalizzi et al., 2010). In epithelial cells, apicobasal polarity is regulated by a conserved set of core complexes, including the PAR, Scribble and Crumbs complexes (Kemphues et al., 1988; Bilder and Perrimon, 2000; Teppas et al., 1984). The polarity proteins composing these complexes interact in a well organized and coordinated-manner creating molecular asymmetry along the apicobasal axis of the cell. In turn, this crosstalk regulates the maturation and stabilization of

the junctions between cells and cytoskeleton in order to strengthen cell polarization (Roignot et al., 2013).

Amongst the different polarity complex, Crumbs has been shown to be a key regulator of apicobasal polarity during development in both vertebrates and invertebrates (Tepass et al., 1990; Fan et al., 2004). Crumbs was identified as the first polarity protein in *D. melanogaster* by Tepass et al. in 1990. The apical polarity protein Crumbs is a transmembrane protein formed by a short intracellular domain and a long extracellular domain (Bulgakova and Knust, 2009). The intracellular tail of Crumbs is involved in regulating apical identity. Within the intracellular tail, the PDZ and the 4.1/Ezrin/Radixin/Moesin (FERM)-binding domains, interact directly or indirectly with cytoskeletal proteins and components of the PAR complex, especially Par6 and the atypical protein kinase C (aPKC) (Polesello et al., 2002; Kempkens et al., 2006). On the other hand, the extracellular domain has recently been found to be involved in the formation of homophilic Crumbs-Crumbs interactions that allow for communication between cells (Thompson et al., 2013). In *Drosophila* and *C. elegans* there is only one *crumbs (crb)*, while in mammals there are three (*Crb1*, *Crb2* and *Crb3*) and in zebrafish five (*crb1*, *crb2a, crb2b*, *crb3a* and *crb3b*) different paralogs 14 (Omori and Malicki, 2006).

In *Drosophila*, mutations in *crb* cause failure of positioning and maintenance of adherens and tight junctions, and in consequence, loss of apicobasal polarity and disruption of tissue integrity (Grawe et al., 1996; Tepass, 1996; Wodarz et al., 1993). However, overexpression of *crb* and *crb3* in *Drosophila* and *Xenopus* respectively leads to an expansion of the apical membrane domain ("apicalization"), inducing transition from a single-layer epithelium to a multilayer epithelium (LaPrise et al., 2010; Klebes et al., 2000; Chalmers et al., 2005). In zebrafish, *crb1*, *crb2a (ome)* and *crb2b* have been studied in the central nervous system (CNS), including the retina and photoreceptors. Mutations in *crb2a* cause loss of apicobasal polarity in neuroepithelium and loss of retinal patterning (Malicki and Driever, 1999; Wei and Malicki, 2002). Overall, these studies confirm a role for Crumbs in specifying the apical domain of epithelial cells and maintaining junctional organization. However, the role that Crumbs plays during trabeculation remains unknown.

Here, taking advantage of zebrafish as a model organism, I study *in vivo* at single cell resolution changes in CM apicobasal polarity during cardiac trabeculation. Moreover, I show which

factors regulate CM apicobasal polarity during this process. In addition, I dissect the role of the polarity complex Crumbs in regulating CM junctional rearrangements and the formation of the trabecular network.

2. Results and discussion

2.1 Establishment of apicobasal polarity in CMs and its regulation during cardiac trabeculation in zebrafish

CMs have been shown to change their shape from the characteristic cobblestone epithelial phenotype into the mesenchymal motile cell phenotype during delamination (Staudt et al., 2014; Liu et al., 2010). Moreover, N-cadherin localization has been found to change very dynamically during cardiac trabeculation (Cherian et al., 2016). However, CMs have never been considered as classical epithelia cells, and CM polarity in the context of cardiac trabeculation has never been studied.

In order to study apicobasal polarity in CMs during cardiac trabeculation, I have generated new transgenic lines using two different transgenes, Podocalyxin and Mark3a. Using these transgenic animals I was able to label *in vivo* the apical and basolateral membranes respectively of CMs. Then, I analyzed *Tg(−0.2myl7:EGFP-podxl)*;*Tg(myl7:MKATE-CAAX)* and *Tg(−0.2myl7:mark3a-TagRFP-T); Tg(myl7:ras-GFP)* hearts before (54 hpf) and after (82 hpf) the onset of trabeculation in zebrafish. At 54 hpf, compact-layer CMs appeared polarized as is shown by the apical localization of EGFP-Podocalyxin and the basolateral localization of Mark3a-TagRFP-T (Figure 1A-A" and Figure 2A-A"). Later, at 82 hpf, I found that delaminated CMs were depolarized, as is shown by the localization of both EGFP-Podocalyxin and Mark3a-TagRFP-T all around the cell membrane (**Figure 1B-B"** and **Figure 2B-B").** Interestingly, compact-layer CMs remained polarized (**Figure 1B-B"** and **Figure 2B-B"**). In this study, I have shown that compact-layer CMs display apicobasal polarity. Moreover, I established that the apical cell membrane is the abluminal side of CMs, and that the basal surface faces the lumen of the ventricle in the heart and is attached to the cardiac jelly that separates endocardium and myocardium.

To further explore the different changes in CM polarity during cardiac trabeculation, I examined live imaging movies of *Tg(−0.2myl7:EGFP-podxl)*;*Tg(myl7:MKATE-CAAX)* larvae at single cell resolution. Spinning disc time-lapses showed that CMs undergo apical constriction,

as shown by the accumulation of EGPF-Podocalyxin at the apical side (**Figure 5A**). Then, constricting CMs in the compact-layer undergo depolarization prior to delamination, as shown by the relocalization of EGFP-Podocalyxin all around the cell membrane (**Figure 5B**). After they depolarize, CMs delaminate and settle into the trabecular layer. Once CMs are in the trabecular layer, I observed that a subset of cells repolarize again (**Figure 5C**), and over time they undergo a second wave of depolarization (**Figure 5D**). These data are consistent with previous evidences showing repolarization of *Drosophila* neuroblasts prior to undergoing asymmetric cell division (Yu et al., 2000; Prehoda, 2009). Here, I describe that CMs undergo apical constriction and depolarization prior to delaminate, suggesting that cardiac trabeculation is an EMT-like process.

Next, I wanted to understand whether Nrg and ErbB2 signaling or blood flow and contractility were involved in the formation of apical constriction and CM depolarization. First, I treated *Tg(−0.2myl7:EGFP-podxl)*;*Tg(myl7:MKATE-CAAX)* embryos at 56 hpf with the ErbB2 inhibitor PD16839 and found that at 100 hpf larvae do not show any apical constriction or depolarized CMs (**Figure 7**). Next, to investigate the role of Nrg, I used Nrg2a gene trap zebrafish mutants (Westcot et al., 2015). At 82 hpf, I found that *nrg2a-/-* showed a significant reduction in the number of apical constrictions compared to *nrg2a+/-* (**Figure 8A-B'** and **Figure 8E**), while at 100 hpf, *nrg2a-/-* exhibit also a significant reduction in the number of delaminated CMs (**Figure 8C-D'** and **Figure 8F**). Moreover, I also analysed *Tg(−0.2myl7:EGFP-podxl)*;*Tg(myl7:MKATE-CAAX)* embryos after stopping blood flow and contractility by using tricaine, 2,3-butanedione monoxime (BDM), or *tnnt2a* morpholino. Tricaine and BDM-treated larvae at 100 hpf did not exhibit any apical constriction or depolarized CM (**Figure 9A-C"** and **Figure 10**). In addition, I injected *tnnt2a* morpholino into *Tg(−0.2myl7:EGFP-podxl)*;*Tg(myl7:MKATE-CAAX)* embryos at the one-cell stage. At 100 hpf, *tnnt2a* morphants did not exhibit apical constriction or depolarized CMs (**Figure 9D-D"**). These data show that both Nrg/ErbB2 signaling and blood flow and contractility are required not only for cardiac trabeculation, but also for apical constriction formation and CM depolarization.

Activation of Notch signaling in the endocardium has been shown to be important for proper formation of trabeculae in the heart (Grego-Bessa et al., 2007; Luxán et al., 2016). However a possible role for myocardial Notch during trabeculation has never been elucidated. To study

whether Notch signaling might have a role in the myocardium during cardiac trabeculation, I took advantage of the *Tg(TP1:Venus-PEST)* line that expresses a destabilized YFP in cells where Notch signaling is activated. At all of the different stages analyzed, I only found *TP1:Venus-PEST*-postive CMs in the compact-layer and never in the trabecular layer (**Figure 11**). These observations were confirmed by lineage tracing experiments (**Figure 11D-F**). Moreover, I observed that CMs neighboring a CM undergoing apical constriction were Notch-positive, but not the constricting CM (**Figure 12**). Although, Nrg/ErbB2 and Notch signaling have been studied during trabeculation, their interaction has never been completely elucidated (Samsa et al., 2015; Han et al., 2016). Here, I analyzed Notch expression in *nrg2a* mutants and found that Nrg2a is required for myocardial Notch activation (**Figure 13**). These data show that an interesting subpopulation of Notch-positive CMs has been identified and suggest a role for Notch within the myocardium in selecting CMs to enter in the trabecular layer. To test if Notch has a role preventing CMs to enter into the trabecular layer, I blocked Notch function using two different inhibitors DAPT and LY411575 before the onset of trabeculation. However, I did not observe an increase in the number of apical constriction (**Figure 14**), delaminating (**Figure 15**) or proliferating CMs (**Figure 16**). Taken together, these data indicate that CM apicobasal polarity is regulated by Nrg/ErbB2 signaling and blood flow and contractility but not Notch signaling.

2.2 Role of the polarity complex Crumbs in regulating junctional rearrangement in CMs during cardiac trabeculation in zebrafish

During EMT, epithelial apicobasal polarity is regulated by the coordination of polarity complexes and cellular rearrangements, where the Crumbs complex plays a key role (Hurd et al., 2003; Kempkens et al., 2006). To investigate which Crumbs genes are expressed in the developing zebrafish heart I performed transcriptomic analysis of isolated embryonic zebrafish hearts at 52 hpf and 7 dpf. These analyses revealed that *crb2a* is the highest Crumbs gene expressed at early stages (**Figure 18**). In order to understand if there is a role for *crb2a* in cardiac trabeculation, I performed Crb2a immunostaining in the embryonic zebrafish heart at different developmental stages. I found that Crb2a is highly enriched at the junctions of compact-layer CMs before trabeculation begins (50 hpf) and is localized homogenously in the apical membrane of all compact-layer CMs once trabeculation has started (80 hpf) (**Figure 19**). Interestingly, these changes in Crb2a localization in CMs coincide with the onset of cardiac trabeculation. Therefore, I hypothesize that Crb2a is required as a junctional protein

before trabeculation, forming homophilic Crumbs-Crumbs interactions between CMs in the compact wall. However once trabeculation starts, I speculate that Crb2a is no longer needed for homophilic interactions at the junctions, and becomes apically localized to function exclusively as an apical determinant of the apical membrane identity of CMs. Similar observations suggesting a role for Crumbs in mediating cell-cell adhesion has been recently reported in the zebrafish retina (Wei and Malicki, 2002) and *Drosophila* salivary glands (Roper et al., 2012).

To further study the possible role of Crb2a during cardiac trabeculation, I studied *crb2a* mutants (Malicki et al., 1996). At 36 hpf, *crb2a*-/- showed defects in heart looping formation (**Figure 22A-C'**). At 48 hpf, mutants displayed slight reduction in the atrial fractional shortening (**Figure 22A-C'** and **Figure 22E**) and 40% show no circulation (**Figure 22D**). In addition, I tested whether defects in fractional shortening might be due to defects in myocardial sarcomeres by staining for α-Actinin in *crb2a*-/-, and found no differences in myofibril structures when compared to wild-type (WT) (**Figure 23F-G'**). Next, I analyzed these mutants after the onset of trabeculation. At 80 hpf, while WT larvae display a single layer of CMs in the compact wall, *crb2a*-/- hearts are smaller, rounded, and display a more disorganized compact wall with more elongated CMs and multilayering (**Figure 24A-B'''**). At 100 hpf, I observed that *crb2a*-/- fail to form trabeculae (**Figure 24C-E'**). In addition, I also found that CM polarity in *crb2a*-/- is affected (**Figure 24F-G'**).

Given the role of the polarity complex Crumbs in regulating tight and adherens junctions (Flores-Benitez and Knust, 2015), I decided to look into the junctional rearrangements in *crb2a*-/-. 79 hpf larvae stained for N-cadherin and ZO-1 revealed that localization of both junctional proteins is mislocalized in mutant CMs (**Figure 29**). Overall, my data suggest a role for Crb2a in the regulation of CM polarity and junctional rearrangements during cardiac trabeculation in zebrafish.

Lastly, to understand whether Crb2a plays a cell-autonomous role in CMs during cardiac trabeculation, I performed several CM-transplantation experiments. Firstly, I generated chimeric hearts by cell transplantation at the mid-blastula stage. When mutant CMs were transplanted into WT hearts, mutant CMs were only observed in the trabecular layer, while heterozygous or WT CMs were found in both compact and trabecular layers (**Figure 30**). These data suggest a cell-autonomously role for Crb2a in CMs during cardiac trabeculation.

Conclusion

In conclusion, I have characterized and established the apicobasal polarity in CMs for the first time *in vivo*, proposing cardiac trabeculation as an EMT-like process. I have described that Nrg/ErbB2 signaling and blood flow and contractility regulates CM polarity during myocardial trabeculation. Moreover, my results indicate that myocardial Notch signaling does not regulate seeding and expansion of the trabecular layer but it might be involved in maintaining the shape of compact-layer CMs upon Nrg/ErbB2 activation. In addition, I identified a new role for Crb2a in regulating the correct establishment of adherens and tight junctions in CMs, being essential for the correct formation of trabecular ridges during cardiac development.

Adams, R.H., Diella, F., Hennig, S., Helmbacher, F., Deutsch, U., and Klein, R. (2001). The Cytoplasmic Domain of the Ligand EphrinB2 Is Required for Vascular Morphogenesis but Not Cranial Neural Crest Migration. Cell *104*, 57-69.

Adams, R.H., Wilkinson, G.A., Weiss, C., Diella, F., Gale, N.W., Deutsch, U., Risau, W., and Klein, R. (1999). Roles of ephrinB ligands and EphB receptors in cardiovascular development: demarcation of arterial/venous domains, vascular morphogenesis, and sprouting angiogenesis. Genes & Development *13*, 295-306.

Alvers, A.L., Ryan, S., Scherz, P.J., Huisken, J., and Bagnat, M. (2014). Single continuous lumen formation in the zebrafish gut is mediated by smoothened-dependent tissue remodeling. Development (Cambridge, England) *141*, 1110-1119.

Anderson, D.C., Gill, J.S., Cinalli, R.M., and Nance, J. (2008). Polarization of the C. elegans embryo by RhoGAP-mediated exclusion of PAR-6 from cell contacts. Science (New York, NY) *320*, 1771-1774.

Ando, J., and Yamamoto, K. (2009). Vascular Mechanobiology
Endothelial Cell Responses to Fluid Shear Stress. Circulation Journal *73*, 1983-1992.

Antunes, M., Pereira, T., Cordeiro, J.V., Almeida, L., and Jacinto, A. (2013). Coordinated waves of actomyosin flow and apical cell constriction immediately after wounding. The Journal of Cell Biology *202*, 365.

Aranda, V., Haire, T., Nolan, M.E., Calarco, J.P., Rosenberg, A.Z., Fawcett, J.P., Pawson, T., and Muthuswamy, S.K. (2006). Par6–aPKC uncouples ErbB2 induced disruption of polarized epithelial organization from proliferation control. Nature Cell Biology *8*, 1235.

Arita, Y., Nakaoka, Y., Matsunaga, T., Kidoya, H., Yamamizu, K., Arima, Y., Kataoka-Hashimoto, T., Ikeoka, K., Yasui, T., Masaki, T.*, et al.* (2014). Myocardium-derived angiopoietin-1 is essential for coronary vein formation in the developing heart. Nature Communications *5*, 4552.

Artavanis-Tsakonas, S., Rand, M.D., and Lake, R.J. (1999). Notch Signaling: Cell Fate Control and Signal Integration in Development. Science *284*, 770.

Assémat, E., Bazellières, E., Pallesi-Pocachard, E., Le Bivic, A., and Massey-Harroche, D. (2008). Polarity complex proteins. Biochimica et Biophysica Acta (BBA) - Biomembranes *1778*, 614-630.

Audebert, S., Navarro, C., Nourry, C., Chasserot-Golaz, S., Lécine, P., Bellaiche, Y., Dupont, J.-L., Premont, R.T., Sempéré, C., Strub, J.-M.*, et al.* (2004). Mammalian Scribble Forms a Tight Complex with the betaPIX Exchange Factor. Current Biology *14*, 987-995.

Auman, H.J., Coleman, H., Riley, H.E., Olale, F., Tsai, H.-J., and Yelon, D. (2007). Functional Modulation of Cardiac Form through Regionally Confined Cell Shape Changes. PLoS Biology *5*, e53.

Bachmann, A., Schneider, M., Theilenberg, E., Grawe, F., and Knust, E. (2001). Drosophila Stardust is a partner of Crumbs in the control of epithelial cell polarity. Nature *414*, 638.

Bakkers, J. (2011). Zebrafish as a model to study cardiac development and human cardiac disease. Cardiovascular Research *91*, 279-288.

Balda, M.S., and Matter, K. (2009). Tight junctions and the regulation of gene expression. Biochimica et Biophysica Acta (BBA) - Biomembranes *1788*, 761-767.

Berdougo, E., Coleman, H., Lee, D.H., Stainier, D.Y.R., and Yelon, D. (2003). Mutation of weak atrium/atrial myosin heavy chain disrupts atrial function and influences ventricular morphogenesis in zebrafish. Development *130*, 6121.

Bilder, D., Li, M., and Perrimon, N. (2000). Cooperative Regulation of Cell Polarity and Growth by Drosophila Tumor Suppressors. Science *289*, 113.

Bilder, D., and Perrimon, N. (2000). Localization of apical epithelial determinants by the basolateral PDZ protein Scribble. Nature *403*, 676.

Böhm, H., Brinkmann, V., Drab, M., Henske, A., and Kurzchalia, T.V. (1997). Mammalian homologues of C. elegans PAR-1 are asymmetrically localized in epithelial cells and may influence their polarity. Current Biology *7*, 603-606.

Bondue, A., and Blanpain, C. (2010). Mesp1. Circulation Research *107*, 1414.
Bos, J.L., Rehmann, H., and Wittinghofer, A. (2007). GEFs and GAPs: Critical Elements in the Control of Small G Proteins. Cell *130*, 385.

Braitsch, C.M., Kanisicak, O., van Berlo, J.H., Molkentin, J.D., and Yutzey, K.E. (2013). Differential expression of embryonic epicardial progenitor markers and localization of cardiac fibrosis in adult ischemic injury and hypertensive heart disease. Journal of molecular and cellular cardiology *65*, 10.1016/j.yjmcc.2013.1010.1005.

Brand, T. (2003). Heart development: molecular insights into cardiac specification and early morphogenesis. Developmental Biology *258*, 1-19.

Brodu, V., and Casanova, J. (2006). The RhoGAP crossveinless-c links trachealess and EGFR signaling to cell shape remodeling in Drosophila tracheal invagination. Genes & Development *20*, 1817-1828.

Bu, Z., and Callaway, D.J.E. (2011). Chapter 5 - Proteins MOVE! Protein dynamics and long-range allostery in cell signaling. In Advances in Protein Chemistry and Structural Biology, R. Donev, ed. (Academic Press), pp. 163-221.

Bulgakova, N.A., and Knust, E. (2009). The Crumbs complex: from epithelial-cell polarity to retinal degeneration. Journal of Cell Science *122*, 2587.

Campanale, J.P., Sun, T.Y., and Montell, D.J. (2017). Development and dynamics of cell polarity at a glance. Journal of Cell Science *130*, 1201.

Cavodeassi, F. (2018). Dynamic Tissue Rearrangements during Vertebrate Eye Morphogenesis: Insights from Fish Models. Journal of Developmental Biology *6*, 4.

Chalmers, A.D., Pambos, M., Mason, J., Lang, S., Wylie, C., and Papalopulu, N. (2005). aPKC, Crumbs3 and Lgl2 control apicobasal polarity in early vertebrate development. Development *132*, 977.

Chen, C.-L., Gajewski, K.M., Hamaratoglu, F., Bossuyt, W., Sansores-Garcia, L., Tao, C., and Halder, G. (2010). The apical-basal cell polarity determinant Crumbs regulates Hippo signaling in Drosophila. Proceedings of the National Academy of Sciences of the United States of America *107*, 15810-15815.

Chen, H., Shi, S., Acosta, L., Li, W., Lu, J., Bao, S., Chen, Z., Yang, Z., Schneider, M.D., Chien, K.R.*, et al.* (2004). BMP-10 is essential for maintaining cardiac growth during murine cardiogenesis. Development (Cambridge, England) *131*, 2219-2231.

Cherian, A.V., Fukuda, R., Augustine, S.M., Maischein, H.-M., and Stainier, D.Y.R. (2016). N-cadherin relocalization during cardiac trabeculation. Proceedings of the National Academy of Sciences of the United States of America *113*, 7569-7574.

Chi, N.C., Shaw, R.M., Jungblut, B., Huisken, J., Ferrer, T., Arnaout, R., Scott, I., Beis, D., Xiao, T., Baier, H.*, et al.* (2008). Genetic and Physiologic Dissection of the Vertebrate Cardiac Conduction System. PLoS Biology *6*, e109.

Clark, B.S., Cui, S., Miesfeld, J.B., Klezovitch, O., Vasioukhin, V., and Link, B.A. (2012). Loss of Llgl1 in retinal neuroepithelia reveals links between apical domain size, Notch activity and neurogenesis. Development (Cambridge, England) *139*, 1599-1610.

Clement, C.A., Kristensen, S.G., Møllgård, K., Pazour, G.J., Yoder, B.K., Larsen, L.A., and Christensen, S.T. (2009). The primary cilium coordinates early cardiogenesis and hedgehog signaling in cardiomyocyte differentiation. Journal of Cell Science *122*, 3070-3082.

Costa, M., Raich, W., Agbunag, C., Leung, B., Hardin, J., and Priess, J.R. (1998). A Putative Catenin–Cadherin System Mediates Morphogenesis of the Caenorhabditis elegans Embryo. The Journal of Cell Biology *141*, 297-308.

Costa, M., Wilson, E.T., and Wieschaus, E. (1994). A putative cell signal encoded by the folded gastrulation gene coordinates cell shape changes during Drosophila gastrulation. Cell *76*, 1075-1089.

D'Amato, G., Luxán, G., del Monte-Nieto, G., Martínez-Poveda, B., Torroja, C., Walter, W., Bochter, M.S., Benedito, R., Cole, S., Martinez, F.*, et al.* (2016). Sequential Notch activation regulates ventricular chamber development. Nature cell biology *18*, 7-20.

D'Amico, L., Scott, I.C., Jungblut, B., and Stainier, D.Y.R. (2007). A Mutation in Zebrafish hmgcr1b Reveals a Role for Isoprenoids in Vertebrate Heart-Tube Formation. Current Biology *17*, 252-259.

Dachsel, J.C., Ngok, S.P., Lewis-Tuffin, L.J., Kourtidis, A., Geyer, R., Johnston, L., Feathers, R., and Anastasiadis, P.Z. (2013). The Rho Guanine Nucleotide Exchange Factor Syx Regulates the Balance of Dia and ROCK Activities To Promote Polarized-Cancer-Cell Migration. Molecular and Cellular Biology *33*, 4909-4918.

Das, S., and Knust, E. (2018). A dual role of the extracellular domain of Drosophila Crumbs for morphogenesis of the embryonic neuroectoderm. Biology Open *7*, bio031435.

David, D.J.V., Tishkina, A., and Harris, T.J.C. (2010). The PAR complex regulates pulsed actomyosin contractions during amnioserosa apical constriction in Drosophila. Development *137*, 1645.

Del Monte, G., Grego-Bessa, J., Gonzalez-Rajal, A., Bolos, V., and De La Pompa, J.L. (2007). Monitoring Notch1 activity in development: evidence for a feedback regulatory loop. Dev Dyn *236*, 2594-2614.

den Hollander Anneke, I., Davis, J., van der Velde-Visser Saskia, D., Zonneveld Marijke, N., Pierrottet Chiara, O., Koenekoop Robert, K., Kellner, U., van den Born, L.I., Heckenlively John, R., Hoyng Carel, B.*, et al.* (2004). CRB1 mutation spectrum in inherited retinal dystrophies. Human Mutation *24*, 355-369.

Drees, F., Pokutta, S., Yamada, S., Nelson, W.J., and Weis, W.I. (2005). α-Catenin Is a Molecular Switch that Binds E-Cadherin-β-Catenin and Regulates Actin-Filament Assembly. Cell *123*, 903-915.

Fanning, A.S., Ma, T.Y., and Anderson, J.M. (2002). Isolation and functional characterization of the actin binding region in the tight junction protein ZO-1. The FASEB Journal *16*, 1835-1837.

Ferrer-vaquer, A., Viotti, M., and Hadjantonakis, A.-K. (2010). Transitions between epithelial and mesenchymal states and the morphogenesis of the early mouse embryo. Cell Adhesion & Migration *4*, 447-457.

Fiévet, B., Louvard, D., and Arpin, M. (2007). ERM proteins in epithelial cell organization and functions. Biochimica et Biophysica Acta (BBA) - Molecular Cell Research *1773*, 653-660.

Fischer, A., Schumacher, N., Maier, M., Sendtner, M., and Gessler, M. (2004). The Notch target genes Hey1 and Hey2 are required for embryonic vascular development. Genes & Development *18*, 901-911.

Flores-Benitez, D., and Knust, E. (2015). Crumbs is an essential regulator of cytoskeletal dynamics and cell-cell adhesion during dorsal closure in Drosophila. eLife *4*, e07398.

Franco, D., Christoffels, V.M., and Campione, M. (2014). Homeobox transcription factor Pitx2: The rise of an asymmetry gene in cardiogenesis and arrhythmogenesis. Trends in Cardiovascular Medicine *24*, 23-31.

Franke, J.D., Montague, R.A., and Kiehart, D.P. (2010). Nonmuscle myosin II is required for cell proliferation, cell sheet adhesion and wing hair morphology during wing morphogenesis. Developmental biology *345*, 117-132.

Frémion, F., Astier, M., Zaffran, S., Guillèn, A., Homburger, V., and Sémériva, M. (1999). The Heterotrimeric Protein G(o) Is Required for the Formation of Heart Epithelium in Drosophila. The Journal of Cell Biology *145*, 1063-1076.

Garnaas, M.K., Moodie, K.L., Liu, M.-l., Samant, G.V., Li, K., Marx, R., Baraban, J.M., Horowitz, A., and Ramchandran, R. (2008). Syx, a RhoA guanine exchange factor, is essential for angiogenesis in vivo. Circulation research *103*, 710-716.

Gassmann, M., Casagranda, F., Orioli, D., Simon, H., Lai, C., Klein, R., and Lemke, G. (1995). Aberrant neural and cardiac development in mice lacking the ErbB4 neuregulin receptor. Nature *378*, 390-394.

Gavert, N., and Ben-Ze'ev, A. (2008). Epithelial-mesenchymal transition and the invasive potential of tumors. Trends in Molecular Medicine *14*, 199-209.

Geling, A., Steiner, H., Willem, M., Bally-Cuif, L., and Haass, C. (2002). A gamma-secretase inhibitor blocks Notch signaling in vivo and causes a severe neurogenic phenotype in zebrafish. EMBO reports *3*, 688-694.

Genevet, A., and Tapon, N. (2011). The Hippo pathway and apico–basal cell polarity. Biochemical Journal *436*, 213.

Genova, J.L., Jong, S., Camp, J.T., and Fehon, R.G. (2000). Functional Analysis of Cdc42 in Actin Filament Assembly, Epithelial Morphogenesis, and Cell Signaling during Drosophila Development. Developmental Biology *221*, 181-194.

Geoffrey Burns, C., and MacRae, C.A. (2006). Purification of hearts from zebrafish embryos. BioTechniques *40*, 278-282.

Gerety, S.S., Wang, H.U., Chen, Z.-F., and Anderson, D.J. (1999). Symmetrical Mutant Phenotypes of the Receptor *EphB4* and Its Specific Transmembrane Ligand *ephrin-B2* in Cardiovascular Development. Molecular Cell *4*, 403-414.

Ghaye, A.P., Bergemann, D., Tarifeño-Saldivia, E., Flasse, L.C., Von Berg, V., Peers, B., Voz, M.L., and Manfroid, I. (2015). Progenitor potential of nkx6.1-expressing cells throughout zebrafish life and during beta cell regeneration. BMC Biology *13*, 70.

Gloerich, M., Bianchini, J.M., Siemers, K.A., Cohen, D.J., and Nelson, W.J. (2017). Cell division orientation is coupled to cell–cell adhesion by the E-cadherin/LGN complex. Nature Communications *8*, 13996.

Gopalakrishnan, S., Hallett, M.A., Atkinson, S.J., and Marrs, J.A. (2007). aPKC-PAR complex dysfunction and tight junction disassembly in renal epithelial cells during ATP depletion. American Journal of Physiology-Cell Physiology *292*, C1094-C1102.

Grawe, F., Wodarz, A., Lee, B., Knust, E., and Skaer, H. (1996). The Drosophila genes crumbs and stardust are involved in the biogenesis of adherens junctions. Development *122*, 951.

Grego-Bessa, J., Luna-Zurita, L., Monte, G.d., Bolós, V., Melgar, P., Arandilla, A., Garratt, A.N., Zang, H., Mukouyama, Y.-s., Chen, H.*, et al.* (2007). Notch Signaling is Essential for Ventricular Chamber Development. Developmental cell *12*, 415-429.

Haigo, S.L., Hildebrand, J.D., Harland, R.M., and Wallingford, J.B. (2003). Shroom Induces Apical Constriction and Is Required for Hingepoint Formation during Neural Tube Closure. Current Biology *13*, 2125-2137.

Han, P., Bloomekatz, J., Ren, J., Zhang, R., Grinstein, J.D., Zhao, L., Burns, C.G., Burns, C.E., Anderson, R.M., and Chi, N.C. (2016). Coordinating cardiomyocyte interactions to direct ventricular chamber morphogenesis. Nature *534*, 700-704.

Hartsock, A., and Nelson, W.J. (2008). Adherens and Tight Junctions: Structure, Function and Connections to the Actin Cytoskeleton. Biochimica et biophysica acta *1778*, 660-669.

Higuchi, H., and Takemori, S. (1989). Butanedione Monoxime Suppresses Contraction and ATPase Activity of Rabbit Skeletal Muscle. The Journal of Biochemistry *105*, 638-643.

Hsu, Y.-C., Willoughby, J.J., Christensen, A.K., and Jensen, A.M. (2006). Mosaic Eyes is a novel component of the Crumbs complex and negatively regulates photoreceptor apical size. Development (Cambridge, England) *133*, 4849-4859.

Hurd, T.W., Gao, L., Roh, M.H., Macara, I.G., and Margolis, B. (2003). Direct interaction of two polarity complexes implicated in epithelial tight junction assembly. Nature Cell Biology *5*, 137.

Ichimura, K., Powell, R., Nakamura, T., Kurihara, H., Sakai, T., and Obara, T. (2013). Podocalyxin regulates pronephric glomerular development in zebrafish. Physiological Reports *1*, e00074.

Ikenouchi, J., Matsuda, M., Furuse, M., and Tsukita, S. (2003). Regulation of tight junctions during the epithelium-mesenchyme transition: direct repression of the gene expression of claudins/occludin by Snail. Journal of Cell Science *116*, 1959.

Itoh, M., Nagafuchi, A., Moroi, S., and Tsukita, S. (1997). Involvement of ZO-1 in Cadherin-based Cell Adhesion through Its Direct Binding to α Catenin and Actin Filaments. The Journal of Cell Biology *138*, 181-192.

Ivanovitch, K., Temiño, S., and Torres, M. (2017). Live imaging of heart tube development in mouse reveals alternating phases of cardiac differentiation and morphogenesis. eLife *6*, e30668.

Izaddoost, S., Nam, S.-C., Bhat, M.A., Bellen, H.J., and Choi, K.-W. (2002). Drosophila Crumbs is a positional cue in photoreceptor adherens junctions and rhabdomeres. Nature *416*, 178.

Jaffe, S.H., Friedlander, D.R., Matsuzaki, F., Crossin, K.L., Cunningham, B.A., and Edelman, G.M. (1990). Differential effects of the cytoplasmic domains of cell adhesion molecules on cell aggregation and sorting-out. Proceedings of the National Academy of Sciences of the United States of America *87*, 3589-3593.

Jenni, R., Rojas, J., and Oechslin, E. (1999). Isolated Noncompaction of the Myocardium. New England Journal of Medicine *340*, 966-967.

Jiménez-Amilburu, V., Rasouli, S.J., Staudt, D.W., Nakajima, H., Chiba, A., Mochizuki, N., and Stainier, D.Y.R. (2016). In Vivo Visualization of Cardiomyocyte Apicobasal Polarity Reveals Epithelial to Mesenchymal-like Transition during Cardiac Trabeculation. Cell Reports *17*, 2687-2699.

Jin, S.-W., Beis, D., Mitchell, T., Chen, J.-N., and Stainier, D.Y.R. (2005). Cellular and molecular analyses of vascular tube and lumen formation in zebrafish. Development *132*, 5199.

Johansson, A., Driessens, M., and Aspenstrom, P. (2000). The mammalian homologue of the Caenorhabditis elegans polarity protein PAR-6 is a binding partner for the Rho GTPases Cdc42 and Rac1. Journal of Cell Science *113*, 3267.

Johnson, K., Grawe, F., Grzeschik, N., and Knust, E. (2002). Drosophila Crumbs Is Required to Inhibit Light-Induced Photoreceptor Degeneration. Current Biology *12*, 1675-1680.

Jongbloets, B.C., and Pasterkamp, R.J. (2014). Semaphorin signalling during development. Development *141*, 3292.

Kemphues, K.J., Priess, J.R., Morton, D.G., and Cheng, N. (1988). Identification of genes required for cytoplasmic localization in early C. elegans embryos. Cell *52*, 311-320.

Kempkens, Ö., Médina, E., Fernandez-Ballester, G., Özüyaman, S., Le Bivic, A., Serrano, L., and Knust, E. (2006). Computer modelling in combination with in vitro studies reveals similar binding affinities of Drosophila Crumbs for the PDZ domains of Stardust and DmPar-6. European Journal of Cell Biology *85*, 753-767.

Kiehart, D.P., Galbraith, C.G., Edwards, K.A., Rickoll, W.L., and Montague, R.A. (2000). Multiple Forces Contribute to Cell Sheet Morphogenesis for Dorsal Closure in Drosophila. The Journal of Cell Biology *149*, 471.

Kikuchi, K., Holdway, J.E., Werdich, A.A., Anderson, R.M., Fang, Y., Egnaczyk, G.F., Evans, T., MacRae, C.A., Stainier, D.Y.R., and Poss, K.D. (2010). Primary contribution to zebrafish heart regeneration by gata4(+) cardiomyocytes. Nature *464*, 601-605.

Kim, J.-B., Islam, S., Kim, Y.J., Prudoff, R.S., Sass, K.M., Wheelock, M.J., and Johnson, K.R. (2000). N-Cadherin Extracellular Repeat 4 Mediates Epithelial to Mesenchymal Transition and Increased Motility. The Journal of Cell Biology *151*, 1193.

Klebes, A., and Knust, E. (2000). A conserved motif in Crumbs is required for E-cadherin localisation and zonula adherens formation in Drosophila. Current Biology *10*, 76-85.

Kolahgar, G., Bardet, P.-L., Langton, P.F., Alexandre, C., and Vincent, J.-P. (2011). Apical deficiency triggers JNK-dependent apoptosis in the embryonic epidermis of Drosophila. Development (Cambridge, England) *138*, 3021-3031.

Krebs, L.T., Xue, Y., Norton, C.R., Shutter, J.R., Maguire, M., Sundberg, J.P., Gallahan, D., Closson, V., Kitajewski, J., Callahan, R.*, et al.* (2000). Notch signaling is essential for vascular morphogenesis in mice. Genes & Development *14*, 1343-1352.

Lai, J.K.H., Collins, M.M., Uribe, V., Jiménez-Amilburu, V., Günther, S., Maischein, H.-M., and Stainier, D.Y.R. (2018). The Hippo pathway effector Wwtr1 regulates cardiac wall maturation in zebrafish. Development *145*.

Lamers, W.H., and Moorman, A.F.M. (2002). Cardiac Septation. Circulation Research *91*, 93.
Laprise, P. (2011). Emerging Role for Epithelial Polarity Proteins of the Crumbs Family as Potential Tumor Suppressors. Journal of Biomedicine and Biotechnology *2011*, 868217.

Laprise, P., Beronja, S., Silva-Gagliardi, N.F., Pellikka, M., Jensen, A.M., McGlade, C.J., and Tepass, U. (2006). The FERM Protein Yurt Is a Negative Regulatory Component of the Crumbs Complex that Controls Epithelial Polarity and Apical Membrane Size. Developmental cell *11*, 363-374.

Laprise, P., Paul, S.M., Boulanger, J., Robbins, R.M., Beitel, G., and Tepass, U. (2010). Epithelial polarity proteins regulate Drosophila tracheal tube size independently of the luminal matrix pathway. Current biology *20*, 55.

Le, A.T., and Stainier, D.Y.R. (2004). Fibronectin Regulates Epithelial Organization during Myocardial Migration in Zebrafish. Developmental Cell *6*, 371-382.

Le, A.T., Yelon, D., and Stainier, D.Y.R. (2005). Hand2 Regulates Epithelial Formation during Myocardial Differentiation. Current Biology *15*, 441-446.

Le, T.L., Yap, A.S., and Stow, J.L. (1999). Recycling of E-Cadherin: A Potential Mechanism for Regulating Cadherin Dynamics. The Journal of Cell Biology *146*, 219-232.

Lee, J., Fei, P., Packard, R.R.S., Kang, H., Xu, H., Baek, K.I., Jen, N., Chen, J., Yen, H., Kuo, C.C.J.*, et al.* (2016). 4-Dimensional light-sheet microscopy to elucidate shear stress modulation of cardiac trabeculation. The Journal of Clinical Investigation *126*, 1679-1690.

Lee, K.F., Simon, H., Chen, H., Bates, B., Hung, M.-C., and Hauser, C. (1995a). Requirement for neuregulin receptor erbB2 in neural and cardiac development. Nature *378*, 394-398.

Letizia, A., Ricardo, S., Moussian, B., Martín, N., and Llimargas, M. (2013). A functional role of the extracellular domain of Crumbs in cell architecture and apicobasal polarity. Journal of Cell Science.

Li, J., Miao, L., Shieh, D., Spiotto, E., Li, J., Zhou, B., Paul, A., Schwartz, R.J., Firulli, A.B., Singer, H.A.*, et al.* (2016). Single cell lineage tracing reveals that oriented cell division contributes to trabecular morphogenesis and regional specification. Cell reports *15*, 158-170.

Lin, Y.F., Swinburne, I., and Yelon, D. (2012). Multiple influences of blood flow on cardiomyocyte hypertrophy in the embryonic zebrafish heart. Developmental Biology *362*, 242-253.

Lindsay, J., Jiao, X., Sakamaki, T., Casimiro Mathew, C., Shirley Lawrence, A., Tran Thai, H., Ju, X., Liu, M., Li, Z., Wang, C.*, et al.* (2008). ErbB2 Induces Notch1 Activity and Function in Breast Cancer Cells. Clinical and Translational Science *1*, 107-115.

Liu, J., Bressan, M., Hassel, D., Huisken, J., Staudt, D., Kikuchi, K., Poss, K.D., Mikawa, T., and Stainier, D.Y.R. (2010). A dual role for ErbB2 signaling in cardiac trabeculation. Development *137*, 3867-3875.

López-Novoa, J.M., and Nieto, M.A. (2009). Inflammation and EMT: an alliance towards organ fibrosis and cancer progression. EMBO Molecular Medicine *1*, 303-314.

Luxán, G., D'Amato, G., MacGrogan, D., and de la Pompa, J.L. (2016). Endocardial Notch Signaling in Cardiac Development and Disease. Circulation Research *118*, e1.

Mably, J.D., Burns, C.G., Chen, J.-N., Fishman, M.C., and Mohideen, M.-A.P.K. (2003). heart of glass Regulates the Concentric Growth of the Heart in Zebrafish. Current Biology *13*, 2138-2147.

Malicki, J., and Driever, W. (1999). oko meduzy mutations affect neuronal patterning in the zebrafish retina and reveal cell-cell interactions of the retinal neuroepithelial sheet. Development *126*, 1235.

Malicki, J., Neuhauss, S.C., Schier, A.F., Solnica-Krezel, L., Stemple, D.L., Stainier, D.Y., Abdelilah, S., Zwartkruis, F., Rangini, Z., and Driever, W. (1996). Mutations affecting development of the zebrafish retina. Development *123*, 263.

Malone, M.H., Sciaky, N., Stalheim, L., Hahn, K.M., Linney, E., and Johnson, G.L. (2007). Laser-scanning velocimetry: A confocal microscopy method for quantitative measurement of cardiovascular performance in zebrafish embryos and larvae. BMC Biotechnology *7*, 40.

Männer, J. (1993). Experimental study on the formation of the epicardium in chick embryos. Anatomy and Embryology *187*, 281-289.

Martin, A.C., Gelbart, M., Fernandez-Gonzalez, R., Kaschube, M., and Wieschaus, E.F. (2010). Integration of contractile forces during tissue invagination. The Journal of Cell Biology *188*, 735.

Martin, A.C., Kaschube, M., and Wieschaus, E.F. (2009). Pulsed actin-myosin network contractions drive apical constriction. Nature *457*, 495.

Médina, E., Lemmers, C., Lane-Guermonprez, L., and Bivic, A. (2012). Role of the Crumbs complex in the regulation of junction formation in Drosophila and mammalian epithelial cells. Biology of the Cell *94*, 305-313.

Medioni, C., Astier, M., Zmojdzian, M., Jagla, K., and Sémériva, M. (2008). Genetic control of cell morphogenesis during Drosophila melanogaster cardiac tube formation. The Journal of Cell Biology *182*, 249-261.

Meyer, D., and Birchmeier, C. (1995). Multiple essential functions of neuregulin in development. Nature *378*, 386-390.

Micalizzi, D.S., Farabaugh, S.M., and Ford, H.L. (2010). Epithelial-Mesenchymal Transition in Cancer: Parallels Between Normal Development and Tumor Progression. Journal of Mammary Gland Biology and Neoplasia *15*, 117-134.

Mizuno Keiko, S.A., Hirose Tomonori, Kitamura Koichi, Kutsuzawa Koici, Futaki Maasaki, Amano Yoshiko and Ohno Shigeo (2003). Self-association of PAR-3-mediated by the Conserved N-terminal Domain Contributes to the Development of Epithelial Tight Junctions. Journal of Biological Chemistry *278*, 31240-31250.

Moorman, A.F.M., and Christoffels, V.M. (2003). Cardiac Chamber Formation: Development, Genes, and Evolution. Physiological Reviews *83*, 1223-1267.

Morin, X., and Bellaïche, Y. (2011). Mitotic Spindle Orientation in Asymmetric and Symmetric Cell Divisions during Animal Development. Developmental Cell *21*, 102-119.

Mosimann, C., Kaufman, C.K., Li, P., Pugach, E.K., Tamplin, O.J., and Zon, L.I. (2011). Ubiquitous transgene expression and Cre-based recombination driven by the ubiquitin promoter in zebrafish. Development *138*, 169-177.

Nakaoka, Y., Nishida, K., Narimatsu, M., Kamiya, A., Minami, T., Sawa, H., Okawa, K., Fujio, Y., Koyama, T., Maeda, M.*, et al.* (2007). Gab family proteins are essential for postnatal maintenance of cardiac function via neuregulin-1/ErbB signaling. Journal of Clinical Investigation *117*, 1771-1781.

Nance, J., and Priess, J.R. (2002). Cell polarity and gastrulation in <em>C. elegans</em&gt. Development *129*, 387.

Navis, A., Marjoram, L., and Bagnat, M. (2013). Cftr controls lumen expansion and function of Kupffer's vesicle in zebrafish. Development *140*, 1703-1712.

Ngok, S.P., Lin, W.-H., and Anastasiadis, P.Z. (2014). Establishment of epithelial polarity – GEF who is minding the GAP? Journal of Cell Science *127*, 3205.

Nikolaidou, K.K., and Barrett, K. (2004). A Rho GTPase Signaling Pathway Is Used Reiteratively in Epithelial Folding and Potentially Selects the Outcome of Rho Activation. Current Biology *14*, 1822-1826.

Ninov, N., Borius, M., and Stainier, D.Y. (2012). Different levels of Notch signaling regulate quiescence, renewal and differentiation in pancreatic endocrine progenitors. Development *139*, 1557-1567.

Ninov, N., Hesselson, D., Gut, P., Zhou, A., Fidelin, K., and Stainier, D.Y.R. (2013). Metabolic regulation of cellular plasticity in the pancreas. Current biology *23*, 1242-1250.

Noda, Y., Takeya, R., Ohno, S., Naito, S., Ito, T., and Sumimoto, H. (2001). Human homologues of the Caenorhabditis elegans cell polarity protein PAR6 as an adaptor that links the small GTPases Rac and Cdc42 to atypical protein kinase C. Genes Cells *6*, 107-119.

Ohata, S., Aoki, R., Kinoshita, S., Yamaguchi, M., Tsuruoka-Kinoshita, S., Tanaka, H., Wada, H., Watabe, S., Tsuboi, T., Masai, I.*, et al.* (2011). Dual Roles of Notch in Regulation of Apically Restricted Mitosis and Apicobasal Polarity of Neuroepithelial Cells. Neuron *69*, 215-230.

Omori, Y., and Malicki, J. (2006). *oko meduzy* and Related *crumbs* Genes Are Determinants of Apical Cell Features in the Vertebrate Embryo. Current Biology *16*, 945-957.

Osmani, N., Vitale, N., Borg, J.-P., and Etienne-Manneville, S. (2006). Scrib Controls Cdc42 Localization and Activity to Promote Cell Polarization during Astrocyte Migration. Current Biology *16*, 2395-2405.

Paige, S.L., Plonowska, K., Xu, A., and Wu, S.M. (2015). Molecular Regulation of Cardiomyocyte Differentiation. Circulation Research *116*, 341.

Paluch, E., and Heisenberg, C.-P. (2009). Biology and Physics of Cell Shape Changes in Development. Current Biology *19*, R790-R799.

Pashmforoush, M., Lu, J.T., Chen, H., Amand, T.S., Kondo, R., Pradervand, S., Evans, S.M., Clark, B., Feramisco, J.R., Giles, W.*, et al.* (2004). Nkx2-5 Pathways and Congenital Heart Disease: Loss of Ventricular Myocyte Lineage Specification Leads to Progressive Cardiomyopathy and Complete Heart Block. Cell *117*, 373-386.

Passer, D., van de Vrugt, A., Atmanli, A., and Domian, I. (2016). Atypical Protein Kinase C Dependent Polarized Cell Division is Required for Myocardial Trabeculation. Cell reports *14*, 1662-1672.

Pérez-Pomares, J.M., and de la Pompa, J.L. (2011). Signaling During Epicardium and Coronary Vessel Development. Circulation Research *109*, 1429.

Pérez-Pomares José, M., and Muñoz-Chápuli, R. (2002). Epithelial–mesenchymal transitions: A mesodermal cell strategy for evolutive innovation in Metazoans. The Anatomical Record *268*, 343-351.

Person, A.D., Klewer, S.E., and Runyan, R.B. (2005). Cell Biology of Cardiac Cushion Development. In International Review of Cytology (Academic Press), pp. 287-335.

Peshkovsky, C., Totong, R., and Yelon, D. (2011). Dependence of cardiac trabeculation on neuregulin signaling and blood flow in zebrafish. Developmental Dynamics *240*, 446-456.

Peterkin, T., Gibson, A., Loose, M., and Patient, R. (2005). The roles of GATA-4, -5 and -6 in vertebrate heart development. Seminars in Cell & Developmental Biology *16*, 83-94.

Pilot, F., and Lecuit, T. (2005). Compartmentalized morphogenesis in epithelia: From cell to tissue shape. Developmental Dynamics *232*, 685-694.

Polesello, C., Delon, I., Valenti, P., Ferrer, P., and Payre, F. (2002). Dmoesin controls actin-based cell shape and polarity during Drosophila melanogaster oogenesis. Nature Cell Biology *4*, 782.

Prehoda, K.E. (2009). Polarization of Drosophila Neuroblasts During Asymmetric Division. Cold Spring Harbor Perspectives in Biology *1*, a001388.

Qian, L., Liu, J., and Bodmer, R. (2005). Slit and Robo Control Cardiac Cell Polarity and Morphogenesis. Current Biology *15*, 2271-2278.

Raich, W.B., Agbunag, C., and Hardin, J. (1999). Rapid epithelial-sheet sealing in the Caenorhabditis elegans embryo requires cadherin-dependent filopodial priming. Current Biology *9*, 1139-S1131.

Ramkumar, N., Omelchenko, T., Silva-Gagliardi, N.F., McGlade, C.J., Wijnholds, J., and Anderson, K.V. (2016). Crumbs2 Promotes Cell Ingression During the Epithelial-to-Mesenchymal Transition at Gastrulation. Nature cell biology *18*, 1281-1291.

Rasouli, S.J., and Stainier, D.Y.R. (2017). Regulation of cardiomyocyte behavior in zebrafish trabeculation by Neuregulin 2a signaling. Nature Communications *8*, 15281.

Ratheesh, A., and Yap, A.S. (2012). A bigger picture: classical cadherins and the dynamic actin cytoskeleton. Nature Reviews Molecular Cell Biology *13*, 673.

Reuter, H., Henderson, S.A., Han, T., Ross, R.S., Goldhaber, J.I., and Philipson, K.D. (2002). The Na+/Ca2+ Exchanger Is Essential for the Action of Cardiac Glycosides. Circulation Research *90*, 305.

Revenu, C., Streichan, S., Donà, E., Lecaudey, V., Hufnagel, L., and Gilmour, D. (2014). Quantitative cell polarity imaging defines leader-to-follower transitions during collective migration and the key role of microtubule-dependent adherens junction formation. Development *141*, 1282.

Richardson, E.C.N., and Pichaud, F. (2010). Crumbs is required to achieve proper organ size control during Drosophila head development. Development *137*, 641.

Rodriguez-Boulan, E., and Macara, I.G. (2014). Organization and execution of the epithelial polarity programme. Nature reviews Molecular cell biology *15*, 225-242.

Rohr, S., Bit-Avragim, N., and Abdelilah-Seyfried, S. (2006). Heart and soul/PRKCi and nagie oko/Mpp5 regulate myocardial coherence and remodeling during cardiac morphogenesis. Development *133*, 107.

Röper, K. (2012). Anisotropy of Crumbs and aPKC Drives Myosin Cable Assembly during Tube Formation. Developmental Cell *23*, 939-953.

Royer, C., and Lu, X. (2011). Epithelial cell polarity: a major gatekeeper against cancer? Cell Death and Differentiation *18*, 1470-1477.

Ruiz-Villalba, A., Simón, A.M., Pogontke, C., Castillo, M.I., Abizanda, G., Pelacho, B., Sánchez-Domínguez, R., Segovia, J.C., Prósper, F., and Pérez-Pomares, J.M. (2015). Interacting Resident Epicardium-Derived Fibroblasts and Recruited Bone Marrow Cells Form Myocardial Infarction Scar. Journal of the American College of Cardiology *65*, 2057-2066.

Rychter Z, O.B. (1971). Fate of "sinusoidal" intertrabecular spaces of the cardiac wall after development of the coronary vascular bed in chick embryo. Folia Morphol (Praha) *19*, 31-44.

Samsa, L.A., Givens, C., Tzima, E., Stainier, D.Y.R., Qian, L., and Liu, J. (2015). Cardiac contraction activates endocardial Notch signaling to modulate chamber maturation in zebrafish. Development *142*, 4080-4091.

Samsa, L.A., Yang, B., and Liu, J. (2013). Embryonic Cardiac Chamber Maturation: Trabeculation, Conduction and Cardiomyocyte Proliferation. American journal of medical genetics Part C, Seminars in medical genetics *163*, 157-168.

Sankova, B., Machalek, J., and Sedmera, D. (2010). Effects of mechanical loading on early conduction system differentiation in the chick. American Journal of Physiology-Heart and Circulatory Physiology *298*, H1571-H1576.

Sawyer, J.M., Harrell, J.R., Shemer, G., Sullivan-Brown, J., Roh-Johnson, M., and Goldstein, B. (2010). Apical Constriction: A Cell Shape Change that Can Drive Morphogenesis. Developmental biology *341*, 5-19.

Schoenwolf, G.C., and Smith, J.L. (1990). Mechanisms of neurulation: traditional viewpoint and recent advances. Development *109*, 243.

Sedmera, D., Pexieder, T., Vuillemin, M., Thompson Robert, P., and Anderson Robert, H. (2000). Developmental patterning of the myocardium. The Anatomical Record *258*, 319-337.

Sedmera, D., and Thomas Penny, S. (1996). Trabeculation in the embryonic heart. BioEssays *18*, 607-607.

Sehnert, A.J., Huq, A., Weinstein, B.M., Walker, C., Fishman, M., and Stainier, D.Y.R. (2002). Cardiac troponin T is essential in sarcomere assembly and cardiac contractility. Nature Genetics *31*, 106.

Serluca, F.C. (2008). Development of the proepicardial organ in the zebrafish. Developmental Biology *315*, 18-27.

Sherrard, K.M., and Fehon, R.G. (2015). The transmembrane protein Crumbs displays complex dynamics during follicular morphogenesis and is regulated competitively by Moesin and aPKC. Development *142*, 1869.

Shook, D., and Keller, R. (2003). Mechanisms, mechanics and function of epithelial–mesenchymal transitions in early development. Mechanisms of Development *120*, 1351-1383.

Singh, M.K., Christoffels, V.M., Dias, J.M., Trowe, M.-O., Petry, M., Schuster-Gossler, K., Bürger, A., Ericson, J., and Kispert, A. (2005). Tbx20 is essential for cardiac chamber differentiation and repression of Tbx2. Development *132*, 2697.

Sit, S.T., and Manser, E. (2011). Rho GTPases and their role in organizing the actin cytoskeleton. Journal of Cell Science *124*, 679.

Sridurongrit, S., Larsson, J., Schwartz, R., Ruiz-Lozano, P., and Kaartinen, V. (2008). Signaling via the Tgf-β type I receptor Alk5 in heart development. Developmental biology *322*, 208-218.

Staudt, D.W., Liu, J., Thorn, K.S., Stuurman, N., Liebling, M., and Stainier, D.Y.R. (2014). High-resolution imaging of cardiomyocyte behavior reveals two distinct steps in ventricular trabeculation. Development *141*, 585-593.

Steimle, J.D., and Moskowitz, I.P. (2017). TBX5: A Key Regulator of Heart Development. Current topics in developmental biology *122*, 195-221.

Stevenson, B.R., Siliciano, J.D., Mooseker, M.S., and Goodenough, D.A. (1986). Identification of ZO-1: a high molecular weight polypeptide associated with the tight junction (zonula occludens) in a variety of epithelia. The Journal of Cell Biology *103*, 755.

Suri, C., Jones, P.F., Patan, S., Bartunkova, S., Maisonpierre, P.C., Davis, S., Sato, T.N., and Yancopoulos, G.D. (1996). Requisite Role of Angiopoietin-1, a Ligand for the TIE2 Receptor, during Embryonic Angiogenesis. Cell *87*, 1171-1180.

Sweeton, D., Parks, S., Costa, M., and Wieschaus, E. (1991). Gastrulation in Drosophila: the formation of the ventral furrow and posterior midgut invaginations. Development *112*, 775.

Takeichi, M. (1990). Cadherins: A Molecular Family Important in Selective Cell-Cell Adhesion. Annual Review of Biochemistry *59*, 237-252.

Tepass, U. (1996). Crumbs, a Component of the Apical Membrane, Is Required for Zonula Adherens Formation in Primary Epithelia ofDrosophila. Developmental Biology *177*, 217-225.

Tepass, U. (2012). The Apical Polarity Protein Network in Drosophila Epithelial Cells: Regulation of Polarity, Junctions, Morphogenesis, Cell Growth, and Survival. Annual Review of Cell and Developmental Biology *28*, 655-685.

Tepass, U., and Knust, E. (1990). Phenotypic and developmental analysis of mutations at thecrumbs locus, a gene required for the development of epithelia in Drosophila melanogaster. Roux's archives of developmental biology *199*, 189-206.

Tepass, U., and Knust, E. (1993). crumbs and stardust Act in a Genetic Pathway That Controls the Organization of Epithelia in Drosophila melanogaster. Developmental Biology *159*, 311-326.

Tepass, U., Theres, C., and Knust, E. (1990). *crumbs* encodes an EGF-like protein expressed on apical membranes of Drosophila epithelial cells and required for organization of epithelia. Cell *61*, 787-799.

Thiery, J.P., Acloque, H., Huang, R.Y.J., and Nieto, M.A. (2009). Epithelial-Mesenchymal Transitions in Development and Disease. Cell *139*, 871-890.

Thompson, B.J., Pichaud, F., and Röper, K. (2013). Sticking together the Crumbs — an unexpected function for an old friend. Nature Reviews Molecular Cell Biology *14*, 307.

Tilston-Lünel, A.M., Haley, K.E., Schlecht, N.F., Wang, Y., Chatterton, A.L.D., Moleirinho, S., Watson, A., Hundal, H.S., Prystowsky, M.B., Gunn-Moore, F.J.*, et al.* (2016). Crumbs 3b

promotes tight junctions in an ezrin-dependent manner in mammalian cells. Journal of Molecular Cell Biology *8*, 439-455.

Towbin, J.A. (2010). Left Ventricular Noncompaction: A New Form of Heart Failure. Heart Failure Clinics *6*, 453-469.

Toyofuku, T., Zhang, H., Kumanogoh, A., Takegahara, N., Suto, F., Kamei, J., Aoki, K., Yabuki, M., Hori, M., Fujisawa, H.*, et al.* (2004a). Dual roles of Sema6D in cardiac morphogenesis through region-specific association of its receptor, Plexin-A1, with off-track and vascular endothelial growth factor receptor type 2. Genes & Development *18*, 435-447.

Toyofuku, T., Zhang, H., Kumanogoh, A., Takegahara, N., Yabuki, M., Harada, K., Hori, M., and Kikutani, H. (2004b). Guidance of myocardial patterning in cardiac development by Sema6D reverse signalling. Nature Cell Biology *6*, 1204.

Umeda, K., Ikenouchi, J., Katahira-Tayama, S., Furuse, K., Sasaki, H., Nakayama, M., Matsui, T., Tsukita, S., Furuse, M., and Tsukita, S. (2006). ZO-1 and ZO-2 Independently Determine Where Claudins Are Polymerized in Tight-Junction Strand Formation. Cell *126*, 741-754.

van de Pavert, S.A., Kantardzhieva, A., Malysheva, A., Meuleman, J., Versteeg, I., Levelt, C., Klooster, J., Geiger, S., Seeliger, M.W., Rashbass, P.*, et al.* (2004). Crumbs homologue 1 is required for maintenance of photoreceptor cell polarization and adhesion during light exposure. Journal of Cell Science *117*, 4169.

van Weerd, J.H., and Christoffels, V.M. (2016). The formation and function of the cardiac conduction system. Development *143*, 197.

van Wijk, B., Moorman, A.F.M., and van den Hoff, M.J.B. (2007). Role of bone morphogenetic proteins in cardiac differentiation. Cardiovascular Research *74*, 244-255.

VanDusen, N.J., Casanovas, J., Vincentz, J.W., Firulli, B.A., Osterwalder, M., Lopez-Rios, J., Zeller, R., Zhou, B., Grego-Bessa, J., De La Pompa, J.L.*, et al.* (2014a). Hand2 is an essential regulator for two Notch-dependent functions within the embryonic endocardium. Cell Reports *9*, 2071-2083.

Vega-Hernández, M., Kovacs, A., De Langhe, S., and Ornitz, D.M. (2011). FGF10/FGFR2b signaling is essential for cardiac fibroblast development and growth of the myocardium. Development *138*, 3331.

von Gise, A., and Pu, W.T. (2012). Endocardial and Epicardial Epithelial to Mesenchymal Transitions in Heart Development and Disease. Circulation Research *110*, 1628.

Wang, C.C., Jamal, L., and Janes Kevin, A. (2011). Normal morphogenesis of epithelial tissues and progression of epithelial tumors. Wiley Interdisciplinary Reviews: Systems Biology and Medicine *4*, 51-78.

Wang, H.U., Chen, Z.-F., and Anderson, D.J. (1998). Molecular Distinction and Angiogenic Interaction between Embryonic Arteries and Veins Revealed by ephrin-B2 and Its Receptor Eph-B4. Cell *93*, 741-753.

Wei, X., and Malicki, J. (2002). nagie oko, encoding a MAGUK-family protein, is essential for cellular patterning of the retina. Nature Genetics *31*, 150.

Wei, Z., Li, Y., Ye, F., and Zhang, M. (2015). Structural Basis for the Phosphorylation-regulated Interaction between the Cytoplasmic Tail of Cell Polarity Protein Crumbs and the Actin-binding Protein Moesin. The Journal of Biological Chemistry *290*, 11384-11392.

Wells, C.D., Fawcett, J.P., Traweger, A., Yamanaka, Y., Goudreault, M., Elder, K., Kulkarni, S., Gish, G., Virag, C., Lim, C.*, et al.* (2006). A Rich1/Amot Complex Regulates the Cdc42 GTPase and Apical-Polarity Proteins in Epithelial Cells. Cell *125*, 535-548.

Westcot, S.E., Hatzold, J., Urban, M.D., Richetti, S.K., Skuster, K.J., Harm, R.M., Lopez Cervera, R., Umemoto, N., McNulty, M.S., Clark, K.J.*, et al.* (2015). Protein-Trap Insertional Mutagenesis Uncovers New Genes Involved in Zebrafish Skin Development, Including a Neuregulin 2a-Based ErbB Signaling Pathway Required during Median Fin Fold Morphogenesis. PLOS ONE *10*, e0130688.

Wodarz, A., Grawe, F., and Knust, E. (1993). CRUMBS is involved in the control of apical protein targeting during Drosophila epithelial development. Mechanisms of Development *44*, 175-187.

Wodarz, A., Hinz, U., Engelbert, M., and Knust, E. (1995). Expression of crumbs confers apical character on plasma membrane domains of ectodermal epithelia of drosophila. Cell *82*, 67-76.

Wu, S.K., Gomez, G.A., Michael, M., Verma, S., Cox, H.L., Lefevre, J.G., Parton, R.G., Hamilton, N.A., Neufeld, Z., and Yap, A.S. (2014). Cortical F-actin stabilization generates apical–lateral patterns of junctional contractility that integrate cells into epithelia. Nature Cell Biology *16*, 167.

Wu, X., Tanwar, P.S., and Raftery, L.A. (2008). Drosophila follicle cells: morphogenesis in an eggshell. Seminars in cell & developmental biology *19*, 271-282.

Wu, Y., Sarkissyan, M., and Vadgama, J.V. (2016). Epithelial-Mesenchymal Transition and Breast Cancer. Journal of Clinical Medicine *5*, 13.

Yamanaka, T., Horikoshi, Y., Sugiyama, Y., Ishiyama, C., Suzuki, A., Hirose, T., Iwamatsu, A., Shinohara, A., and Ohno, S. (2003). Mammalian Lgl Forms a Protein Complex with PAR-6 and aPKC Independently of PAR-3 to Regulate Epithelial Cell Polarity. Current Biology *13*, 734-743.

Yap, A.S., Crampton, M.S., and Hardin, J. (2007). Making and breaking contacts: The cellular biology of cadherin regulation. Current opinion in cell biology *19*, 508-514.

Yeaman, C., Grindstaff, K.K., and Nelson, W.J. (1999). New Perspectives on Mechanisms Involved in Generating Epithelial Cell Polarity. Physiological Reviews *79*, 73-98.

Yi, C., Troutman, S., Fera, D., Stemmer-Rachamimov, A., Avila, J.L., Christian, N., Persson, N.L., Shimono, A., Speicher, D.W., Marmorstein, R.*, et al.* (2011). A Tight Junction-Associated

Merlin-Angiomotin Complex Mediates Merlin's Regulation of Mitogenic Signaling and Tumor Suppressive Functions. Cancer cell *19*, 527-540.

Yonemura, S. (2011). Cadherin–actin interactions at adherens junctions. Current Opinion in Cell Biology *23*, 515-522.

Yoruk, B., Gillers, B.S., Chi, N.C., and Scott, I.C. (2012). Ccm3 functions in a manner distinct from Ccm1 and Ccm2 in a zebrafish model of CCM vascular disease. Developmental Biology *362*, 121-131.

Yu, F., Morin, X., Cai, Y., Yang, X., and Chia, W. (2000). Analysis of partner of inscuteable, a Novel Player of Drosophila Asymmetric Divisions, Reveals Two Distinct Steps in Inscuteable Apical Localization. Cell *100*, 399-409.

Zhang, W., Chen, H., Qu, X., Chang, C.P., and Shou, W. (2013). Molecular mechanism of ventricular trabeculation/compaction and the pathogenesis of the left ventricular noncompaction cardiomyopathy (LVNC). American Journal of Medical Genetics Part C: Seminars in Medical Genetics *163*, 144-156.

Zhou, B., and Pu, W.T. (2011). Epicardial epithelial-to-mesenchymal transition in injured heart. Journal of Cellular and Molecular Medicine *15*, 2781-2783.

Zihni, C., Mills, C., Matter, K., and Balda, M.S. (2016). Tight junctions: from simple barriers to multifunctional molecular gates. Nature Reviews Molecular Cell Biology *17*, 564.